The Dissertation Committee for Deqiang An Certifies that this is the approved version of the following dissertation:

Novel Calixpyrrole-like Anion Receptors

Committee:

Jonathan L. Sessler, Supervisor

Eric V. Anslyn

Brian L. Pagenkopf

Jennifer S. Brodbelt

Martin Poenie

Novel Calixpyrrole-like Anion Receptors

by

Deqiang An, B.S., M.S.

Dissertation

Presented to the Faculty of the Graduate School of

The University of Texas at Austin

in Partial Fulfillment

of the Requirements

for the Degree of

Doctor of Philosophy

The University of Texas at Austin

August 2004

Dedication

This manuscript is dedicated to my father.

Acknowledgements

I would like to acknowledge all the people who helped me along my five year's journey in the University of Texas at Austin.

First of all, I would like to thank my supervisor, Professor Jonathan L. Sessler. Thank you so much for providing me the chance to study and work in this nice group. Your mentorship is the light tower that continuously leads me to success.

I would like to thank Dr. Hidekazu Mijaji, Dr. Sato Wataru, Won-seob, and Dr. Toshihisa Mizuno for your kind help and cooperations on several research projects. I would like to thank Dr. Vincent Lynch for your great help on solving the X-ray diffraction structures of all my compounds. I would like to thank Bobbi for being a nice labmate for four years and the proofreader for my dissertation. I would like to thank Dr. Steve Dudek for your precious advice for my research and great friendship. I would like to thank Dr. Wenhao Wei for your brothership and daily Chinese conversation with me around the lunch time.

I would like to thank all other group members in Sessler lab for their non-conservative help and candid discussion for my project. Thank you, Dr. Jackline Veauthier, Dr. Piotr Piatek, Dan, Janan, Wyeth, Leah, Jeong Tae, Patricia, Elisa, Mark, Apolonio, Julian, Jim, and Becky. Without your help, I couldn't have walked so far.

Finally, I would like to thank my wife, Huiyu Jia, my lovely son, Yunhao An, and all my family members in China. They are to whom my heart belongs, forever.

Novel Calixpyrrole-like Anion Receptors

Publication No._____

Deqiang An, Ph.D.

The University of Texas at Austin, 2004

Supervisor: Jonathan L. Sessler

Calix[*n*]pyrroles ($n \geq 4$) are venerable anion receptors that are based on single pyrroles and ketones as building blocks. However, the existence of only one variable, *n*, that defines the nature of the systems, limits this class of macrocycles to only a few core structures. To overcome this limitation, a series of building blocks other than single pyrroles, have been applied to the construction of novel calixpyrrole-like systems. These building blocks include bipyrrole, furan, thiophene, and 1,3-bispyrrolylbenzenes. Based on bipyrrole as the sole building block, a series of calix[*n*]bipyrroles (n = 3, 4) was synthesized. Based on bipyrrole, furan or thiophene as co-building blocks, calix[2]bipyrrole[*m*]furan[*n*]thiophene ($m + n = 2$) were obtained. Based on 1,3-bispyrrolylbenzenes, calix[*n*]bispyrrolylbenzenes (n = 2 - 4) were synthesized. These novel calixpyrrole-like macrocycles contain different core structures than calix[*n*]pyrroles, and thus display different anion binding properties than their parent systems. This, in turn, means that these new systems are not only helping to the chemistry of calixpyrroles, but also giving rise to selective receptors that find applications in anion coordination chemistry.

Table of Contents

List of Tables

List of Figures

List of Schemes

Chapter 1: An Introduction to Calixpyrroles-based Anion Coordination Chemistry

Anions play essential roles in biological systems and are noted environmental pollution. For example, anions are believed to participate in *ca.* 70% of all enzymatic binding events, serving as either enzyme substrates or cofactors. Further, excess phosphate and nitrate, as the result of agricultural run-off and urban use, are responsible for eutrophication in water-ways. The pertechnetate produced during the reprocessing of nuclear fuel, when discharging into the seas or underground water, is also an environmental problem. Given their importance, it is perhaps no surprise that anion coordination chemistry has emerged as an important and fast-growing branch of supramolecular chemistry.

Simmons and Park reported the first synthetic polyammonium-based anion receptors in 1968.[1] Since then, especially over the course of the last two decades, numerous anion receptors have been synthesized and studied. While, a detailed introduction to different kinds of anion receptors is beyond the discussion of this dissertation, several excellent reviews and one book have appeared recently that summarize contributions to this area.[2-6] In spite of these reviews a detailed summary of one approach to anion recognition, one based on the use of calixpyrroles, is appropriate here. This is because this chemistry provides the antecedents for the research projects that provide the basis for this dissertation.

1.1 INTRODUCTION

Calix[4]pyrroles (e.g., **1**), originally named "pyrrole-acetone" and formally known as *meso*-octaalkylporphyrinogens, are macrocycles composed of four pyrrole units linked *via* four di-substituted *meso*-carbons at the α positions. Unlike porphyrin precursors, *meso*-free porphyrinogens (e.g., **2**), calix[4]pyrroles are not readily oxidized to form porphyrin-like structures (Scheme 1.1). As a consequence, the four pyrrole units are all in their neutral, NH-bearing forms in calix[4]pyrroles and no electron delocalization exists within the macrocyclic system as a whole. This lack of delocalization causes the absence of visible absorption or fluorescence emission bands, which, in turn, means that calix[4]pyrroles can not be studied using optical techniques. NMR spectroscopic methods provide a good means for characterizing and studying this class of compounds; such studies can not only provide detailed structural information, but also be used to follow various intermolecular binding events, including anion binding.

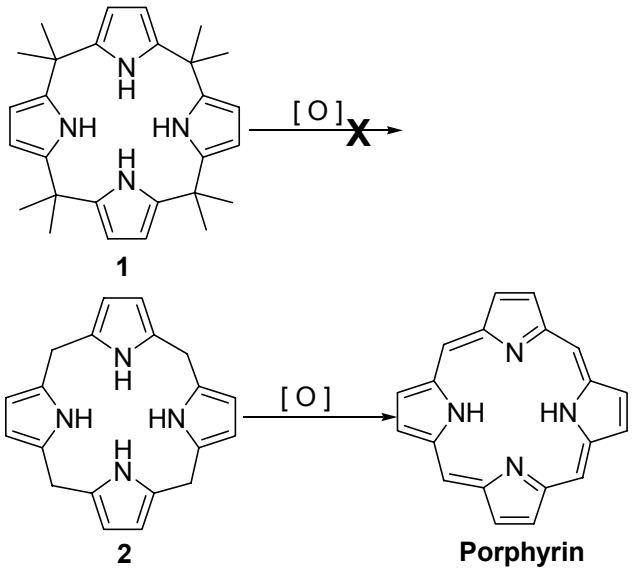

Scheme 1.1 Schematic representation showing the different behavior of porphyrinogens **1** and **2** with respect to oxidation.

1.2 HISTORY

In 1886, Baeyer synthesized a white crystalline material by condensing pyrrole with acetone in the presence of hydrochloric acid.[7] Thirty years later, Chelintzev and Tronov repeated this reaction and proposed a cyclic tetrametric porphyrinogen structure for the product, which later proved to be correct.[8] In 1955, Rothemund and Gage improved this synthesis by using methanesulfonic acid as the catalyst.[9] Other than these important findings, this class of compounds (e.g., **1**) were only studied sporadically in the 100 years following their discovery, most of which merely focused on the refined syntheses of these macrocycles and their meso-substituted derivatives but not their applications.[10-12] This situation changed in the early 1990s when Floriani and coworkers began exploring their metal coordination chemistry extensively, thus reviving interest in these venerable macrocycles after a long dormant period.[13]

In 1996, Sessler and coworkers first reported that this kind of macrocycle could bind anions in organic media, thus demonstrating that this class of macrocycles could be used in novel applications.[14] In this paper, the term calix[4]pyrroles was introduced to highlight the fact these macrocycles displayed conformational behavior similar to that of the calix[4]arenes and, in contrast to porphyrin precursors, did not undergo facile oxidation. Since this seminal report, many new calixpyrrole-based anion receptors have been synthesized and studied, both within the Sessler research group and in other research groups worldwide. This activity has served to establish firmly this branch of anion coordination chemistry. In fact, several reviews[15-16] and a book chapter[17] dealing with calixpyrrole chemistry has already appeared, while further new reports on calixpyrrole-type anion receptors are continuing to appear with increasing regularity.

The development of calixpyrrole-based anion coordination chemistry is reflected in the number of publications appearing each year since 1996 (Figure 1.1, based on a

search using SciFinder Scholar 2004). The number of publications since 1999 has easily averaged more than per year with the peak number appearing in 2002. Whether the decrease seen in 2003 is "real" or simply reflects a statistical variation remains to be seen. However, the tremendous amount of attention devoted to calixpyrroles is providing a strong incentive to branch out and study newer systems, formally analogues of calixpyrroles, such as those described in this dissertation.

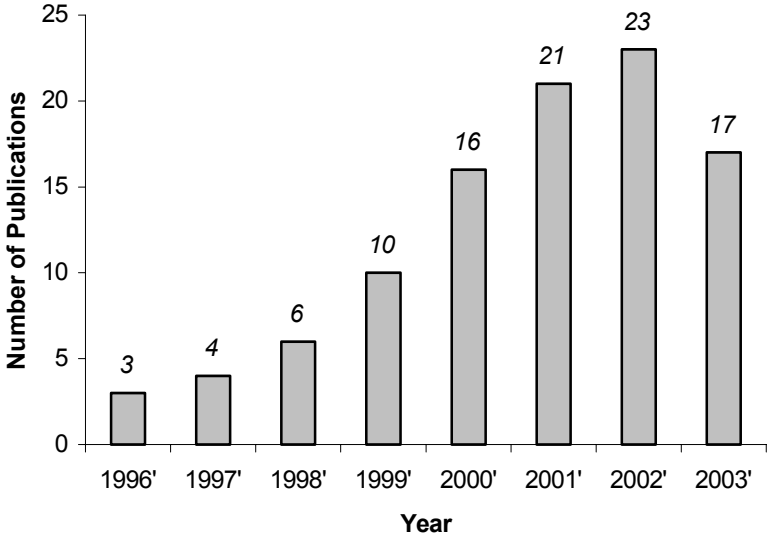

Figure 1.1 Number of publications involving calix[4]pyrrole-based anion coordination chemistry appearing each year during the period of 1996-2003. This graphic is based on the results of a search made using SciFinder 2004.

1.3 ANION BINDING PROPERTIES OF CALIX[4]PYRROLES

As noted above, Sessler and coworker turned their interest towards calix[4]pyrroles–based anion coordination chemistry in the mid-1990's. Their interest was sparked at the time by the sapphyrin-based anion coordination chemistry that was ongoing in their group at that time. The study of sapphyrin as an anion receptor, in turn, can be traced back to 1990, when a crystal structure of the sapphyrin-fluoride anion complex was obtained by Sessler and Ibers.[18] It revealed that in the solid state, the diprotonated form of sapphyrin binds fluoride anion *via* five hydrogen bonding interactions involving the pyrrolic NH protons and the fluoride anion. The question raised by this structure and subsequent analyses was whether neutral pyrrolic macrocycles would bind anions. The calix[4]pyrroles, due to their ease of synthesis, were chosen as a means of addressing this question. Thus, Sessler and coworkers studied calix[4]pyrroles **1** and **3** as anion coordination agents using both solution-phase and solid-phase measurements.[14] NMR spectroscopic titration analyses in CD_2Cl_2 revealed that both compounds are not only effective as 1:1 anion-binding agents in solution, they also show a marked preference for F^- relative to other anions. For example, **1** binds F^- with a much higher affinity constant (K_a = 17,170 M^{-1}) than either Cl^- (350 M^{-1}) or $H_2PO_4^-$ (97 M^{-1}) species[14] that are both bound reasonably well by diprotonated sapphyrin.[19,20] Compound **3** also binds F^-, and to a lesser extent, Cl^-, albeit with a considerably lower affinity than **1**.

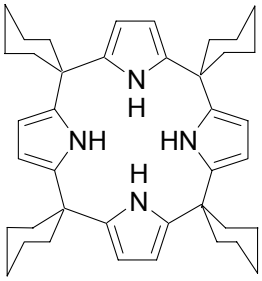

3

X-ray crystal analysis revealed that without anions, compound **1** molecule adopts a 1,3-alternate conformation wherein adjacent rings are oriented in opposite directions. In the presence of chloride anion, the molecule adopts a cone-like conformation such that the four NH protons can hydrogen bond to the halide anions (Scheme 1.2). Compound **3** behaves in the same way in the absence and presence of fluoride anion. These crystal structures clearly show the cooperative hydrogen bonding interactions that exist in the solid state between the four pyrrolic NH protons and the halide anions.

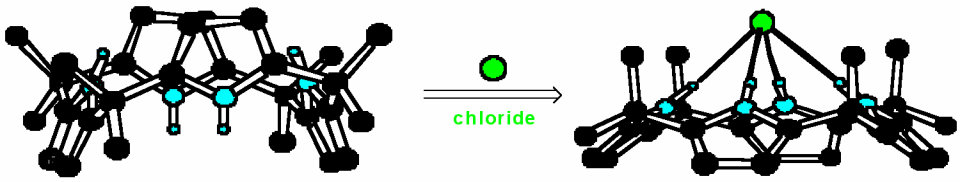

1,3-alternate conformation cone-like conformation

Scheme 1.2 X-ray crystal structures of calix[4]pyrrole **1** in the absence and presence of chloride anion.

1.4 THEORETICAL STUDIES

Calix[4]arenes can adopt four limiting conformations: 1,3-alternate, 1,2-alternate, partial cone, and cone. Calix[4]pyrroles can behave in the same way, something that has been observed experimentally and noted theoretically (Figure 1.2).[21]

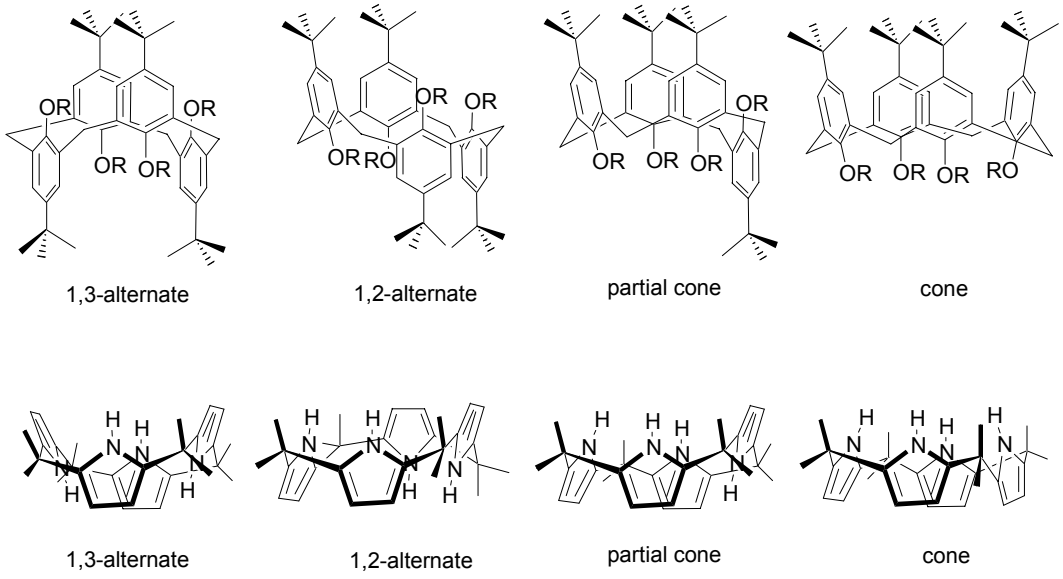

Figure 1.2 Four limiting conformations of representative calix[4]arenes (upper) and calix[4]pyrroles (lower).

Jorgensen investigated the complexation of **1** with anions by carrying out energy minimizations in the gas phase and *via* Monte Carlo simulations in a dichloromethane milieu using the OPLS force field.[21] The gas phase calculations revealed that 1,3-alternate conformation of **1** was the most stable one in the absence of a halide anion, while the cone conformer was not stable under this condition. However, in the presence of halide anions the cone conformation was the most stable among the various possible conformations (Figure 1.3). The solution phase simulation showed that the relative free

energies of binding of chloride, bromide, and iodide with **1** were in excellent agreement with the experimental data. A notable exception is that the theoretical studies predicted a free energy of binding for fluoride anion that was larger than that observed by experiment. This discrepancy is thought to reflect the presence of trace water under the conditions of the experiment. Such a possibility is quite real since the fluoride salt used, tetrabutylammonium fluoride, can never be produced in a completely anhydrous form.

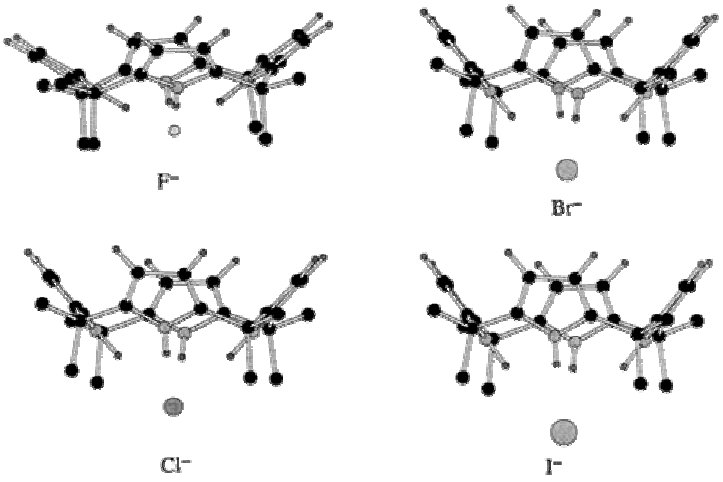

Figure 1.3 Cone-like halide complexes of **1** energy-minimized in the gas phase.

The anomalous nature of the fluoride binding behavior was further explained by the studies of Orozco. These workers showed that the inherent binding preference of **1** for fluoride anion calculated in the gas phase or observed by experiment in pure aprotic solvents, such as dichloromethane, can change dramatically in protic solvents or in the presence of the hydrated cation as co-solute of the anion.[22] Their theoretical studies also served to underscore the importance of considering all relevant factors, including solvent,

hydration, countercation, concentration, binding stoichiometry, and so forth when comparing different experimental results.

Wu also studied the conformation features and anion binding properties of compound **1** theoretically.[23] Geometries and energies were optimized by the BLYP/3-21G and BLYP/6-31G, and BLYP/6-31+G** methods, respectively. Both gas phase and solution phase (CH_2Cl_2) studies revealed a predicted stability sequence for the various conformers of 1,3-alternate > partial cone > 1,2-alternate > cone. This theoretical study also showed that in the case of fluoride anion binding, a 1:1 anion-binding mode would be favored over a 1:2 binding mode. It also predicted a calculated binding energy for chloride anion complexation that was in good agreement with the experimental data.

1.5 SYETHESES OF CALIX[4]PYRROLE CORE MACROCYCLES

There are three general methods for the synthesis of calix[4]pyrroles: a one-pot [1 + 1 + 1 + 1] condensation; [2 + 2] condensations; and [3 + 1] condensations, where the numbers in the brackets refer to the number of pyrrolic subunits in the precursors involved. Among these, the one-pot approach is the most popular for preparing simple calix[4]pyrroles.

1.5.1 One-pot Condensation

As commonly practiced, the one-pot synthesis of calix[4]pyrroles involves the condensation of pyrrole(s) and ketone(s) in a 1:1 ratio in the presence of an acid catalyst. Commonly used catalysts include methanesulfonic acid, trifluoroacetic acid, and boron trifluoride diethyl etherate. Favored solvents include methanol, ethanol, acetonitrile, and dichloromethane. In some cases the reactant ketone can be used in large excess as the solvent. Depending on how many types of pyrroles or ketones are used in the reaction, one-pot condensation can be categorized into homo-condensation and mixed condensation.

1.5.1.1 Homo-condensation

The term homo-condensation is meant to define the reaction of a specific pyrrole with a specific ketone. According to the symmetry of the pyrrole or ketone components, these homo-condensations can be further categorized as symmetric homo-condensations and asymmetric homo-condensations.

A symmetric homo-condensation represents a reaction employing a symmetric pyrrole and a symmetric ketone. Generally such reaction produces one easy-to-separate major product in good yield. One typical example of symmetric homo-condensation is

the synthesis of **1** *via* the condensation of pyrrole with acetone in a 1:1 ratio in methanol using methanesulfonic acid as the acid catalyst.[14] Column chromatography (silica gel, dichloromethane /hexanes 1:1, eluent) affords **1** in yields ranging between 60% and 80% (Scheme 1.3).

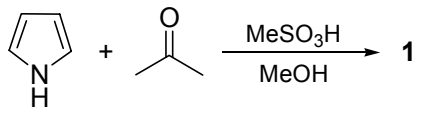

Scheme 1.3 A prototypical symmetric homo-condensation as illustrated *via* the synthesis of calix[4]pyrrole **1**.

An asymmetric homo-condensation normally involves the reaction of a pyrrole with an asymmetric ketone. For example, condensation of pyrrole with *p*-hydroxyacetophenone in methanol in the presence of methanesulfonic acid afforded the desired calix[4]pyrrole **4** in 62% yield (Scheme 1.4).[24] Since each of the four *meso* bridges formed under the conditions contains both a methyl and aryl substituent, the product, actually, consists of a mixture containing four different configurational isomers; these isomers can be difficult to separate and may require tedious separation procedures including careful column chromatography or HPLC techniques.

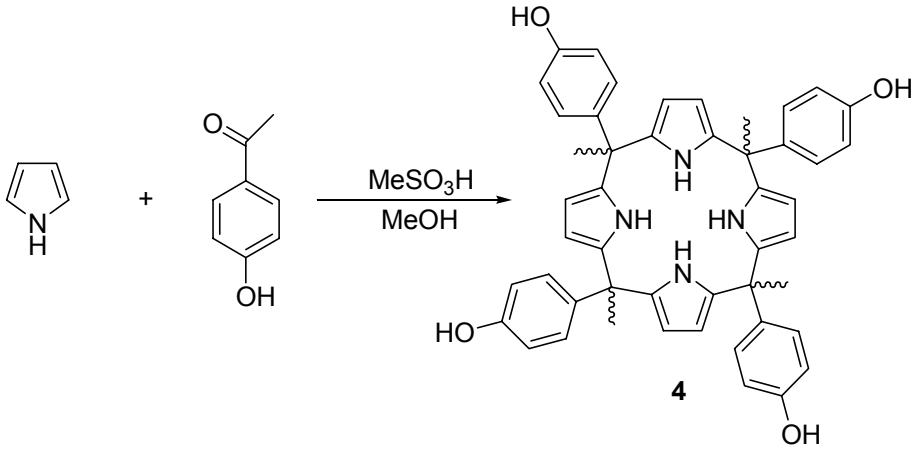

Scheme 1.4 A typical asymmetric homo-condensation showing the synthesis of the tetraphenolic calix[4]pyrrole **4**. As explained in the text, this product is obtained as a mixture of configurational isomers.

1.5.1.2 Mixed Condensation

Mixed condensations involve the condensation of more than one kind of pyrrole with a specific ketone or more than one kind of ketone with a specific pyrrole. Mixed condensations have low yields of individual products due to the fact that a mixture of products is formed. As a result, the reactants ratio must be carefully controlled so as to optimize the yield of the desired products. However, once separated, the various calix[4]pyrroles can often find application in a variety of areas, in part because mixed condensations provide a good entry into functionalized systems. For instance, the calix[4]pyrrole monoester **5** was synthesized by stirring pyrrole, cyclohexanone, and methyl 4-acetylbutyrate in a 2:1:1 ratio under the same reaction conditions as used to prepare **1**.[25] Column chromatography (silica gel; dichloromethane, eluent) afforded **5** in 12% yield (Scheme 1.5).

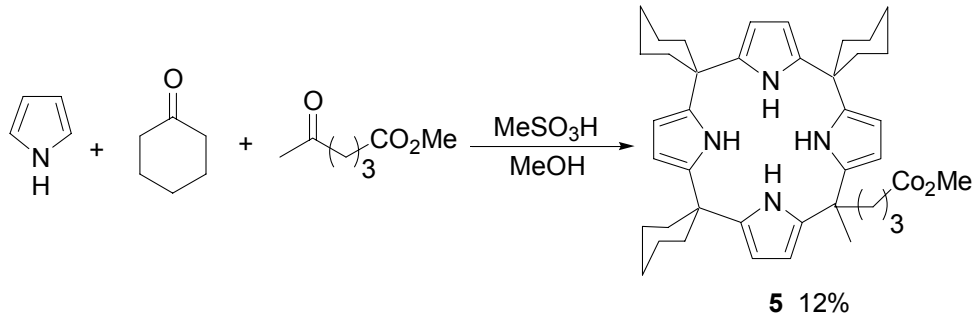

Scheme 1.5 Mixed condensation synthesis of calix[4]pyrrole monoester **5**.

1.5.2 [2 + 2] Condensation

[2 + 2] Condensations refer to acid-catalyzed condensations of two dipyrromethane units, generally synthesized in a predicative step from pyrrole and a ketone, with two ketone units (normally different from those used in the syntheses of the dipyrromethanes). This [2 + 2] approach represents an important means of constructing a variety of calix[4]pyrrole macrocycles, particularly less symmetric ones, that can not be obtained under the less well-controlled one-pot reaction conditions.

Compounds **6-8** are typical of the kinds of products that may be obtained readily using a [2 + 2] approach. These particular products were synthesized from the dipyrromethane precursors **9-11** (Scheme 1.6).[26] These precursors were, in turn, prepared from the condensation of pyrrole with diaryl ketones in ethanol using boron trifluoride diethyl etherate as the catalyst. Once in hand, these precursors were condensed with acetone in a mixed solvent system consisting of ethanol and acetone (1:1 v/v), with the acetone acting both as a solvent and as a reactant. This gave the cyclic products **6-8** in decent yields. By contrast, **9-11** were found not to react further with the original aromatic ketones, either to form linear polymers or cyclic calixpyrrole-type products,

even after prolonged reaction times or *via* the use of elevated temperature. This lack of reactivity may be explained by the steric effect caused by the aryl groups.

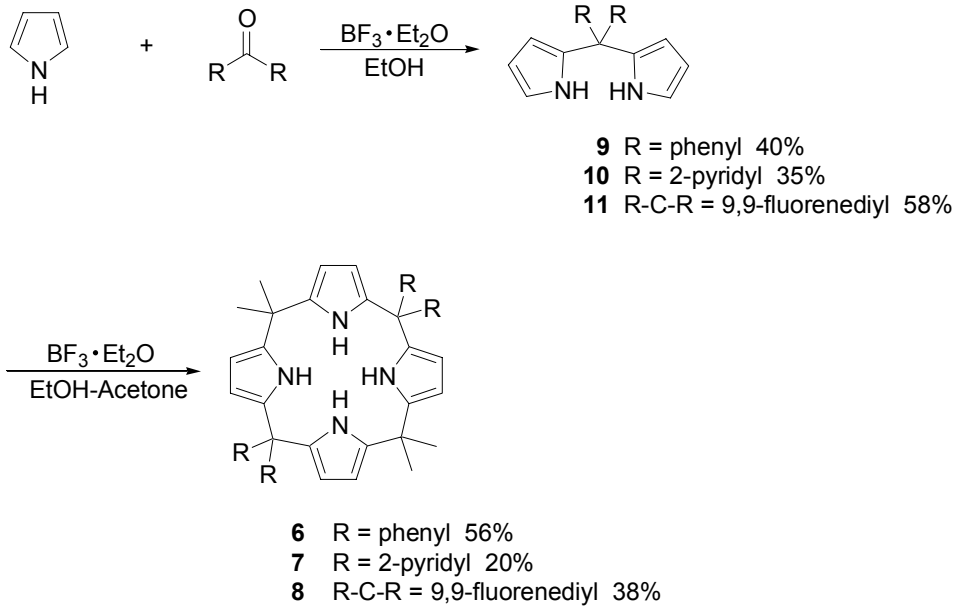

9 R = phenyl 40%
10 R = 2-pyridyl 35%
11 R-C-R = 9,9-fluorenediyl 58%

6 R = phenyl 56%
7 R = 2-pyridyl 20%
8 R-C-R = 9,9-fluorenediyl 38%

Scheme 1.6 [2 + 2] Condensation syntheses of compounds **6-8**.

1.5.3 [3 + 1] Condensation

[3 + 1] Condensations involve the reaction of a tripyrrane or tripyrrane derivative with a pyrrole or pyrrole derivative in the presence of an acid catalyst. Due to the poor stability of most tripyrranes in the presence of acid, such reactions generally procede in low yield. In fact, no true calix[4]pyrroles have been synthesized using this method.

Recently, a "pseudo" calix[4]pyrrole **12** was synthesized using the [3 + 1] method (Scheme 1.7).[27] Tripyrrane dimethanol **13c** was synthesized by reducing the corresponding tripyrrane dialdehyde **13b**, which was synthesized by formylation of tripyrrane **13a**,[28] with sodium borohydride in a mixture of THF and methanol. Treatment of the resulting tripyrrane diol with the tetrathiafulvalene-containing pyrrole **14** in dry

acetonitrile using boron trifluoride diethyl ether as an acidic catalyst afforded the mono-TTF calix[4]pyrrole **12** in 21% yield. Anion binding properties of this compound were studied by both NMR spectroscopic methods and electrochemical techniques. The NMR spectral studies revealed that **12** displays stronger anion binding affinities than does compound **1**. Electrochemical studies showed that the complexation of the anion inside the cavity of **12** shifts the first oxidation wave of the TTF unit towards more cathodic potentials.

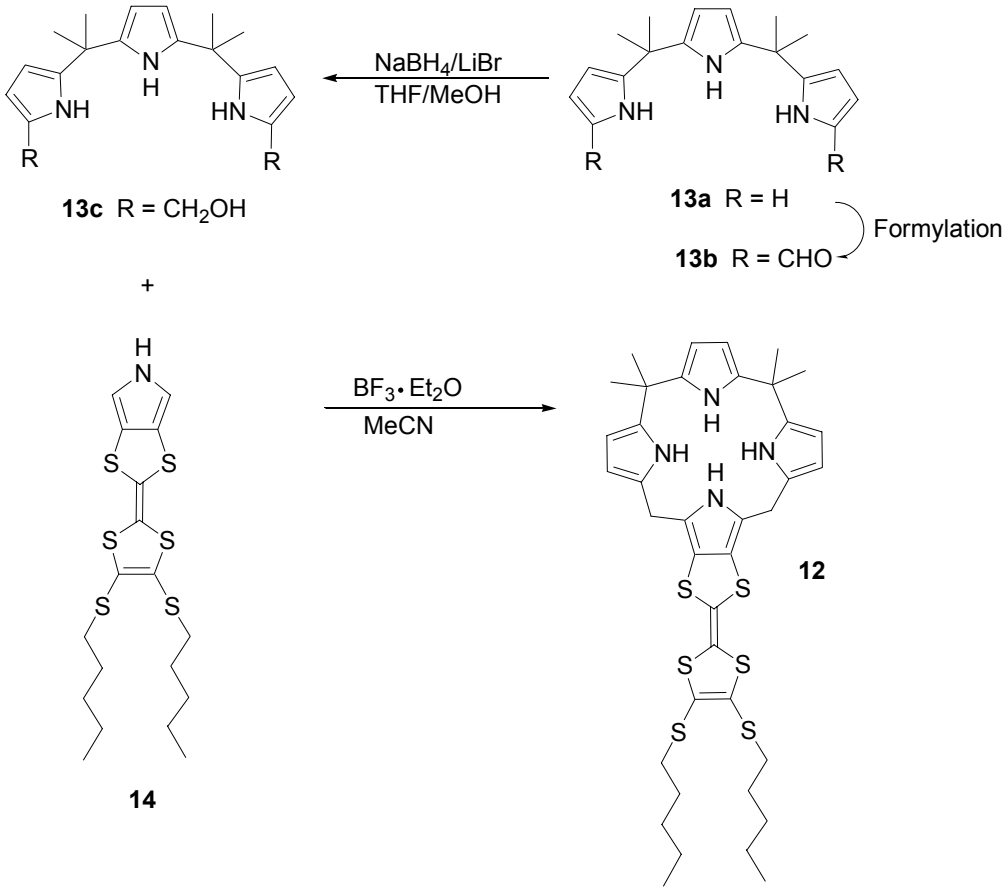

Scheme 1.7 Synthesis of a "pseudo" calix[4]pyrrole **12** *via* a [3 + 1] condensation approach.

1.6 POST-MACROCYCLE FUNCTIONALIZATIONS

Calix[4]pyrroles can be functionalized at either the *β*-positions (C-rim) or *meso* positions. Such substitutions not only affect the anion binding properties of calix[4]pyrroles, but also produce precursors useful for the syntheses of calix[4]pyrrole-based anion sensors, transporting agents, or solid phase for anion separation. Functionalizations at *β*-positions, also called C-rim functionalization, have been extensively explored in this group. The most popular C-rim functionalizations are *β*-octa functionalizations and *β*-mono functionalizations since they produce only one dominant product. *β*-Functionalization procedures intermediate between these two extremes have not been extensively explored due to the production of multiple products, poor reaction control, and difficulties in achieving product separation.

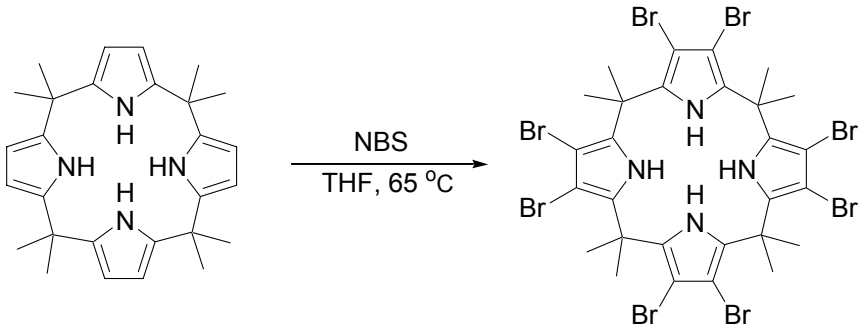

Scheme 1.8 C-rim functionalization synthesis of compound **15**.

β-Octabromocalix[4]pyrrole **15** was synthesized in 90% yield by heating **1** with eight equivalents of NBS reagents in THF at reflux for five hours (Scheme 1.8).[29] This represents an alternative and highly effective synthesis of **15**, since the standard one-pot condensation of 3,4-dibromopyrrole with acetone proved unproductive, presumably due to the instability of 3,4-dibromopyrrole under the reaction conditions.

β-Monosubstituted calix[4]pyrroles were also synthesized and studied (Scheme 1.9). However, their systhesis proved somewhat unusual and serves to illustrate an interesting feature of calix[4]pyrrole chemistry. In particular, it was found that lithiation of **1** with four equivalents of *n*-butyllithium in THF at –78 ˚C produced a polyanion intermediate, which upon treatment with a suitable electrophile followed by quenching with water, gave the *β*-monosubstituted calix[4]pyrroles **16-20** and some *β*-disubstituted calix[4]pyrroles.[30] This method provided a variety of elaborated calix[4]pyrroles, among which systems **16-18** have proved particularly useful as building blocks for further elaboration.

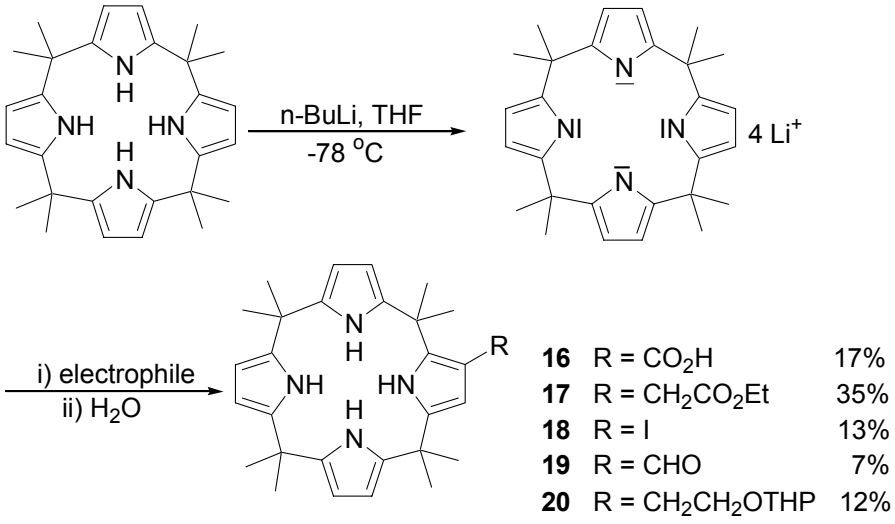

Scheme 1.9 C-rim functionalization syntheses of compounds **16**-**20**.

For instance, the monoiodo derivative **18** was used to produce the *β*-monoethynyl calix[4]pyrrole **21**, a species that , in turn, has served as a versatile builiding block (Scheme 1.10).[31] The synthesis of **21** involved first reacting **18** with excess TMS acetylene in diisopropylamine-DMF at 80 ˚C in the presence of $Pd(PPh_3)_4$-CuI, to give

the TMS protected alkynyl derivative **22** in 73% yield. In a second step, this intermediate was subject to deprotection using tetrabutylammonium fluoride in THF at room temperature; this gave **21** in 89% yield.

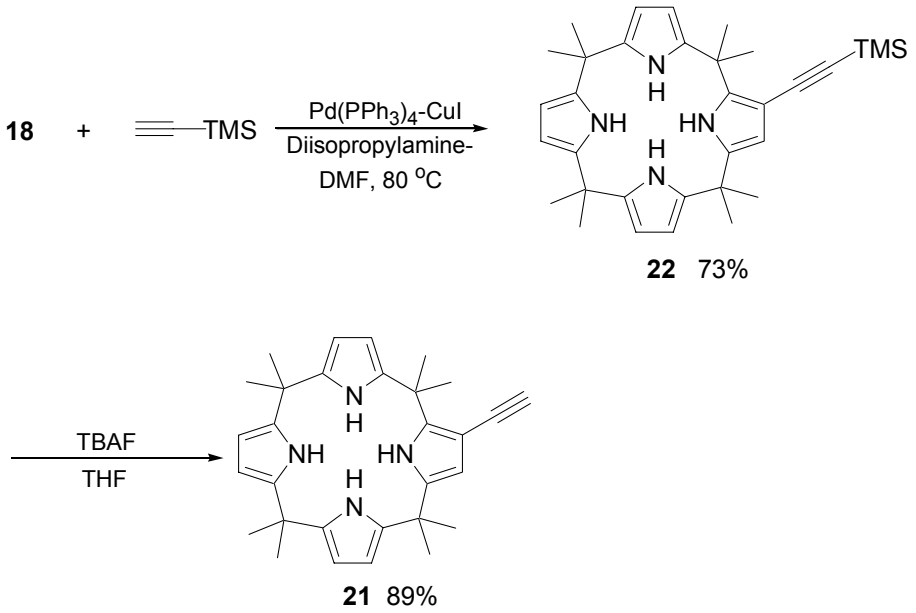

Scheme 1.10 Two step synthesis of building block **21**.

1.7 MODULATING THE ANION BINDING PROPERTIES OF CALIX[4]-PYRROLES

Calix[4]pyrroles have been modified using a variety of methods in an effort to modify their inherent anion binding properties. The known modification methods include C-rim substitution, *meso*-modification, dimerization, and by incorporating a synthetic cover onto one face. C-rim modification will be discussed in greater detail in Chapter 2. The other approaches are reviewed briefly here.

1.7.1 *Meso*-modification

Introduction of aryl or other rigid groups into the *meso*-like positions of calix[4]pyrroles could serve not only to change the intrinsic anion selectivity of the calix[4]pyrrole skeleton, but also, in appropriate cases to introduce secondary binding sites that might allow for selective recognition of cationic, anionic, or neutral guests. A good example of *meso*-modification is provided by compound **4** and its ether derivative.[24] As detailed above, calix[4]pyrrole **4** consists of four isomers that can be separated *via* column chromatography. According to the relative position of the bulky substituted phenyl group, these isomers were identified as being the *αααα*, *ααaβ*, *ααββ*, and *αβαβ* configurational isomers, where the "*α*" and "*β*" nomenclature follows the standard porphyrin convention (Figure 1.4). A single crystal X-ray diffraction analysis of the ethanol adduct of the *αααα* isomer revealed that one ethanol molecule was trapped within the deep cavity that, in turn, was found to be in the expected cone conformation. Solution-phase NMR spectral studies also showed that the Cl^- and $H_2PO_4^-$ affinities of all isomers are lower than those of **1**. On the other hand, the Cl^- over $H_2PO_4^-$ selectivity seen for **1** was found to be reversed in the case of the *αααα* isomer.

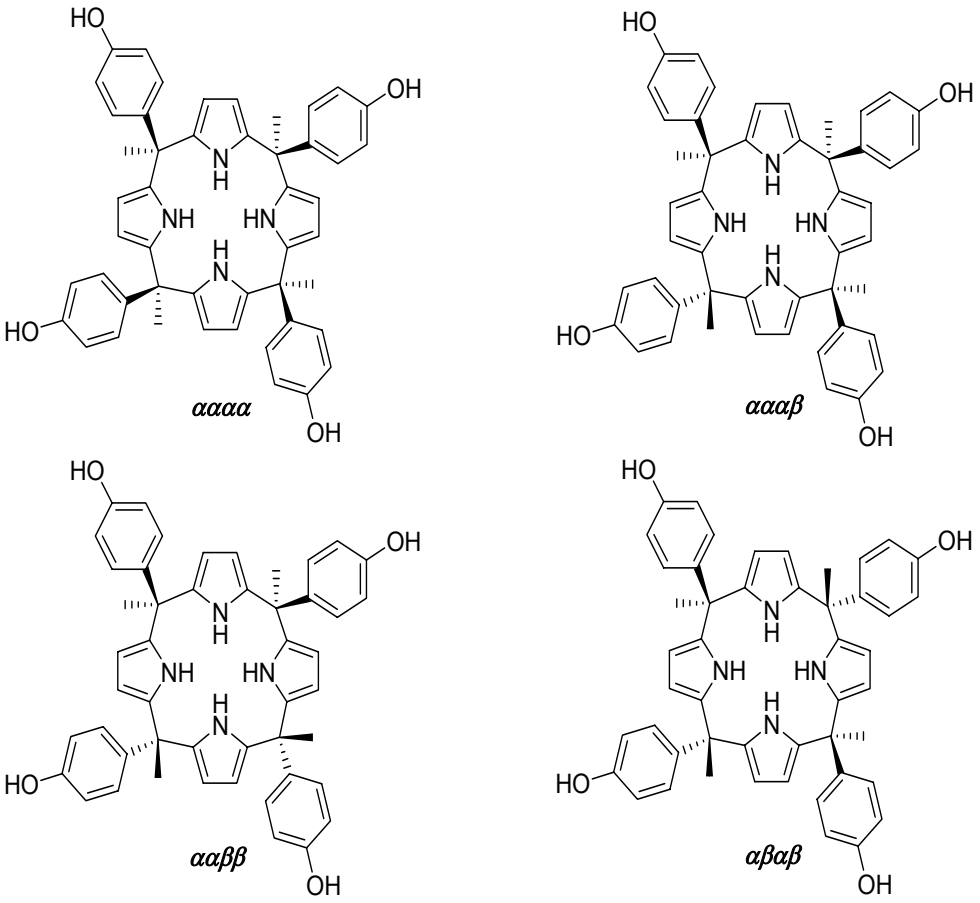

Figure 1.4 Structure isomers of calix[4]pyrrole **4**.

Novel deep cavity calix[4]pyrroles **23** and **24** derived from steroidal ketones were synthesized and studied for their ability to effect the selective recognition of appropriate sized organic anions. Here, the initial "screenings" of binding activity and selectivity were made using FAB-MS.[32] One good receptor, the polyhydroxylated *ααα*β configurational isomer of **24b**, was found in this way to bind both tartaric acid and mandelic acid selectively, while **23** and **24a** were found to be far less effective as receptors for these guests. These findings were rationalized in terms of a combination of

both specific anion-pyrrole NH hydrogen bonding interactions and less well-defined steroid-substrate interactions.

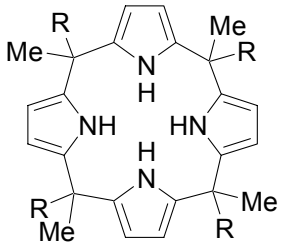

R =

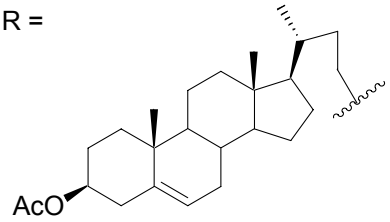

23

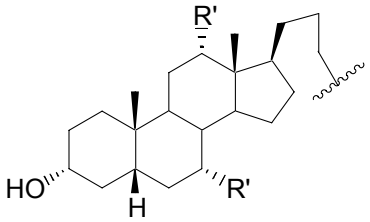

24a R' = H
24b R' = OH

In work that is without prior precedent in the calix[4]pyrrole literature, Gale and coworkers recently reported the synthesis of a new *meso*-modified calix[4]pyrrole, namely the pentapyrrolic calix[4]pyrrole **25** (Scheme 1.11).[33] The fifth pyrrole unit, attached synthetically to a *meso*- position, was expected to act as an ancillary hydrogen bonding doner, thereby enhancing the anion affinities of **25** relative to simple calix[4]pyrroles. Tripyrrolylmethane **26** was synthesized *via* a methanesulfonic acid catalyzed condensation of pyrrole with 2-acetyl-3,4,5-tribromopyrrole. Of further note is the ease of synthesis. In fact, the [2 + 2] mixed condensation of **26** with dimethyl dipyrromethane in acetone afforded **25** in 14% yield.

NMR spectroscopic titration studies carried out in dichloromethane-d_2 revealed that **25** shows enhanced affinities for several common anions of interest. When

compared to **1**, **25** was found to exhibit affinities for Cl^-, Br^-, $H_2PO_4^-$, and HSO_4^-, that are not substantially improved. However, it shows considerably higher affinities for benzoate and acetate. This behavior, as proposed by the authors, can be attributed to the coordination of both oxygen atoms of the carboxylate anion simultaneously by **25**, thus raising the affinity. By contrast, **1** coordinates only one oxygen atom of the carboxylate anion.

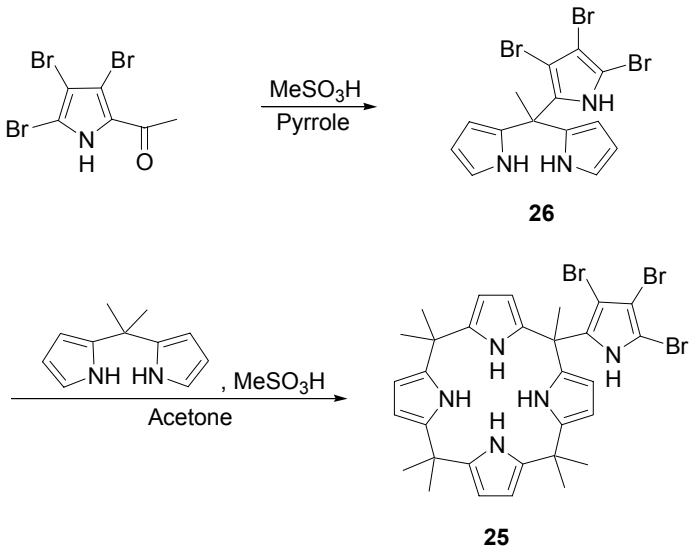

Scheme 1.11 Synthesis of compound **25**.

1.7.2 Dimeric Systems

Calix[4]pyrroles that contain two binding sites, such as **27**, could be used to bind polyanion substates with fit geometries. Self-coupling of **21** afforded dimer **27** in 91% yield (Scheme 1.12).[34] Anion binding studies from ^{1}H NMR titration measurements revealed that **27** binds isophthalate in dichloromethane-d_2 with a binding constant of 4180 M^{-1}, which is five times larger than that for **1** (K_a = 700 M^{-1}). However, **27** binds phthalate and benzoate with much lower binding constants. Job plot data showed a 1:1

binding mode for isophthalate, and a 1:2 binding mode for both phthalate and benzoate. A cooperative binding mode was proposed for the interaction of **27** with isophthalate. Specifically, it was suggested that each of the two carboxylate anionic moieties of isophthalate interacts with the individual calix[4]pyrrole moieties present in **27** (Figure 1.5).

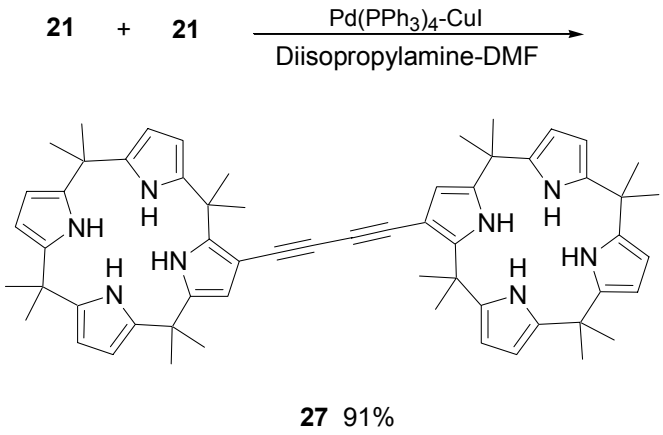

Scheme 1.12 Synthesis of calix[4]pyrrole dimer **27**.

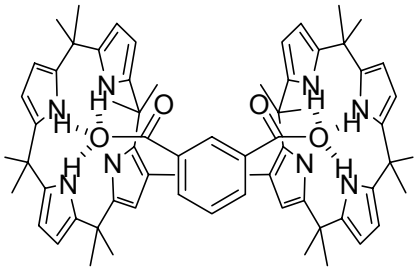

Figure 1.5 Schematic representation of cooperative binding of isophthalate anion by the dimeric calix[4]pyrrole **27**.

1.7.3 Strapped Calix[4]pyrroles

The intrinsic anion binding properties of calix[4]pyrroles can also be modified by covering one face by means of "straps" attached at the 1,3- *meso* positions with flexible linkers. Such strapping could serve to reduce the solvent-host interactions while at the same time enhancing the host-guest interactions. Such modifications of the calix[4]pyrrole skeletons would create different-sized 3-D cavities, therefore allowing for selective "size matched" anion recognition within the cavities.[35-37]

The first strapped calix[4]pyrroles **28** were synthesized by Lee and coworkers using the [2 + 2] condensation methods (Scheme 1.13).[35] Reacting 5-hydroxy-2-pentanone in excess pyrrole in the presence of trifluoroacetic acid afforded the corresponding dipyrromethane **29**, followed by coupling with isophthaloyl dichloride in the presence of pyridine gave the strapped dipyrromethane intermediate **30**. A subsequent [2 + 2] condensation of **29** with acetone then afforded **28** in 16% yield. ITC studies of **28** in DMSO revealed a much larger affinity constant for Cl^- binding (K_a = 1.01×10^5 M^{-1}) in comparison to **1** ($K_a = 1.27 \times 10^3$ M^{-1}).

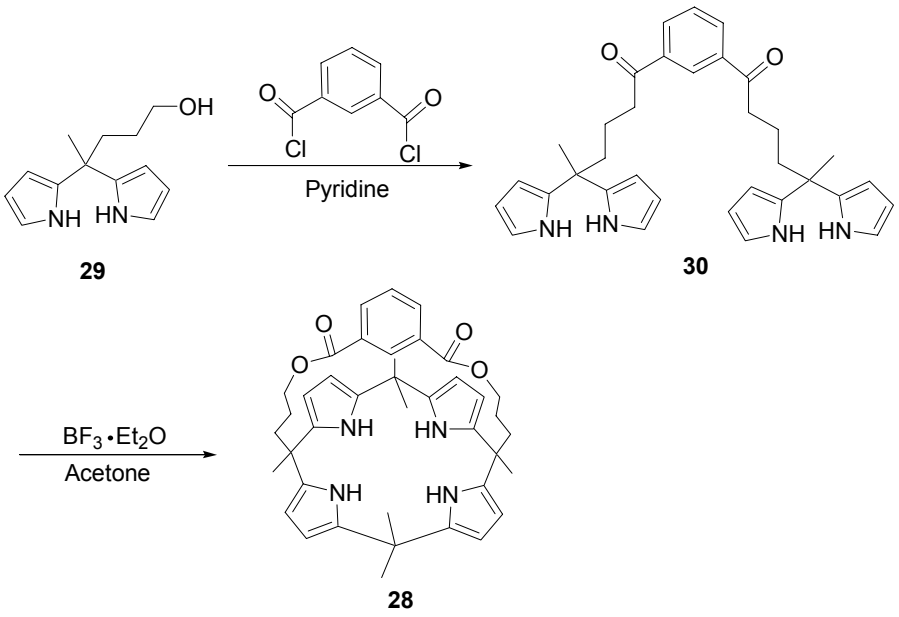

Scheme 1.13 Synthesis of compound **28** *via* a [2 + 2] condensation.

A more general method for synthesizing strapped calix[4]pyrroles was recently developed in the same research group (Scheme 1.14). Specifically, it was found that condensing strapped diketones with pyrrole in the presence of TFA provided the corresponding strapped dipyrromethane intermediate. This intermediate could then be condensed with acetone in a [2 + 2] fashion in the presence of a catalytic amount of boron trifluoride diethyl etherate to produce the desired strapped calix[4]pyrroles **31**-**33**.[36] Anion binding studies revealed that compounds **31**-**33** all displayed enhanced affinities for chloride and bromide anion relative to **1**. The principle difference within the series is that **31** displays the largest Cl^- affinity, while **33** displays the largest Br^- affinity. Considering the lengths of the straps in the three compounds, one may conclude that the anion binding properties are being effectively tuned as the result of modification in the length of the bridging straps.

Current work in the Lee group is focused on the preparation of other strapped calix[4]pyrroles. Among the systems being developed in this context is compound **34**. This novel capped system contains two different kinds of binding elements (calix[4]pyrrole and porphyrin) and could function as a ditopic receptor, as well as a Lewis acid assisted anion receptors in the case of the metalated (porphyrin) derivatives.[37]

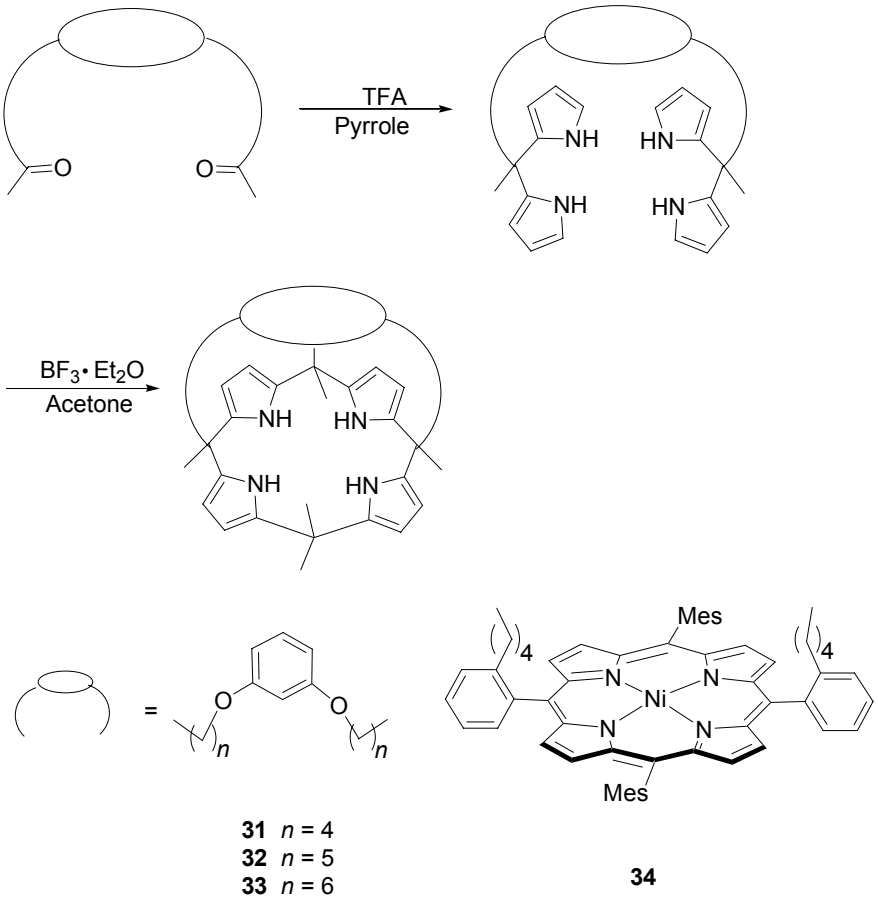

31 *n* = 4
32 *n* = 5
33 *n* = 6

34

Scheme 1.14 General synthesis of strapped calix[4]pyrroles as used to prepare systems **31-34**.

1.8 APPLICATION OF CALIX[4]PYRROLES AND THEIR DERIVATIVES

As easy-to-prepare anion receptors, calix[4]pyrroles have not surprisingly been studied for the ability to effect anion sensing, anion transport, and anion separation. These studies have not only served to flesh out many aspects of calix[4]pyrrole chemistry, but also to highlight their potential utility in various putative practical applications.

1.8.1 Calix[4]pyrrole-based Optical Sensors

Signaling the presence of particular anions either qualitatively or quantitatively through optical means (colorimetric or fluorescent) is a more direct and attractive means of reporting the presence, absence, or specific concentration than through more conventional NMR spectroscopic or ITC titration methods, and thus has considerable appeal as a goal for supramolecular chemists. In an effort to achieve this goal, a variety of known calix[4]pyrrole building blocks were successfully attached to various chromophores or fluorophores. Such an approach has produced several excellent optical anion sensors.

Anion sensors **35-37** were derived from *β*-monosubstituted calix[4]pyrroles, specifically, compounds **16** and **17** (Scheme 1.15).[38] Amide coupling of **16** with 1-aminoanthracene using dicyclohexylcarbodiimide (DCC) and hydroxybenzotriazole (HOBt) in DMF afforded calix[4]pyrrole-anthracene conjugate **35** in 34% yield. Saponification of **17** under basic conditions produced the corresponding acid, which upon coupling with 1-aminoanthrancene and 9-aminomethylanthracene using BOP in DMF afforded conjugates **36** and **37** in 63% and 51% yield, respectively. When these calix[4]pyrrole-anthracene conjugates were titrated with the different anions (studied in the form of their TBA salts), a quenching of the fluorescence was seen; anion binding

event produces electronic changes that are presumably transferred to the anthracene fluorophore through the amide linkage or the amide-alkyl links. Quantitative measures of the fluorescence quenching allowed the affinity constants associated with anion binding to be determined. Among the three conjugates **35-37**, the more closely coupled system **35** proved to be the most sensitive to changes in the anion concentration. Presumably, this reflects both enhanced electronic coupling and an augmentation in the underlying K_a value as the result of the nearby electron withdrawing carbonyl group.

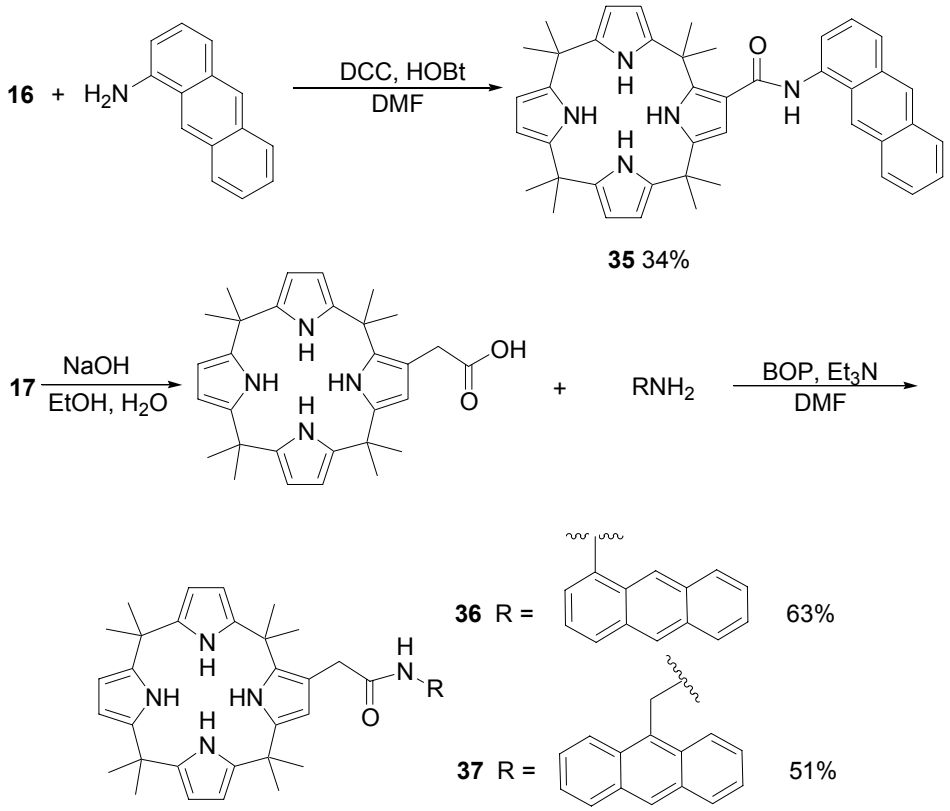

Scheme 1.15 Syntheses of calix[4]pyrrole-based fluorescent anion sensors **35-37**.

The *β*-monoethynyl calix[4]pyrrole **21** represents another calix[4]pyrrole core that was used to prepare sensors in particular conjugates **38-44** (Scheme 1.16).[39] This

approach to optical anion sensor development was considered to be particularly advantageous, not only because of the ease and generality of the synthesis, but also because the π-conjugated acetylene moiety could act as a "molecular wire", thus facilitating efficient "communication", *via* electron (or energy) transfer, between the calix[4]pyrrole anion binding entity and the chromophore-derived reporting subunit. For example, fluorescence measurements showed that **42** was a more sensitive sensor than either **35** or **36** that are predicted on the use of amide or amide-alkyl linkers. In fact, several of these alkyne-linked systems, notably **38**, **39**, **43**, and **44**, were found to act as powerful naked-eye sensors for selected anions in dichloromethane.

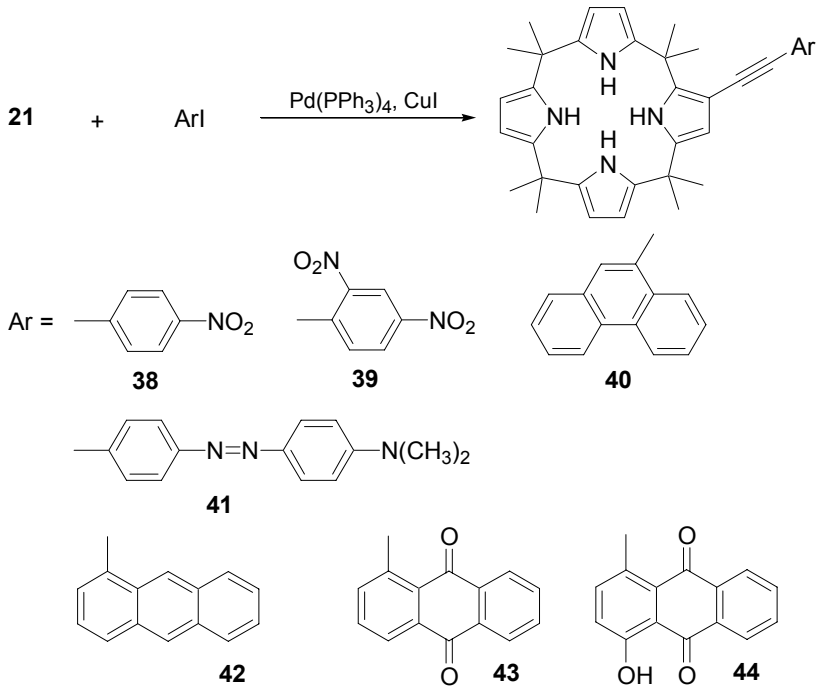

Scheme 1.16 Synthesis of calix[4]pyrrole conjugates **38-44**.

In addition to the sensors noted above, where an optical reporter group is appended to the calix[4]pyrroles at *β*-positions *via* different linkers, a set of so called "second generation" calix[4]pyrrole anion sensors **45-47** were synthesized by attaching a chromophore to the calix[4]pyrrole skeleton at a *meso*- position (Scheme 1.17).[40] These targets were prepared from the mixed condensation of pyrrole, 3-pentanone, and Cbz-protected 3-aminoacetophenone under standard acid-catalyzed conditions. This afforded calix[4]pyrrole **48**, which was deprotected to give the corresponding free amine, which was then reacted with carbonyl chlorides or isothiocyanate to give sensors **45-47** in good yields. The linker moieties present in **45-47** all include ancillary hydrogen bonding donors (either sulfonamides or thiourea), which could provide additional hydrogen bonding interactions with a bound anionic substrate, thus enhancing the overall anion binding affinities. Such cooperative anion binding in turn, was expected to be reflected in efficient fluorescence quenching, making these modified calix[4]pyrroles highly effective anion sensors.

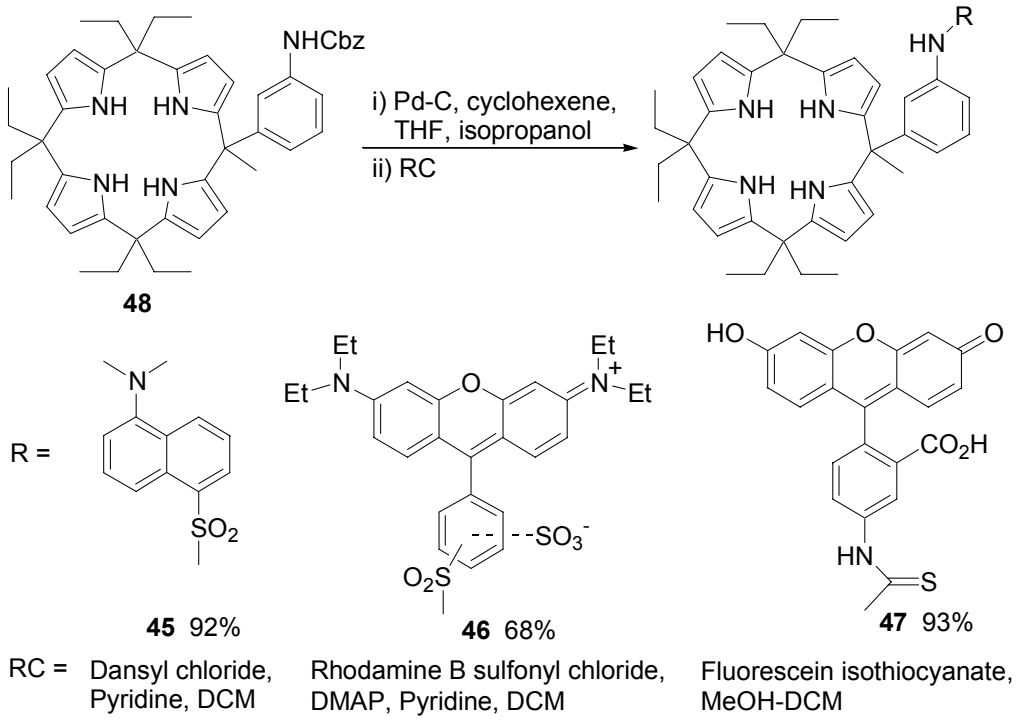

Scheme 1.17 Synthesis of sensors **45-47**.

1.8.2 Calix[4]pyrrole-based Electrochemical Sensors

In an effort to develop an electrochemical anion sensor, a ferrocene moiety was appended to a calix[4]pyrrole. Such a strategy, it was felt, would allow the anion binding event to be monitored *via* a change in the ferrocene/ferrocinium redox potential. As with the optical sensors described above, this was done using both *meso* functionalization and *via* modification of a *β*-pyrrolic position. Thus, compounds **49** and **50** were synthesized based on the calix[4]pyrrole building blocks **16** and **17**,[41] while an alternative system, **51**, was synthesized *via* a mixed condensation involving pyrrole, cyclohexanone, and acetylferrocene.[42] Electrochemical studies showed that for **49** and **50**, the ferrocene/ferrocenium redox couples could be used to sense the presence of anions albeit not in an easily rationalized way. For **51**, cathodic shifts of up to 100 mV (approx.) were

seen upon the addition of excess dihydrogen phosphate in acetonitrile/DMSO (9:1 v/v), as determined using cyclic voltammetric and related voltammetric techniques. NMR spectroscopic titrations in the same solvent system also revealed that one ferrocene CH proton participated in hydrogen bonding interactions with this and other bound anions.

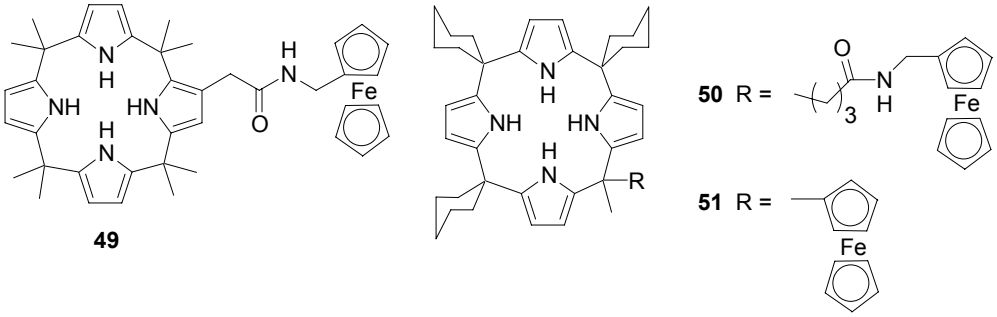

Calix[4]pyrroles were also incorporated into PVC based membranes in an effort to produced ion-selective electrodes (ISEs).[43] Potentiometric studies revealed that at low pH values (between 3.5 and 5.5) the ISEs containing **1** displayed strong anionic responses towards Br^-, Cl^-, and $H_2PO_4^-$, while to a lesser extent, F^-. At high pH values (i.e., 9.0), however, ISEs containing **1** displayed not only cationic responses (positive slope) toward Cl^- and Br^- but also selectivities (i.e., $Br^- < Cl^- < OH^- \approx F^- < HPO_4^{2-}$) that are non-Hofmeister in nature. This phenomenon was then rationalized in that **1** acts as a direct anion binding agents at low pH, but acting, at least in part, as an hydroxide-complexing receptor at higher pH. These results lead to the conclusion that the calixpyrroles and their derivatives could play important roles in the generation of PVC-based ISEs.

1.8.3 Calix[4]pyrrole-based HPLC Supports

Calix[4]pyrrole-modified silica gels could act as new solid-phase HPLC supports. Two such systems, **Gel B** and **Gel M**, not only proved to be effective for the separation

of F^-, Cl^-, Br^-, HSO_4^-, $H_2PO_4^-$, and some Cbz-protected anionic amino acids, but also proved particularly useful in effecting the charge-based separation of nucleotides and oligonucleotides.[44] A mechanism for the HPLC-based separation was proposed as resulting from the weak hydrogen bonding interactions between calix[4]pyrrole moieties and the anionic substrates. These weak interactions, which presumably differ in strength for each anionic substrate in question, lead to selective retention of the anions under conditions of isochratic elution using a competitive solvent system. For instance, HPLC separation of 5'-adenosine monophosphate (AMP), 5'-adenosine diphosphate (ADP), and 5'-adenosine triphosphate (ATP) on **Gel M** revealed that the more highly charged nucleotide is retained longer without the use of ion-pairing agents.

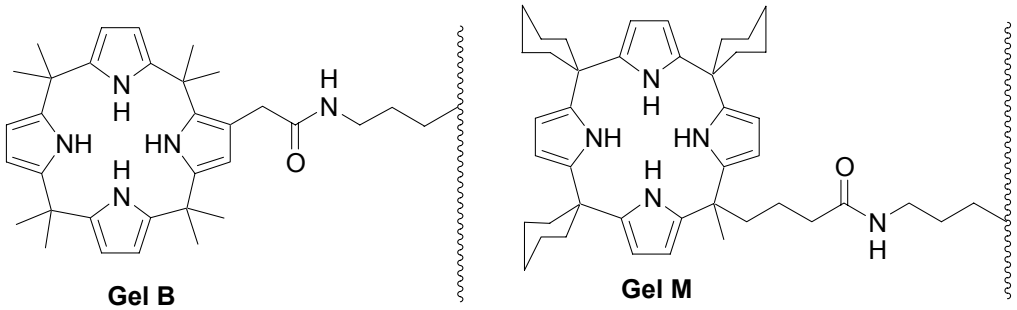

1.8.4 Calix[4]pyrrole-based Anion Transporting Agents

Calix[4]pyrroles have been shown to act as anion carriers capable of transporting anions or anionic substrates through rudimentary model membranes. This transport ability was tested specifically *via* the synthesis of the two cytosine substituted calix[4]pyrroles, **52** and **53**. These systems were synthesized and studied as neutral receptors for 5'-guanosine monophosphate (5'-GMP).[45] Transport studies revealed that good selectivity for 5'-GMP over 5-CMP and 5'-AMP was seen for **52**, which acts as a ditopic receptor by binding both the phosphate "head" of 5'-GMP with the

calix[4]pyrrole core and its purine "center" with cytosine "tail" in a "two point" recognition manner. In these early studies, the "membrane" was a simple aqueous-organic-aqueous Pressman cell. Current work is therefore being devoted to studying these and related anion carriers using more sophisticated membrane models, including liposomes. This work is being carried out by fellow graduate student, Leah Eller.

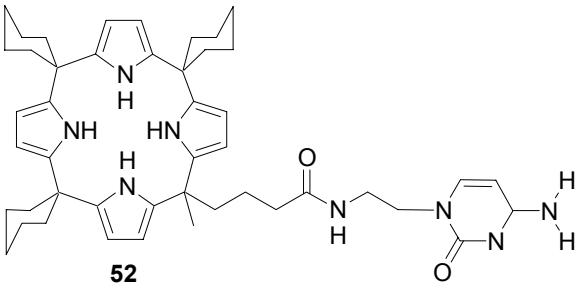

52

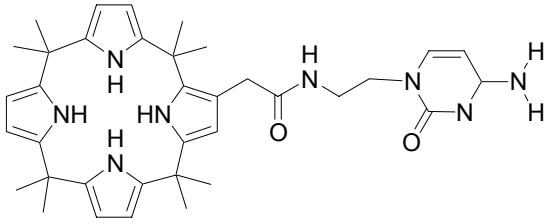

53

1.9 EXPANDED CALIXPYRROLES WITH "LARGER CAVITIES"

As the above discussion should make clear, calix[4]pyrroles show considerable promise as anion receptors. However, due to the small size of their "cavities", calix[4]pyrroles only bind small anions, such as fluoride and chloride, effectively in aprotic solvents. Even in these cases, crystal structures of the resulting anion complexes reveal that the anions sit above the macrocycle planes and not within a well-defined cavity.[14] In addition, the energetic price needed to adopt the cone conformation seen in these complexes could be serving to reduce the overall anion affinities. One way to improve, or at least modulate, the anion binding properties of calix[4]pyrroles would be to "expand" them to produce so called higher order calix[*n*]pyrrole ($n > 4$). Such systems are expected to bind larger anions selectively due to a change in the anion-receptor size or geometry match. However, these higher order structures are likely to prove more flexible than calix[4]pyrroles, which could also affect their anion binding properties.

However, in contrast to calix[4]pyrroles, higher order systems cannot normally be isolated from "one-pot" preparations involving the condensation of pyrrole with acetone. It is now known that this failure reflects the fact that such expanded systems are neither kinetically nor thermodynamically stable under the acid catalyzed reaction conditions. Thus it was only in 1997 that the first calix[*n*]pyrrole was reported. This work, a collaborative effort between the MaKervey and Sessler groups, did not give a free standing calix[*n*]pyrrole. Rather, it produced a calix[5]arene-calix[5]pyrrole conjugate *via* a templated process.[46] Since that time, a number of expanded calixpyrrole or calixpyrrole-like systems have been synthesized and studied in several different laboratories.

1.9.1 Calix[5]pyrrole-Calix[5]arene Conjugate: The First Expanded Calix[*n*]-pyrroles

Although unstable, a peak of low intensity corresponding to normal calix[5]pyrrole was found to be present in the mass spectrum of the reaction mixture obtained from the direct condensation of pyrrole with acetone. However, the corresponding product could never be isolated and it was this observation that spawned efforts to develop a template-bored approach. This led to the preparation of the first expanded calix[5]pyrrole-calix[5]arene pseudo dimer, **54** (Scheme 1.18) as noted above.[46] The actual synthesis of this product was inspired by a prior template-mediated preparation of a calix[4]pyrrole-calix[4]arene pseudo dimer,[47] that was prepared using a calix[4]arene tetraketone. Thus, the calix[5]pyrrole-calix[5]arene **54** was synthesized by reacting calix[5]arene pentaketone with pyrrole in the presence of boron trifluoride diethyl etherate; this afforded **54** in 10% yield.

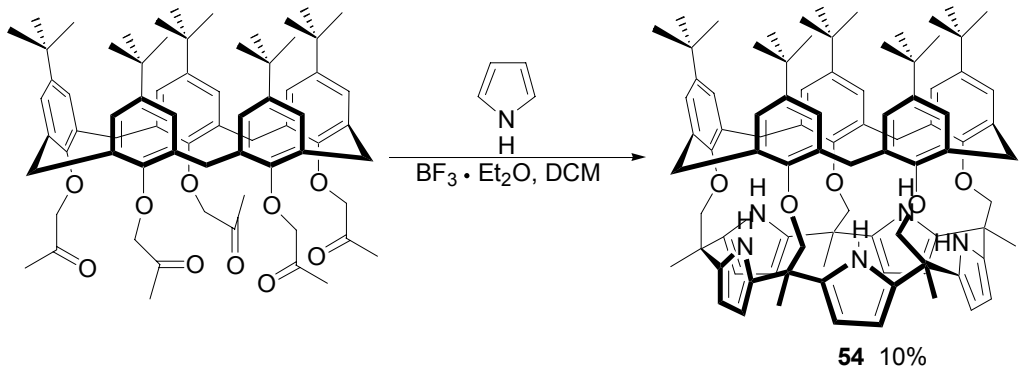

Scheme 1.18 Template synthesis of calix[5]arene-calix[5]pyrrole pseudo dimer **54**.

Preliminary ^{1}H NMR spectroscopic studies revealed that, like the corresponding calix[4]arene-calix[4]pyrrole pseudo dimer, an internal hydrogen bonding array,

involving NH (pyrrolic)-O (phenolic) interactions in **54** served to reduce the ability of this larger system to act as an anion receptor.

1.9.2 Eichen's Syntheses of *Meso*-Hexaarylcalix[6]pyrroles

In what represented an important breakthrough at the time of its publication, Eichen and coworkers reported the synthesis of a series of calix[6]pyrroles. This synthesis is based on the use of the diaryl dipyrromethane building blocks **6** and **7**.[26,48] In particular, reaction of **6** or **7** in a mixture of dry acetone and ethanol (1:1 v/v) in the presence of trifluoroacetic acid gave rise to *meso*-hexaphenylcalix[5]pyrrole **55** and *meso*-hexa(2-pyrridyl)calix[6]pyrrole **56**, respectively (Scheme 1.19).

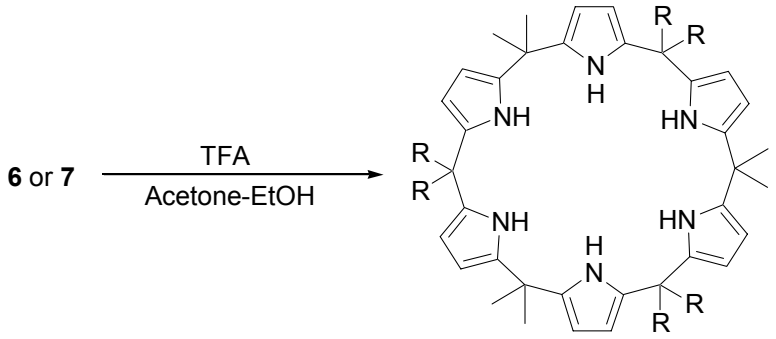

55 R = phenyl, 25%
56 R = 2-pyridyl, 2%

Scheme 1.19 One-pot syntheses of "higher order" calix[6]pyrroles **55** and **56**.

Investigation into the role of the acid catalyst in the synthesis of **55** revealed that, in addition to acting as a catalyst for the reaction, the trihaloacid catalyst plays an independent role as a template, promoting the formation of the calix[6]pyrrole product. A more generalized finding was that trihalogenated comounds, not just the acid, act as effective and selective templates in the template-assisted synthesis of **55**.

NMR-based anion binding studies in acetonitrile-chloroform (1:9) revealed that compared to **1**, **55** binds larger anions such as I^-, BF_4^-, and $CF_3CO_2^-$ quite effectively. By contrast, this expanded system shows relatively reduced affinities for smaller anions, such as F^-, Cl^-, Br^-, and SCN^-. This result is consistent with the general notion that higher affinities are seen when size and geometry of a host and guest are properly matched.[48]

1.9.3 Kohnke's Syntheses of Calix[*n*]pyrroles (*n* = 5, 6)

In a procedure that differs completely from the two methods described above, Kohnke and coworkers introduced a conversion-based method for the syntheses of calix[5]pyrrole **57**[49] and calix[6]pyrrole **58**.[50] In this procedure, readily accessible calix[*n*]furans (*n* = 5, 6) were converted into the corresponding eneketones by oxidative ring-opening of the furan units with *m*-chloroperoxybenzoic acid (MCPBA). After selective reduction of the olefinic double bonds using zinc in acetic acid, a multiketones intermediate was obtained. Treatment of these species, a decaketone and dodecaketone, with excess ammonium acetate in ethanol at reflux, gave **57** and **58** in the yields of 41% and 1%, respectively (Scheme 1.20).

X-ray crystal structures of the 1:1 complexes formed from mixtures of **58** and TBACl and TBABr revealed that the halide ions were encapsulated within the macrocycle cavity *via* six NH-X^- hydrogen bonds. Molecule **58** adopts a cone-like conformation in these anion complexes that is similar to those seen for **1**. However, in the case of **58** the anions are displaced out of the calixpyrrole planes with shorter distances than those in the case of **1**. This is thought to reflect the larger cavity size of macrocycle **58**. Compared to **1**, a stronger interaction with Cl^- was also inferred for **58** relative to **1** as judged from extraction experiments. Unexpectedly, however, a weaker

binding affinity for chloride anion was observed for **57** as compared to **1**; so far, no detailed explanation has been put forward to account for this observation.[49]

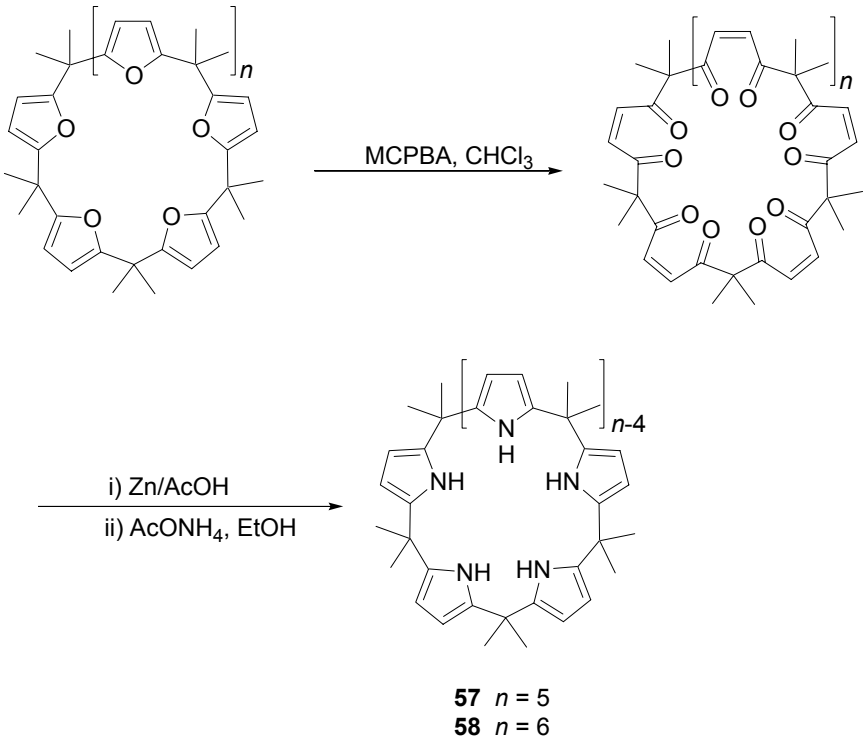

57 *n* = 5
58 *n* = 6

Scheme 1.20 Conversion syntheses of compound **57** and **58**.

1.9.4 Sessler and Marquez's Syntheses of Perfluorinated Calix[*n*]pyrroles (*n* = 5, 6, and 8)

In the course of initial attempts to prepare *β*-octafluorocalix[4]pyrrole **59** *via* a one-pot condensation of 3,4-difluoropyrrole with acetone, two byproducts were seen in the reaction mixture in addition to the desired product. These species, which were produced in isolable quantities, proved to be decafluorocalix[5]pyrrole **60** and hexadecafluorocalix[6]- pyrrole **61**.[51] Under carefully optimized conditions, **60** and **61** could be produced in the yields of 27% and 16%, respectively. On the other hand,

appreciable quantities of dodecafluorocalix[6]pyrrole **62** were only obtained by using a templated approach.[52] Specifically, at reduced temperature (-10 ºC) and in the presence of TBA chloride, the one-pot condensation of 3,4-difluoropyrrole and acetone in methanol in the presence of methanesulfonic acid was found to afford **62** in 20% yield, along with other calixpyrrole products (Scheme 1.21).

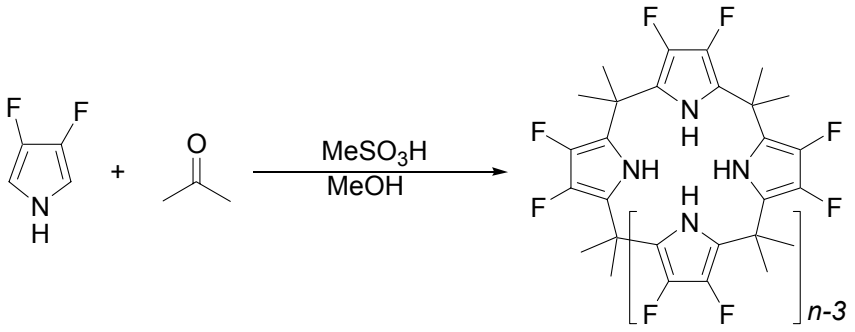

59 *n* = 4
60 *n* = 5
61 *n* = 8
62 *n* = 6

Scheme 1.21 One-pot synthesis of compounds **59-62**.

Single crystal X-ray diffraction structures were obtained in the case of **60** and **61** and provided unequivocal evidence that these products were higher order calixpyrroles. Corresponding solution-phase NMR spectral studies revealed that **60** displays a higher affinity for both the fluoride and chloride anions relative to the corresponding *β*-octafluorocalix[4]pyrrole **59**. Compound **61** was found to have a much weaker affinity for chloride anion; however, it was found to bind the pyrophosphate surprisingly well (affinity of *ca*. 36,000 M^{-1} in acetonitrile-d_3 containing 0.5% v/v D_2O, as judged from standard ^1H NMR spectroscopic titrations).

ITC titration studies carried out in dry acetonitrile revealed that **59** binds chloride anion with an affinity that is higher than those of **60** and **62**. On the other hand, among the three receptors **62** displays the highest bromide affinity.[53] This, once again, is consistent with the notion that effective bindings occur when the sizes and geometries of the host-guest systems are matched.

1.9.5 The First Cryptand-like Calixpyrrole

Cryptand-like calixpyrrole **63** represents another type of rationally designed expanded calixpyrrole. Although not obtained in overly high yield and requiring precursors that are themselves tedious to make, the synthesis of this system is remarkably simple from at least the intellectual perspective: all that is required is the mixing of the diformyl tripyrrane **13b** with its corresponding α-free form **13a** in the presence of an acid catalyst. The resulting condensation produces the cryptant-like calixpyrrole **63** in 15% yield (Scheme 1.22).[28]

X-ray diffraction analysis revealed that the molecule adopts an in-in configuration wherein both *meso*-like bridging carbon atoms are pointing in toward the center of the molecule. The small size of the resulting cavity precludes compound **63** from acting as a so-called *endo* receptor. Still it binds a wide range of anions in CD_2Cl_2 with 1:1 (**63**:F^-), 1:2 (**63**:NO_3^-), and 2:1 (**63**:Cl^-) stoichiometries, as measured by ^1H NMR binding studies. It is thought that in all cases the binding is "calixpyrrole-like" and taking place on the outer surfaces of the cryptand.

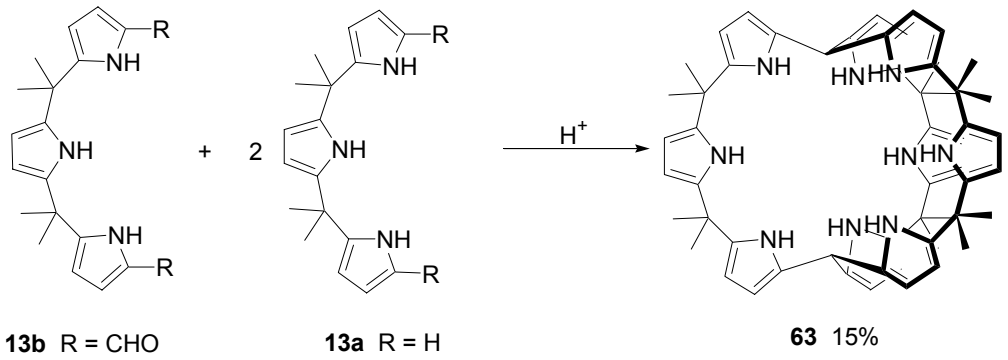

Scheme 1.22 Synthesis of compound **63**.

1.10 RESEARCH PROJECT IN THIS DISSERTATION

The research work summarized in this dissertation actually entails two related but slightly different projects. Accordingly, the presentation that follows will be divided into two parts. The first part will detail continued studies involving calix[4]pyrrole chemistry, while the second part will summarize efforts associated with the design and synthesis of novel calixpyrrole-based anion receptors.

In the first part (Chapter 2), the synthesis of additional *β*-octasubstituted and *β*-monosubstituted calix[4]pyrroles is presented. The systems in question provided platforms that were helpful in detailing how C-rim modification affects the anion binding properties of calix[4]pyrroles.

In the second part, a series of novel calixpyrrole-like systems, with larger cavities than normal calix[4]pyrroles, is described. In contrast to the various calix[*n*]pyrroles summarized in this introductory chapter, these new systems are predicated on the use of building blocks other than pyrrole and modified pyrroles. Specifically, as will be detailed in Chapter 3 to Chapter 5, they are based on the use of larger precursors, such as bipyrrole, furan, thiophene, and 1,3-bispyrrolylbenzene. These novel systems have been studied using both solution-phase anion binding techniques and solid-phase structural methods and their properties have been compared to those of the parent system, calix[4]pyrrole **1**.

The candidate benefits extensively from a collaboration with postdoctoral fellow, Hidekazu Miyaji, in pursuing the first project. Dr. Miyaji was responsible for most of the binding studies, whereas almost all the synthetic work was that of the candidate alone. The second project was almost entirely the result of the candidate's own efforts, especially as regard the design and synthesis. Assistance from fellow Sessler group member, Mr. Won-Seob Cho in making some of the early anion binding measurements

and double checking the later ones carried out by the candidate, is gratefully acknowledged. Thanks is also due to Dr. Vincent Lynch for carrying out the X-diffraction analyses reported in this dissertation. All single crystals used for these analyses were grown by the candidate.

Chapter 2: *β*-Halogenated Calix[4]pyrroles: Fine-tuning the Anion Binding Properties of Calix[4]pyrrole

2.1 INTRODUCTION

As introduced in Chapter 1, the anion binding properties of calix[4]pyrroles can be changed through such modifications as adding specific *meso*-substituents, forming cavities *via* single side strapping, or through the introduction of ancillary anion binding sites. In addition to these methods, C-rim modification remains one of the more attractive means for improving the anion binding properties of normal calix[4]pyrroles. It has thus been a point of interest to explore the range and scope of "adjustment" in affinities this approach permits.

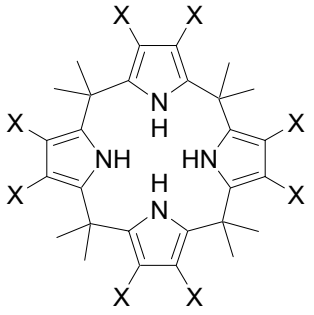

15 X = Br

59 X = F

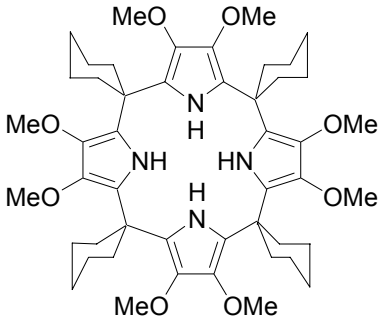

64

In the context of work providing new easy-to-make anion binding agents, two *β*-octasubstituted calix[4]pyrroles, **15** and **64**, were first reported in 1997 by Gale et al.,[29] while *β*-octafluorocalix[4]pyrrole **59** was later reported by Anzenbacher, Jr. et al. in 2000.[54] Interestingly, anion binding studies revealed that **15** and **59** show enhanced affinities for various anions of interest relative to normal calix[4]pyrrole **1**, while **64**

shows decreased affinities relative to **3**. This phenomenon was attributed to an electronic effect arising from the substituent groups at the *β*-pyrrolic positions. These effects, in particular, are thought to increase the acidity of the pyrrole NH protons thus increasing their hydrogen binding donor ability.

2.2 RESEARCH GOAL

Although the effect of three different kinds of *β*-pyrrolic substituents, namely methoxy, bromo and fluoro, had been previously reported in the case of the octa-substituted systems, it was thought likely that more detailed insights could be obtained by further exploring this area *via* synthesis and anion studies of both *β*-octahalogenated and *β*-monohalogenated calix[4]pyrroles. The systems bearing 2-7 halogen atoms at *β*-pyrrolic positions, however, are not included in this study due to difficulties associated with their synthesis and separation.

In the context of this work, we sought to complete more fully the series of *β*-octahalogenated calix[4]pyrroles through the synthesis of *β*-octachlorocalix[4]pyrrole. We also wanted to prepare and study calix[4]pyrrole systems bearing only a single substituent but characterized by different electronegativities (i.e. I, Br, Cl and F). The replacement of a *β*-pyrrolic proton by a halogen atom is potentially beneficial because it might allow the effect of substituents on the anion binding properties of calix[4]pyrroles to be studied in greater detail. Also, this generalized approach is advantageous because these *β*-monohalogenated calix[4]pyrroles could be useful synthetic intermediates for a range of functionalized calix[4]pyrroles, as discussed briefly in Chapter 1.

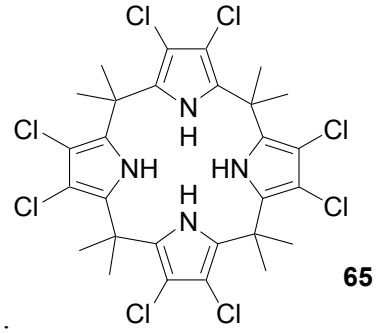

65

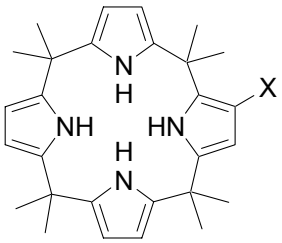

66 X = F

67 X = Cl

68 X = Br

18 X = I

2.3 *β*-OCTACHLOROCALIX[4]PYRROLE

2.3.1 Synthesis

So far two synthetic methods have been developed that allow for the synthesis of *β*-octasubstituted calix[4]pyrroles. As introduced in Chapter 1, *β*-octabromo-calix[4]pyrrole **15** was synthesized using post-macrocycle functionalization method *via* bromination of calix[4]pyrrole **1** with NBS reagent in THF.[29] This generalized approach is advantageous because calix[4]pyrrole **1** is simple-to-make starting material that is easy to scale up. Thus the key to this approach is finding convenient reagents that allow facile replacement of the *β*-pyrrolic protons. On the other hand, there are advantages to the direct one-step synthesis approach.

Both *β*-octamethoxycalix[4]pyrrole **64**[29] and *β*-octafluorocalix[4]pyrrole **59**[54] were synthesized using the one-pot homo-condensation method. Specifically, **64** was synthesized by reacting 3,4-dimethoxypyrrole and acetone in acetic acid, while **59** was synthesized by stirring 3,4-difluoropyrrole and acetone in methanol in the presence of methanesulfonic acid for 5 days. In the case of **59**, a longer than normal reaction time proved necessary, a finding that presumably reflects the poor reactivity of 3,4-difluoropyrrole due to the electron withdrawing effect of the two fluorine groups at the *β*-pyrrolic positions. Unfortunately, while straightforward, this chemistry is somewhat limited because the starting material, the appropriate 3,4-disubstituted pyrrole, must be synthesized separately and sometimes *via* tedious multistep syntheses.

In the case of the octachloro target **65**, the post-macrocycle functionalization method was tried first. Here, N-chlorosuccinimide (NCS), a venerable chlorinating reagent, was used in attempt to perchlorinate **1**. This reagent has been used to chlorinate porphyrin compounds and in this case it proved possible to replace off eight *β*-pyrrolic protons by eight chlorine atoms.[55] However, applying the same reaction conditions, i.e.

heating calix[4]pyrrole **1** and eight equivalents of NCS at reflux in THF while irradiating with UV light, failed to give the desired compound. Rather, decomposition products were obtained (Scheme 2.1).

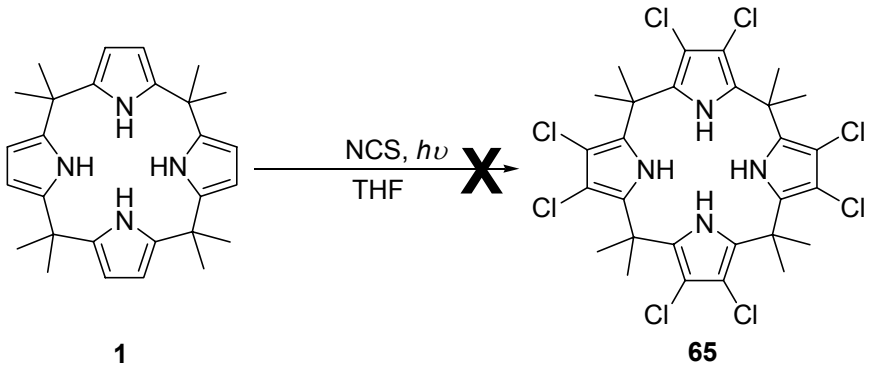

1 **65**

Scheme 2.1 Failed synthesis of **65** from **1**.

Considering that the reaction conditions may be too harsh for either **1**, or the product **65**, or both, milder conditions were adopted in which the reaction mixture was stirred at room temperature either with or without irradiation. However, in neither case was the target compound obtained and, again, only a mixture of uncharacterized products was produced as inferred from TLC and mass spectrometric analysis. Taking into account that NCS is relatively mild compared to other known chlorinating reagents such as chlorine and sulfuryl chloride, no further attempts at direct post-synthetic chlorination were attempted for the synthesis of **65**.

Given this lack of success, efforts were then devoted to preparing **65** from 3,4-dichloropyrrole **69**, *via* the one-pot condensation approach. 3,4-Dichloropyrrole **69**, the requisite staring material, was synthesized in three steps from commercially available ethyl acetylacetate and acetylacetaldehyde dimethyl acetal according to the literature procedure summarized in Scheme 2.2.[56]

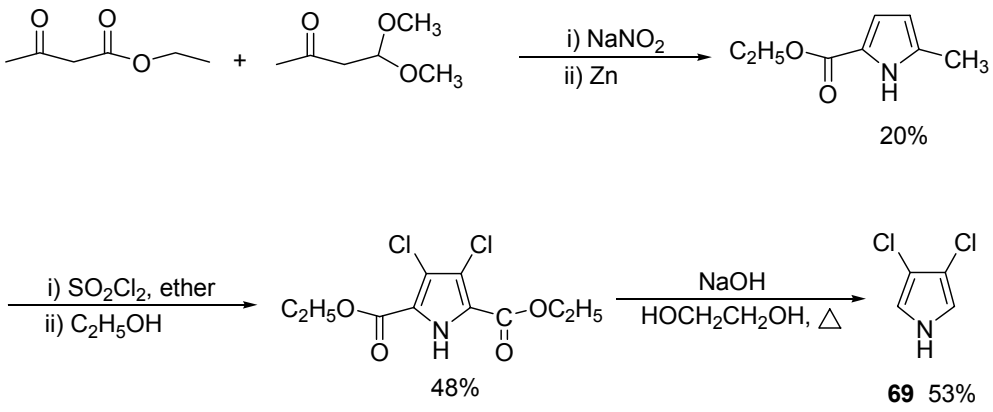

Scheme 2.2 Synthesis of 3,4-dichloropyrrole **69**.[56]

Unfortunately, and in contrast to what proved true for the synthesis of **59**, attempts to synthesize **65** by condensing **69** with acetone under normal reaction condition (i.e. stirring in methanol in the presence of methanesulfonic acid) failed to produce appreciable quantities of product even after prolonged reaction times (several days). This was deemed a surprising result since compared to 3,4-difluoropyrrole, **69** should theoretically be more reactive due to the weaker electron withdrawing effects from the chlorine substituents. However, it could be that this enhanced electronic benefit is offset by unfavorable steric effects. While this latter hypothesis remains to be tested *via* additional experimentation, the key point from a synthetic perspective is that condensation of **69** and acetone in dichloromethane in the presence of boron trifluoride diethyl etherate was found to afford **65** in 56% yield.

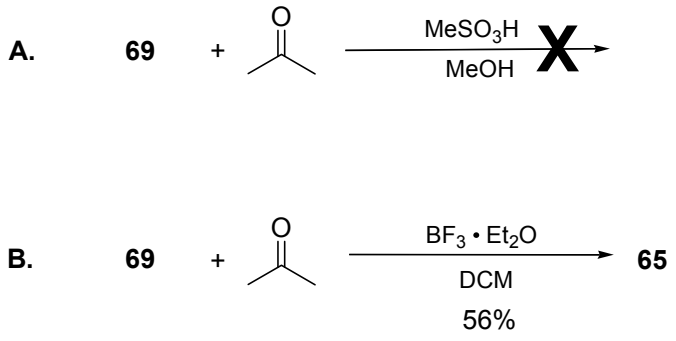

Scheme 2.3 Synthesis of **65** from 3,4-dichloropyrrole **69**.

Inspired by the fact that higher order calix[*n*]pyrroles (*n* = 5, 6, and 8) are formed together with calix[4]pyrrole from 3,4-difluoropyrrole under the conditions of the one-pot homo-condensation, we looked for analogous species in the case of the 3,4-dichloropyrrole. However, under the reaction conditions of Scheme 2.3B, ones involving modifications in either reagent concentrations or reaction temperature, no higher order *β*-chlorinated calix[*n*]pyrrole (n > 4) systems could be separated from the reaction mixture. In fact, none were actually detected *via* MS analysis. This failure is consistent with the notion, invoked for other fluorine-free higher order calixpyrroles, that any higher order species formed under the acidic reaction conditions simply reequillibrate "back" to the parent calix[4]pyrrole product. Presumably, the electron withdrawing effect from the *β*-pyrrolic chlorine is simply not strong enough to decrease this reequilibration process *via* a raising of the transition state energy leading to the first carbocation intermediate that would be produced upon breaking up of a calix[*n*]pyrrole (*n* > 4) core..

2.3.2 Charaterization

Compound **65** was characterized by standard spectroscopic techniques including ^{1}H NMR, ^{13}C NMR, and HR-MS. It was also characterized by X-ray diffraction analysis (Figure 2.1).

Diffraction-grade crystals of *β*-octachlorocalix[4]pyrrole **65** were grown by slow evaporation of a dichloromethane solution of **65** in an atmosphere saturated with hexanes vapor. X-ray crystal analysis revealed that the molecule adopts a 1,3-alternate conformation in the solid state. This system thus exists in a conformation similar to that seen in the solid-state structures of **1** and **59** but different from the flattened 1,2-alternate conformation found in the case of **15**. However, in contrast to what is observed for **59**, there are no intermolecular hydrogen bonding interactions in the crystal structure of **65**. Again, this presumably reflects the weaker electronegativity of chlorine compared to fluorine. Figure 2.2 shows the unit cell packing diagram of **65**.

a)

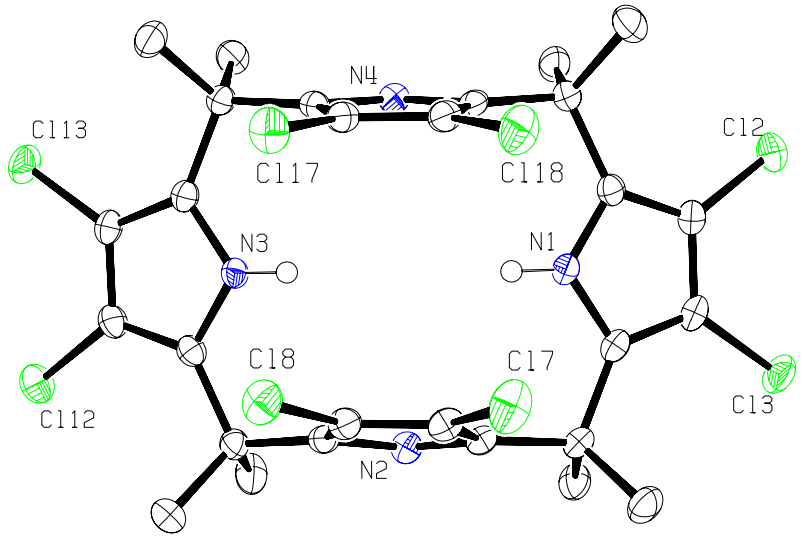

b)

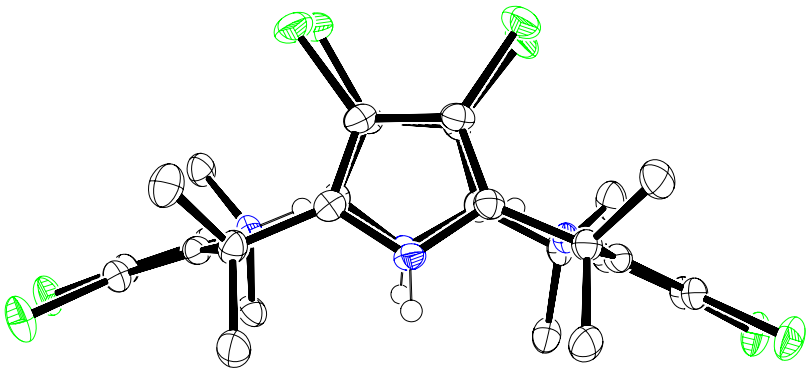

Figure 2.1 Ortep view of molecule structure of **65** as determined by X-ray diffraction analysis. a) Top view; b) side view. Thermal ellipsoids are scaled to the 50% probability level. The molecule adopts a 1,3-alternate conformation in the solid state.

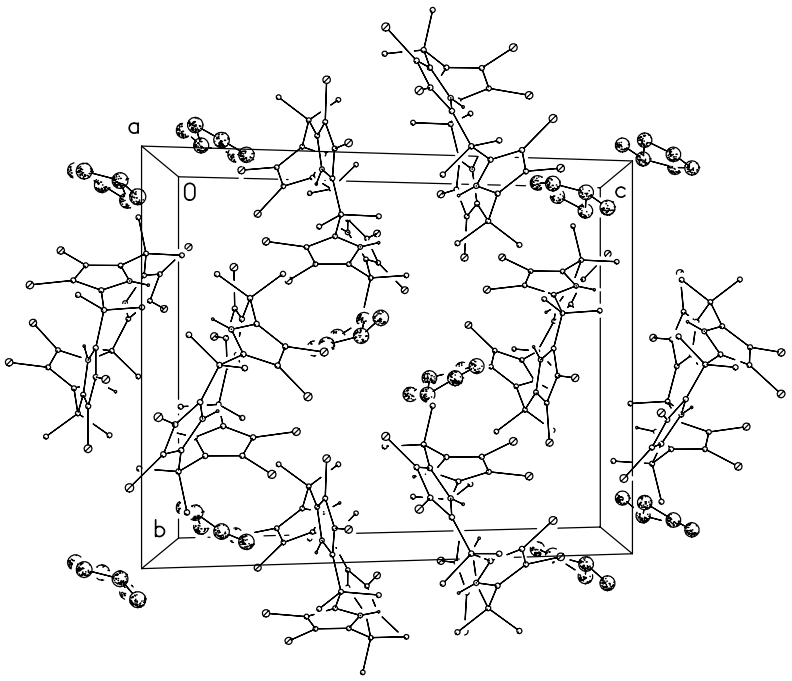

Figure 2.2 Schematic representation of the unit cell packing diagram of **65** as seen in the solid state.

2.3.3 Anion Binding Studies

Anion binding studies of compound **65** were made using ^{1}H NMR spectroscopic titrations carried out in dichloromethane-d_2. Data analysis and stability constant determinations were made using the Wilcox non-linear method (Appendix A) for fitting the binding profiles to a 1:1 calixpyrrole-anion solution complex model (Table 2.1). Table 2.1 also includes the stability constant for compounds **1**, **3**, **15**, **59**, and **64** with anions from either published or unpublished sources for comparison.

Table 2.1 Stability constants for compounds **1**, **3**, **15**, **59, 64,** and **65** with anionic substrates in CD_2Cl_2 at 298 K.

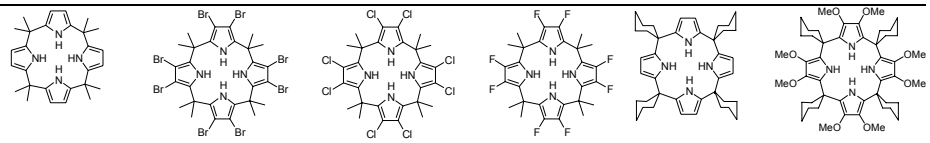

	1[a]	**15**[b]	**65**	**59**[c]	**3**[a]	**64**[b]
F^-	>10,000	>10,000	>10,000	>10,000	3,600	170
Cl^-	350	4,300	5,300	>10,000	117	<10
$H_2PO_4^-$	97	650	1,100	>10,000	<10	-

[a] From ref. 14. [b] From ref. 29. [c] Unpublished results.

Table 2.1 clearly showed that the electron donating groups at *β*-pyrrolic positions decrease the anion affinities of the basic calix[4]pyrrole core, as can be easily seen by comparing the affinity constants for compound **64** with those of **3**. By contrast, electron withdrawing groups enhance the anion affinities of the calix[4]pyrrole skeleton, as becomes readily apparent by comparison of the K_a data for **15**, **59**, **65**, and **1**. However, these *β*-pyrrolic substituents would only change the anion affinity strength of the corresponding macrocycles, while not likely modulate their anion selectivities. This is reasonable because these simple substituents would not change the geometries and cavity sizes of the parent calix[4]pyrrole core.

Looking carefully at compound **65**, we see that it does display enhanced anion affinities relative to **1** for the anions of interest at least with the factors enhancement falling between those of **15** and **65**. This in turn is in accord with the electronegativities of the halogen substituents in question. In fact, very good linear correlation exists between the chloride anion affinities and the electronegativities of *β*-pyrrolic substitution

groups for the compounds **1**, **15**, and **65** (Figure 2.3). The equation used for making this correlation is:

$$K_a = 4647 \times N - 9416 \qquad \text{Equation } \mathbf{2.1}$$

where A represents anion affinity (M^{-1}); N represents Pauling's electronegativity; 4647 and 9416 represent constants.

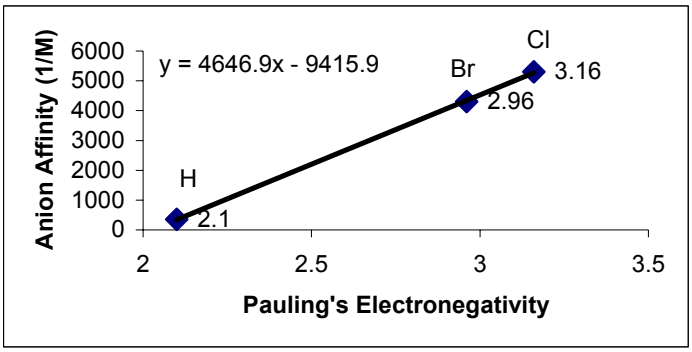

Figure 2.3 Correlation between the chloride anion affinities of calix[4] and electronegativities of the *β*-pyrrolic halogen elements.

2.4 *β*-MONOHALOGENATED CALIX[4]PYRROLES

2.4.1 Synthesis and Characterization

Theoretically, mono-halogen substituted calix[4]pyrroles could be synthesized from either of the two methods used for the syntheses of octahalogen-substituted calix[4]pyrroles. However, considering the difficulty in controlling the product distribution obtained from one-pot mixed condensations, the post macrocycle functionalization method was considered a more attractive approach to the syntheses of such target systems (Scheme 2.4).

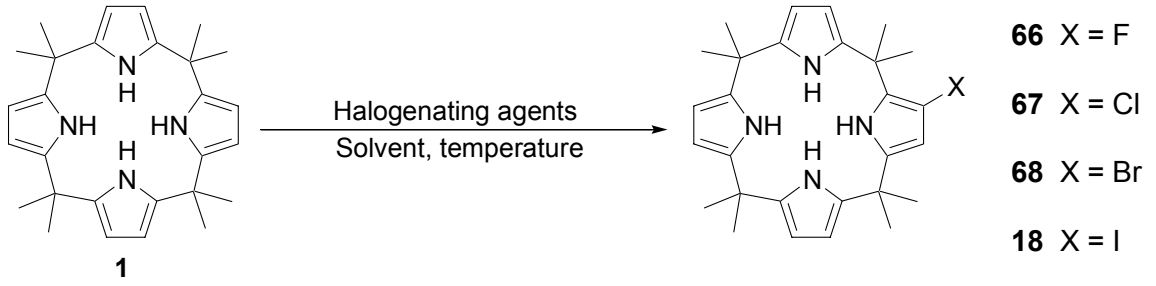

Scheme 2.4 Proposed synthesis of **66-68** and **18** from **1** using post-macrocycle functionalization methods.

Table 2.2 shows the reaction conditions used for the syntheses of compounds **66-68** and **18**.[57] The monofluorocalix[4]pyrrole **66** was synthesized in 15% yield by reacting calix[4]pyrrole **1** with 1.2 equiv. of N-fluoropyridinium triflate in THF at 60 ˚C. The monochlorocalix[4]pyrrole **67** was synthesized in 33% yield by reacting **1** with 1.5 equiv. of NCS reagent in THF at 60 ˚C. Similarly, the monobromocalix[4]pyrrole **68** was synthesized in 21% yield by treating calix[4]pyrrole **1** with 1.2 equiv. of NBS in THF at 60 ˚C. The synthesis of monoiodocalix[4]pyrrole **18**[30] was mentioned in Chapter 1. In the context of the present study it was actually synthesized in a different way.

Specifically, it was obtained in 20% yield by treating *meso*-octamethylcalix[4]pyrrole **1** with I_2 and $PhI(CF_3CO_2)_2$ in CH_2Cl_2 at ambient temperature.

As a general rule multi-halogen substituted calix[4]pyrrole products were seen in all cases, as inferred from TLC and mass spectrometric analyses of the reaction mixture. However, no attempts were made to isolate these products due to perceived difficulties in effecting their separation.

Table 2.2 Reaction conditions used for the syntheses of **66-68** and **18**.

Reactant	Halogenating agents	Solvents	Temperature (˚C)	Products (Yields %)
	$(Py\text{-}F)^+ \cdot CF_3SO_3^-$	THF	60	**66** (15)
1	NCS	THF	60	**67** (33)
	NBS	THF	60	**68** (21)
	$PhI(CF_3CO_2^-)_2$	CH_2Cl_2	25	**18** (20)

2.4.2 Characterization

Compounds **66-68** and **18** were characterized using standard spectroscopic techniques including ^{1}H NMR and ^{13}C NMR spectroscopy and HR-MS. They were additionally characterized by elemental analysis. With the exception of the mono-fluoro derivative **66** that showed evidence for intermolecular aggregation under certain conditions, all compounds gave data that were in accord with their proposed structures. Furthermore, in the case of **66**, weak ^{19}F-^{1}H splittings (J = 3.3 Hz) were also observed for the CH_{py} signals. Such splittings were not seen in the case of **67**, **68,** and **18**.

2.4.3 Anion Binding Studies

The solution-phase anion binding properties of calix[4]pyrroles **18, 66-68** were studied using ^{1}H NMR titration methods. As expected, the addition of anions caused the pyrrole NH resonances to shift to lower field (Figure 2.4). The actual extent of this downfield shift, however, was found to be a function of anion concentration, receptor, and choice of anion. This point is illustrated in Figure 2.4, which shows the chemical shifts of the pyrrole NH protons of compounds **18, 66-68** observed upon the addition of up to 4 equiv. of tetrabutylammonium chloride (TBACl).

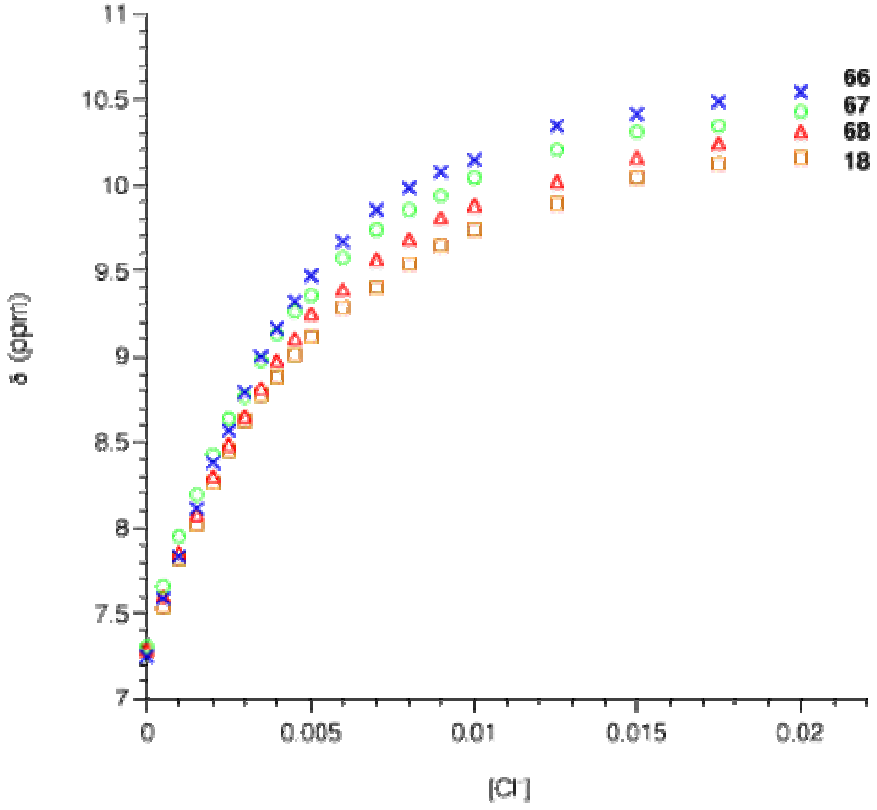

Figure 2.4 ^{1}H NMR titration curves of the mono halogen calix[4]pyrroles **66-68** and **18** (5 mmol) in CD_2Cl_2 observed upon treatment with TBACl.

Table 2.3 Anion binding constants for compounds **1**, **18**, **66-68** as deduced from ^{1}H NMR spectroscopic titrations carried out in CD_2Cl_2 at 298 K.[a]

Anions	K_a (M^{-1})				
	1	**18**	**68**	**67**	**66**
F^-	>10,000[b]	>10,000	> 10,000	>10,000	>10,000
Cl^-	350[b]	610	650	780	870
Br^-	10[b]	49	53	80	62
I-	<10[b]	<5	<5	<5	<5
$H_2PO_4^-$	97[b]	100	180	230	130
HSO_4^-	<10[b]	<5	6	13	<5

[a] Anions were added as their tetrabutylammonium salts; estimated errors were <10%.

[b] Data from ref. 14.

Table 2.3 lists the anion binding constants for compounds **18** and **66-68** as deduced from ^{1}H NMR spectroscopic titrations carried out in CD_2Cl_2 at 298K. The K_a values tabulated in Table 2.3 confirm that, in analogy to what is true for *β*-octahalogenated calix[4]pyrroles, the mono-halogen substituted calix[4]pyrroles **18**, **66-68** bind anions more strongly than does the parent system **1**. As expected, the monofluorocalix[4]pyrrole **66** displays the highest affinity for chloride anion. However, it is actually the mono-chlorocalix[4]pyrrole **67** that binds bromide, dihydrogen phosphate and hydrogen sulfate anions most strongly, and not the monofluoro derivative **66**. These findings lead to the consideration that factors other than just substituent electronegativity effects could be controlling the anion properties of receptor **66**. Based on the intermolecular NH-F interactions observed in the solid state of octafluorocalix[4]pyrrole **59**, the lower than expected anion affinities seen in the case of

66 are thought to reflect a competition between intermolecular NH-F hydrogen bonding interactions and NH-A^- anion binding events (A^- = F^-, Cl^-, Br^-, I^-) as illustrated schematically in Figure 2.5.

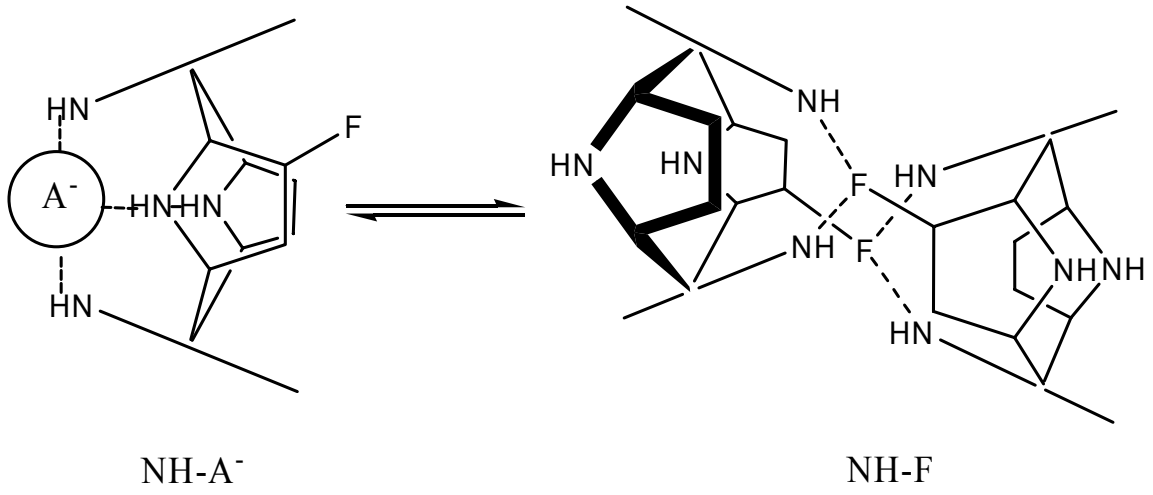

Figure 2.5 Proposed competition between intermolecular NH-F hydrogen bonding interactions and NH-A^- anion binding.

While not a proof, the above explanation would also help provide a rationale for the fact that in contrast to what was seen in the case of *β*-octahalogenated calix[4]pyrroles, no correlation between the anion affinities and *β*-halogen electronegativities was found to exist in the case of the *β*-monohalogenated calix[4]pyrroles.

2.4.4 Concentration and Temperature-dependent NMR Spectroscopic Studies of 66

In order to provide additional evidence for the presence of the proposed intermoleculer NH-F hydrogen bonding interactions in the case of **66**, concentration dependent ^{1}H NMR spectroscopic studies were carried out in CD_2Cl_2 solution (Figure 2.6). In particular, the ^{1}H NMR spectral changes for the four NH protons of **66** were observed as its concentration was varied between 2.5 mM and 50 mM,. At high concentrations the NH peaks shifted to slightly lower fields. While not a complete proof of the proposed aggregation, these observations are consistent with the proposed formation of intermolecular dimers, or possibly other higher order species at greater concentrations.

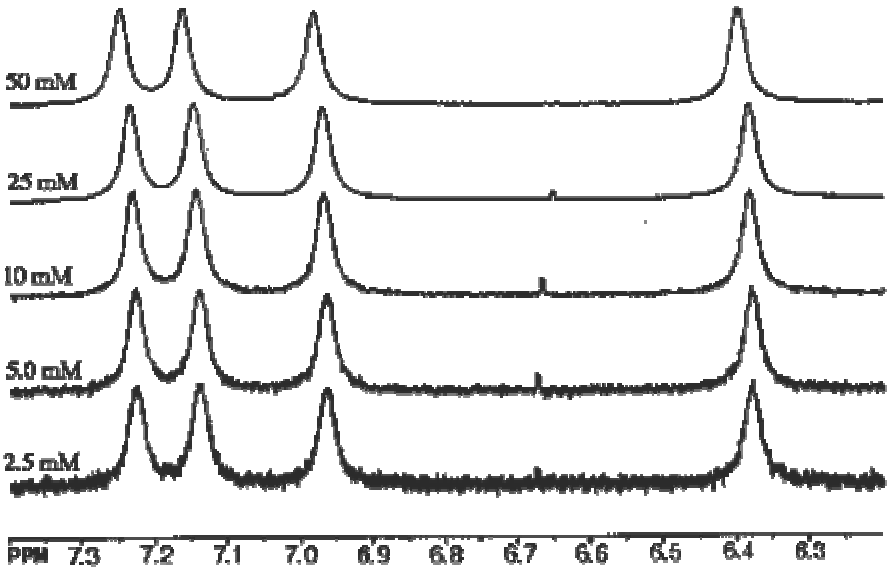

Figure 2.6 A set of analogous ^{1}H NMR spectra showing the concentration dependent shifts observed for the four NH proton signals of mono-fluorocalix[4]pyrrole **66** in CD_2Cl_2 at 298 K.

Compound **66** was further studied by carrying out a temperature dependent ^{1}H NMR analysis (Figure 2.7). It was observed that the four NH peaks observed for **66** in CD_2Cl_2 (50 mM), appearing at 7.25, 7.16, 6.98, and 6.40 ppm at 25˚C, are shifted to 7.39, 7.31, 7.08, and 6.53 ppm, respectively, when the spetrum is recorded at -40 ˚C. Cooling to -60 ˚C caused the two peaks resonating at 7.39 and 7.31 ppm at -40 ˚C to shift even further downfield to 7.41 and 7.32 ppm, respectively. However, the two peaks appearing at 7.08 and 6.53 ppm at -40 ˚C were found to be shifted "upfield" to 7.04 and 6.50 ppm. A ^{19}F NMR spectral analysis of **66** also revealed that the ^{19}F peak observed for a 50 mM solution of **66** in CD_2Cl_2, appearing at -165.18 ppm at 0 ˚C, is shifted to –165.12 ppm, –165.04 ppm, -164.95 ppm, and -164.83 ppm, at -20 ˚C, -40 ˚C, -60 ˚C, and -80 ˚C, respectively.

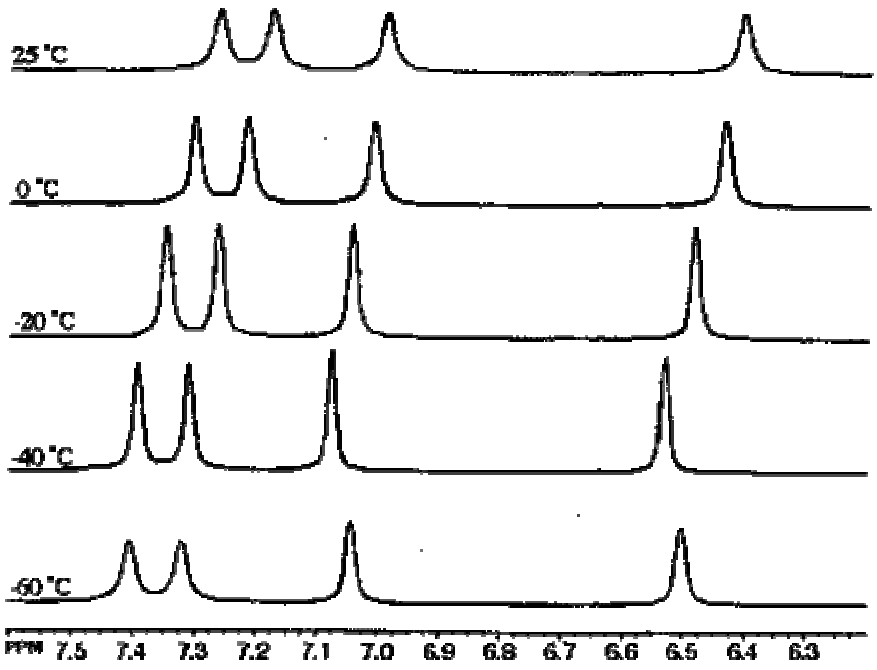

Fig. 2.7 A set of ^{1}H NMR spectra showing the changes in the signals for the four NH protons of monofluorocalix[4]pyrrole **66** in CD_2Cl_2 (50mM) observed as a function of temperature.

The downfield shifts of the NH and ^{19}F NMR peaks of **66** observed at high concentration and low temperature are consistent with the proposed intermolecular NH-F hydrogen bonding interactions. Both high concentration and low temperature are expected to increase this intermolecular association, a proven, that in turn, should lead to a downfield shift in the δ values. Such shifts are what are seen by experiment true for the ^{19}F signals and for all of the NH signals down to at least -40 ˚C. However, at even lower temperature (<-40 ˚C), two of the NH proton resonances shift upfield. This latter, unexpected observation, could reflect a "freezing out" of the more stable 1,3-alternate conformation from amongst the mixture of rapidly equilibrating cone, partial cone, 1,2-alternate and 1,3-alternate conformers that exist in the absence of a strongly bound substrate. The key point is that at low temperature, the 1,3-alternate dimeric form of **66** is expected to dominate among different conformations. In this proposed dimeric form, two of the four NH protons on each monomeric subunit are expected to interact with fluorine atoms and therefore produce NMR signals that are shifted to lower field. By contrast, the other two pyrrole NH protons are expected to experience ring current effects as the result of adjacent pyrroles and thus be subject to an influence that shifts the corresponding signals to higher field. This point is illustrated in Figure 2.8, which shows an idealized representation of the proposed 1,3-alternate dimeric form of **66**.

a)

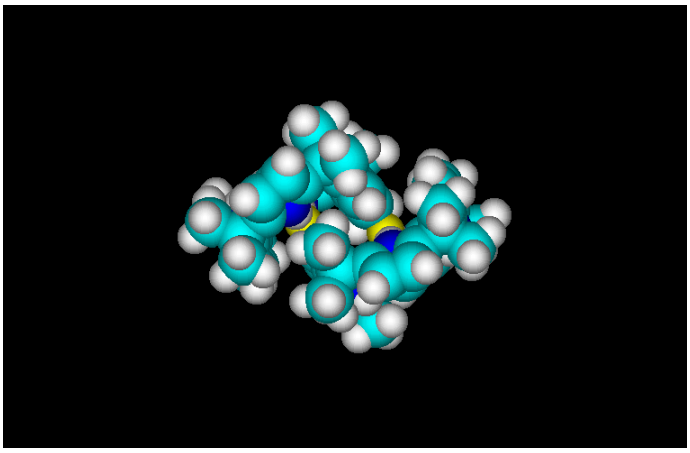

b)

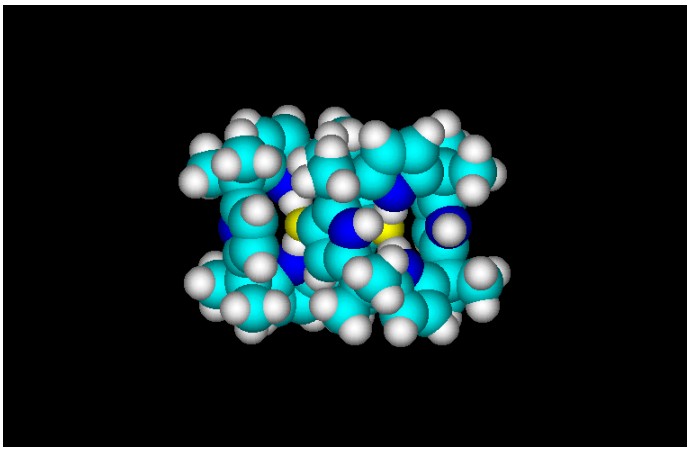

Figure 2.8 Schematic representation of the 1,3-alternate dimer of **66**. a) Top view; b) side view.

2.5 CONCLUSION

In conclusion, *β*-octachlorocalix[4]pyrrole **65** was successfully synthesized using the one-pot homo-condensation method. Anion binding studies revealed that in analogy to what was observed in the case of the *β*-octabromocalix[4]pyrrole **15** and the *β*-octafluorocalix[4]pyrrole **59**, the chlorinated system **65** displays enhanced anion affinities relative to **1** with the extent of the enhancement lying between that seen for **15** and **59**. In the specific case of chloride anion binding, the stability constants of compounds **1**, **15**, and **65** were found to correlate linearly with the electronegativities of the *β*-pyrrolic. Such a correlation was taken as support for the notion that the *β*-pyrrolic substituents have a clear effect on the anion affinities of calix[4]pyrroles. Such C-rim modifications have little effect, however, on the inherent anion selectivities.

A series of mono-halogen atom substituted calix[4]pyrroles, namely compounds **18, 66**-**68**, were also synthesized and, as above, their anion binding characteristics were studied. In the case of chloride anion binding, an affinity sequence of **66** > **67** > **68** > **18** > **1** was observed. This is in accord with the electronegativity sequence of F > Cl > Br > I > H. However, in the case of other anions, specifically bromide, dihydrogen phosphate, and hydrogen sulfate anions, it was the monochlorocalix[4]pyrrole **67**, not monofluoro derivative **66**, that displays the highest affinity. These disparate results in the case of **66** are rationalized in terms of the combined, albeit competing, effects of intermolecular NH-F and NH-anion hydrogen bonding interactions. Such complexities notwithstanding, the present results serve to underscore in very clear fashion how halogenation of the *β*-pyrrolic positions may be used to fine-tune the anion binding properties of calix[4]pyrroles.

Chapter 3: Calix[*n*]bipyrroles: Synthesis, Characterization, and Anion Binding Studies

3.1 INTRODUCTION

As versatile building blocks, bipyrroles have been extensively applied for the syntheses of many expanded porphyrins, among which rosarins[58] and their higher order homologues[59] are good representatives.

These macrocycles are of interest as possible design analogues of novel calixpyrroles because they were all synthesized using simple, albeit effective one-pot condensation procedures. For example, rosarins are easily synthesized in 70% yield from the acid-catalyzed condensation of a bipyrrole with an aldehyde. By controlling carefully both the reaction conditions and the structure of the reactants, not only rosarins but also their higher order homologues can be obtained in a single step using an analogous one-pot procedure. The thought was thus that this methodology, with appropriate modifications, might be applicable to the synthesis of calixpyrroles.

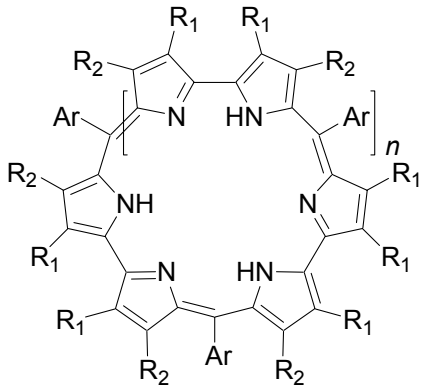

Rosarins and higher order homologues

n = 1; R_1 = Me, R_2 = Et; Ar = Ph.
n = 1, 2; R_1 = R_2 = Et; Ar = Ph.
n = 1, 2, 4, 6; R_1 = R_2 = Et; Ar = 2,6-dichlorophenyl.

3.2 RESEARCH GOAL

As far as we were aware, bipyrroles had not yet been used as building blocks for the synthesis of calixpyrrole systems at the outset of this research. We thus sought to use this moiety to produce a series of bipyrrole-based calixpyrrole systems, namely, calix[*n*]bipyrroles ($n \geq 3$). Specifically, the thought was various calix[*n*]bipyrroles could be synthesized *via* the one-pot condensation of a bipyrrole and a ketone in the presence of an acid catalyst (Scheme 3.1).

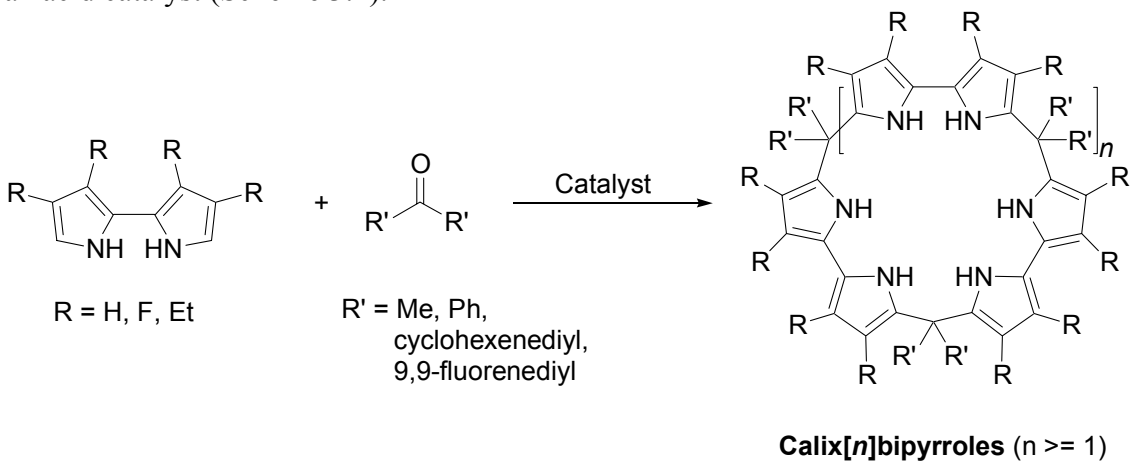

Scheme 3.1 Proposed synthesis of calix[*n*]bipyrroles *via* a one-pot condensation procedure.

From a synthetic perspective the chemistry of Scheme 3.1 is attractive. This is because bipyrroles represent readily available precursors in the Sessler group. Furthermore, bipyrroles represent larger building blocks than normal pyrroles, and thus the proposed calixpyrrole analogues, once prepared, should have larger cavity sizes and different anion binding properties than both the calix[4]pyrroles and their higher order calix[*n*]pyrrole homologues.

3.3 SYNTHESIS

3.3.1 Synthesis of Calix[3]bipyrrole 70 and Calix[4]bipyrrole 71

Calix[3]bipyrrole **70** and calix[4]bipyrrole **71** were synthesized using the one-pot condensation shown in Scheme 3.2.[60] The requisite bipyrrole, **72**, was synthesized in two steps from pyrrole and 2-pyrrolidinone according to a literature procedure.[61] Once this precursor was in hand, it was condensed with acetone in methanol in the presence of methanesulfonic acid. A set of optimized reaction conditions that involved stirring the reaction mixture at ambient temperature for 2 h, followed by quenching with saturated aqueous sodium bicarbonate, was derived. After purification by column chromatography (silica gel; dichloromethane eluent for **70**, followed by dichloromethane/ethyl acetate 98:2 v/v, eluent for **71**), this procedure yielded targets compounds **70** and **71** in yields of 24% and 29%, respectively.

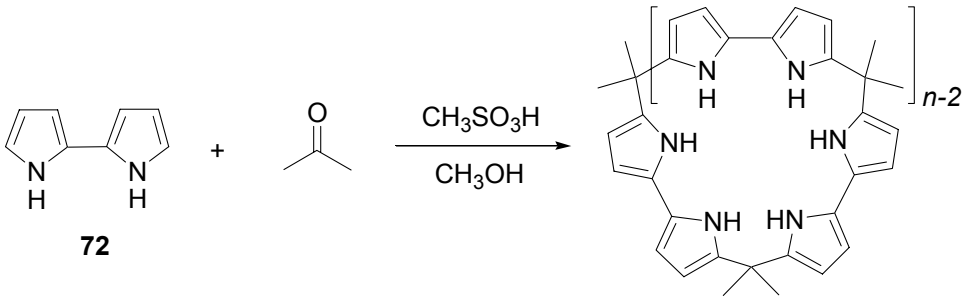

70 *n* = 3

71 *n* = 4

Scheme 3.2 Synthesis of calix[3]bipyrrole **70** and calix[4]bipyrrole **71**.

Both calix[3]bipyrrole **70** and calix[4]bipyrrole **71** are pale green solids. Compound **70** is so unstable that it could only be stored under Ar at low temperature for one week. In contrast, and most interestingly, compound **71** proved so much more stable

than **70** that it could be stored under analogous conditions for several months without decomposition. The difference in relative stability between these two compounds, we think, could reflect steric effects. The triangular structure of **70** and its inherent rigidity might contribute to a high degree of structural tension that could destabilize the molecule. Such steric effects should be far less pronounced in the case of the more flexible, square-like system, **71**.

The condensation of bipyrrole **72** with acetone under other reaction conditions was also attempted in an attempt to produce calix[*n*]bipyrroles. Most of these attempts proved unsuccessful. For example, reaction either in dichloromethane in the presence of boron trifluoride diethyl etherate, or in acetonitrile in the presence of trifluoroacetic acid, gave rise to what appeared to be a very slow reaction and afforded calix[*n*]pyrroles in only low yields. This result can be rationalized by noting that as a nucleophile, bipyrrole **72** is less reactive than normal pyrrole due to the electron withdrawing effect of the appended pyrrole subunit attached to whichever pyrrolic entity is involved in the reaction.

3.3.2 Attempted Syntheses of *β*-Substituted Calix[*n*]bipyrroles

Consistent with various failed attempts to produce *β*-substituted calix[4]pyrroles, efforts to synthesize calix[*n*]bipyrroles bearing *β*-substituents proved unsuccessfully. For example, the attempted condensation between 3,3',4,4'-tetrafluoro-2,2'-bipyrrole **73**[62] and 3,3',4,4'-tetraethyl-2,2'-bipyrrole **74** with acetone under the optimized reaction used to prepare **70** and **71** (Scheme 3.3), failed to give isolable quantities of product, even after prolonged reaction time. In the case of bipyrrole **73**, the electron withdrawing effects from the four fluorine substituents might attribute to the low nucleophilicity of bipyrrole unit. As to bipyrrole **74**, which should be more nucleophilic due to the electron donating

effects from the four ethyl substituents, we attribute this lack of success to steric effects resulting from the interaction between the acetone-derived incipient *meso*-methyl groups and the β-alkyl substituents present on the bipyrrole. Such effects would serve to inhibit both the various condensation steps and the final cyclization process.

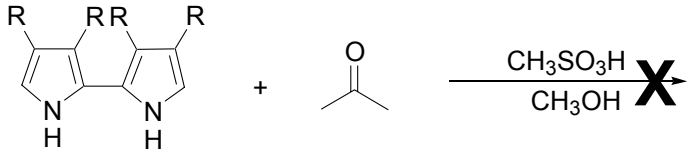

73 R = F
74 R = Et

Scheme 3.3 Summary of unsuccessful attempts made in an effort to synthesize calix[*n*]bipyrroles from bipyrrole **73** and **74**.

3.3.3 Synthesis of *Meso*-Substituted Calix[*n*]bipyrroles

The reaction of 2,2'-bipyrrole **72** with ketones other than acetone were also explored in an effort to prepare calix[*n*]bipyrroles bearing substituents other than methyl groups at the *meso*- positions (Scheme 3.4). Attempted syntheses included condensing bipyrrole **72** with cyclohexanone, benzophenone, and 9-fluorenone under the same reaction condition as used for synthesis of **70** and **71**.

In the case of cyclohexanone, such a reaction afforded the calix[3]bipyrrole **75** in 14% yield (Scheme 3.4). By contrast, only trace quantities of the corresponding calix[4]bipyrrole were produced as judge from mass spectrometric analysis. This putative trace product was not isolated (Scheme 3.4).

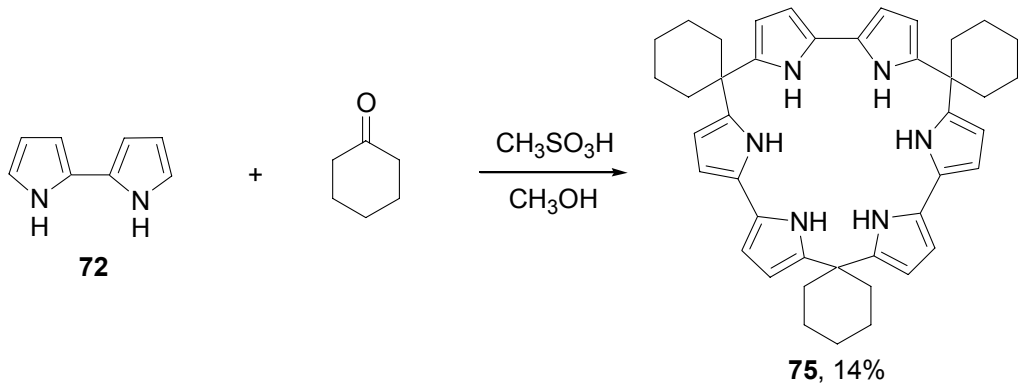

Scheme 3.4 Synthesis of calix[3]bipyrrole **75** from bipyrrole **72** and cyclohexanone.

Interestingly, benzophenone and 9-fluorenone were found to react with **72** differently, in spite of the fact that they are both aryl ketones. In the case of benzophenone, no cyclized products were produced, and the condensation reaction appeared to stop right after the first step. In particular, one bipyrrole and one benzophenone were found to react to give an intermediate, which after purification *via* column chromatography (silica gel, dichloromethane/methanol 97:3 v/v, eluent) afforded **76** as a red solid in 48% yield (Scheme 3.5). The formation of this product stands in contrast to what is seen in the case of the corresponding condensation reaction involving pyrrole. Here, the diphenyl dipyrromethane intermediate is produced, but again no further reaction takes place.[26] In analogy to this is latter observation, attempts to react **76** with bipyrrole in the presence of acid catalyst proved unproductive. This shows that this intermediate is quite stable under the reaction conditions.

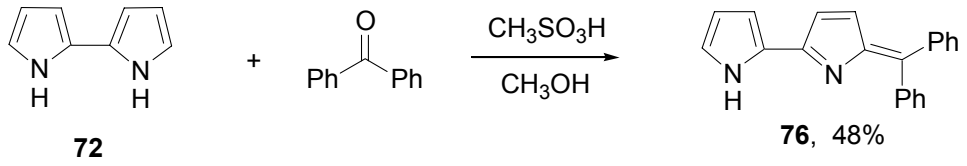

Scheme 3.5 Reaction of bipyrrole **72** with benzophenone to afford compound **76**.

In the case of 9-fluorenone, reaction with bipyrrole was found to afford the corresponding calix[3]- and calix[4]bipyrroles **77** and **78** in 7% and 17% yields, respectively. Both compounds are dark red solids but, unfortunately, proved unstable even at low temperature and under Ar. At the present time it is not clear why this cyclization proceeded so well, while the corresponding reaction involving benzophenone stopped right after the first condensation step. It is also not understood at present why 9-fluorenone reacts with bipyrrole in a way that is so different from the way it reacts with pyrrole; in the latter case, only a 9,9-fluorenediyl-bridged dipyrromethane is produced.[26] One reasonable explanation, we think, might involve steric effects. In the case of 9-fluorenone, more planar structures are produced. By contrast, the use of benzophenone would produce, however, the bulky phenyl groups that might serve to preclude any further condensation process. On the other hand, bipyrrole is a larger and more flexible building block than pyrrole, which might help to reduce any incipient steric hindrance effects during the various condensation reactions summarized above.

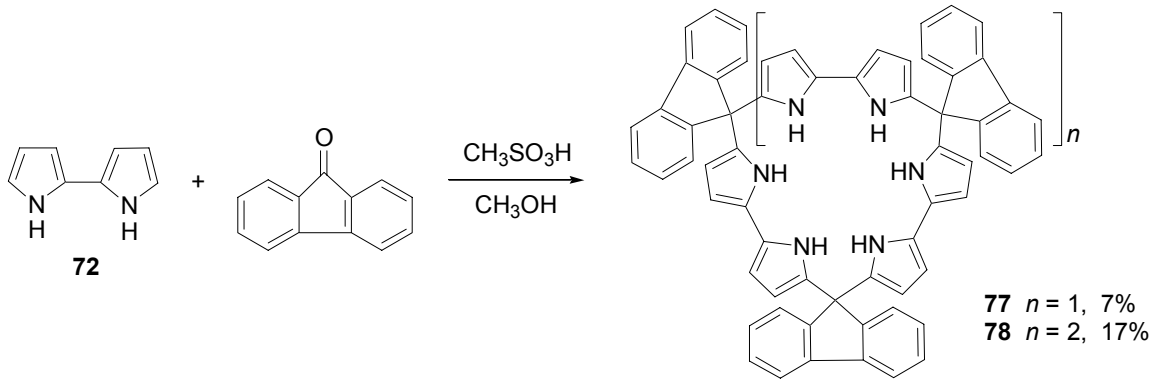

Scheme 3.6 Synthesis of calix[3]bipyrrole **77** and calix[4]bipyrrole **78** from bipyrrole **72** and 9-fluorenone.

In summary, calix[*n*]bipyrroles free of β-pyrrolic substituents can be synthesized in good yield *via* the acid catalyzed condensation of α,β-unsubstituted bipyrrole with different ketones. So far attempts to synthesize the corresponding β-substituted calix[*n*]bipyrroles have proved unsuccessful.

3.4 CHARACTERIZATION

All products were characterized by standard spectroscopic techniques including ^{1}H NMR, ^{13}C NMR, and HR-MS. Calix[4]bipyrrole **71** was also characterized using X-ray diffraction analysis. In the case of the calix[3]bipyrrole **70**, attempts to obtain diffraction grade crystals in the absence of an anion proved unsuccessful. However, crystals of the chloride anion complex of **70** were obtained, and the detailed X-ray analysis will be introduced later.

Diffraction-grade crystals of calix[4]bipyrrole **71** were grown from a tetrahydrofuran solution of the macrocycle layered with water on the bottom and methanol on the top. The ensuing X-ray structural analysis revealed that the molecule adopts a 1,3-alternate conformation in the solid state, with adjacent bipyrrole units oriented in opposite directions and each bipyrrole unit bonded to a tetrahydrofuran molecule through two NH (pyrrole)-O (THF) hydrogen bonds (Figure 3.1). The nitrogen-to-oxygen distances are 2.8874(17) Å and 2.8877(18) Å, respectively; the nitrogen-hydrogen-oxygen angles are 168.4(16)º and 169.2(16)º, respectively. The two bipyrrole units at opposite positions are almost parallel to each other, while the plane of each bipyrrole unit is perpendicular to the plane of the tetrahydrofuran molecule to which it is bound *via* hydrogen bonds. As a result, the whole molecule displays a square-like shape, showing a grid-like packing mode in the unit cell packing diagram (Figure 3.2).

a)

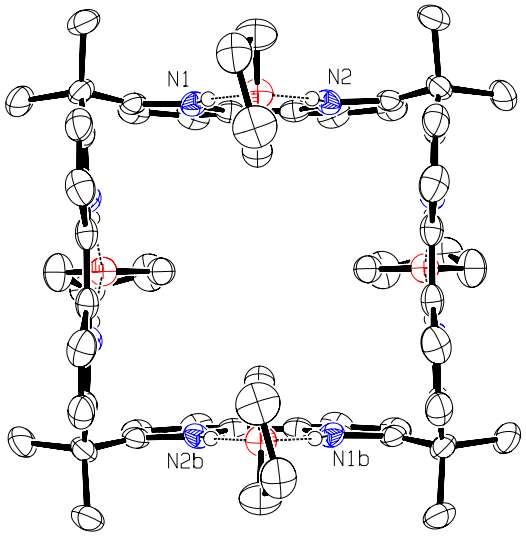

b)

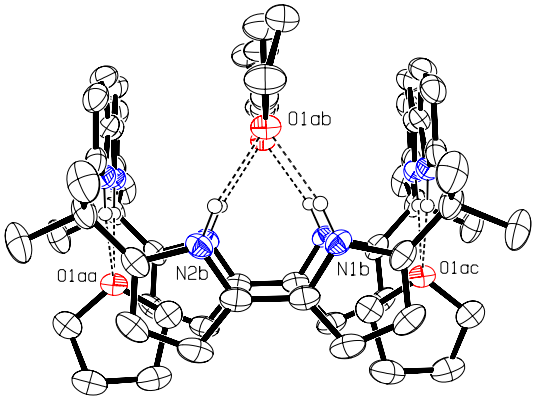

Figure 3.1 Ortep view of the molecular structure of **71**·4THF. a) Top view; b) side view. Thermal ellipsoids are scaled to the 30% probability level. Most hydrogen atoms have been removed for clarity. Dashed lines are indicative of NH---O hydrogen bonding interactions.

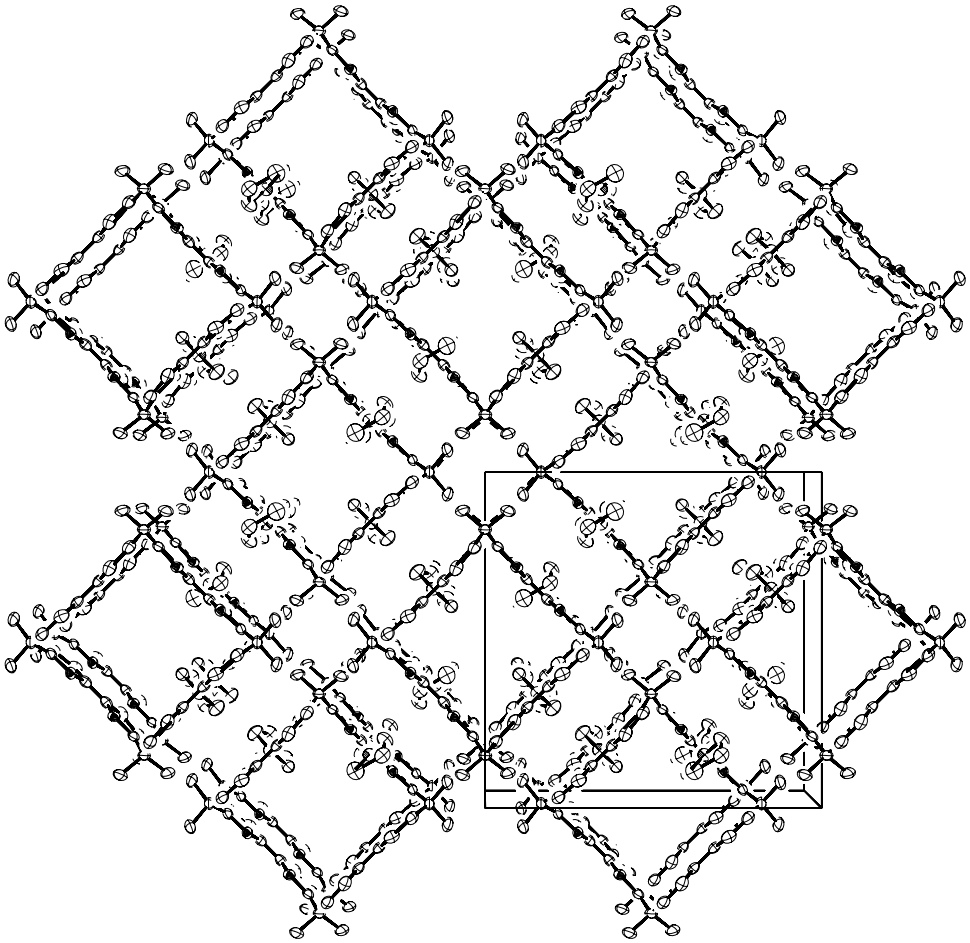

Figure 3.2 Unit cell packing diagram for **71**·4THF. The view is down the **c**-axis.

3.5 ANION BINDING STUDIES

The anion binding properties of calix[3]bipyrrole **70** and calix[4]bipyrrole **71** were studied using X-ray diffraction analysis in the solid state and using ^{1}H NMR spectroscopic titration and isothermal titration calorimetry (ITC) methods in organic solution.

3.5.1 Calix[3]bipyrrole 70

Diffraction-grade crystals of a chloride anion complex of **70** were obtained by slow evaporation of a dichloromethane solution of **70** containing an excess of tetrabutylammonium chloride. X-ray diffraction-based structural analysis revealed that the calix[3]bipyrrole core adopts a cone-like conformation, with the six pyrrolic NH protons involved in hydrogen bonding interactions with a bound chloride anion (Figure 3.3). The nitrogen-to-chloride distances are in the range of 3.338(7)-3.382(8) Å; the hydrogen-to-chloride distances are in the range of 2.46-2.59 Å; and the nitrogen-hydrogen-chloride angles are in the range of 147.5º-175.5º.

The cone-like conformation seen in the chloride complex of **70** resembles that of the chloride complex of **1**,[14] differing mainly in the numbers of hydrogen bonds observed between the pyrrolic macrocycles and the bound chloride anions. The greater number of such interactions seen in the case of [**70**·Cl]$^{-}$ was later found to be prognostic of a solution-state chloride anion affinity.

a)

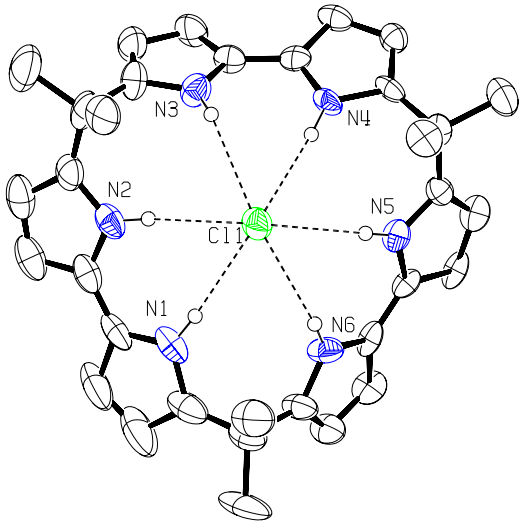

b)

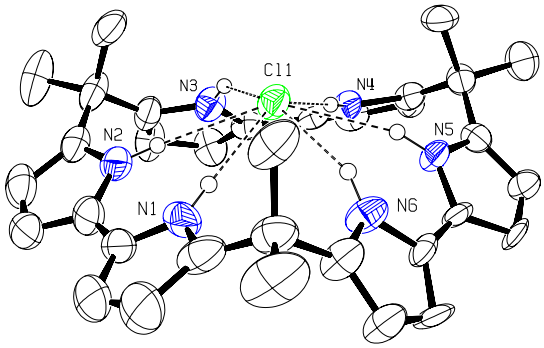

Figure 3.3 Ortep view of the molecular structure of [**70**·Cl]$^-$. a) Top view; b) side view. Displacement ellipsoids are scaled to the 50% probability level. Most hydrogen atoms have been removed for clarity. Dashed lines are indicative of N-H---Cl$^-$ hydrogen bonding interactions.

In the solid state structure of [**70**·Cl]$^-$, the chloride anion resides 1.189(5) Å above the N_6 root-mean-square plane of the calix[3]bipyrrole core. This out-of-plane distance is shorter than 2.319(3) Å seen in the case of [**1**·Cl]$^-$. Presumably, this difference simply reveales the very reasonable expectation that the cavity that can be formed by

calix[3]bipyrrole **70** is larger than the one that can be formed by calix[4]pyrrole **1**. While not established by these solid-state analyses, the expectation was that the larger core structure present in **70**, compared to **1**, would be reflected in relative higher affinities towards larger anions.

Initial solution-phase anion binding studies were carrying out *via* standard ^{1}H NMR spectroscopic titrations in acetonitrile-d_3. These analyses revealed that calix[3]bipyrrole **70** behaves as a strong anion receptor for halide anions (Cl^-, Br^- and I^-) in acetonitrile. For instance, after the addition of ca. 0.1 equiv. of chloride anion (as its tetrabutylammonium salt) to a ca. 2 mM solution of calix[3]bipyrrole **70** in acetonitrile-d_3, the pyrrole N*H* peak, originally present at 8.52 ppm, was seen to split into two distinct peaks, one at 8.52 ppm corresponding to the free calix[3]bipyrrole, and one at 10.29 ppm corresponding to the calix[3]pyrrole bound with chloride anion ([**70**·Cl]$^-$). Further additions of chloride anion caused the intensity of the peak at 8.52 ppm to decrease along with a concurrent increase in the size of the peak at 10.29 ppm. Such changes are considered to reflect a simultaneous decrease in the amount of free **70** and an increase in the chloride anion complex [**70**·Cl]$^-$. After the addition of ca. 0.7 equiv., the peak at 8.52 ppm could no longer be observed and only the peak at 10.29 ppm could be seen in the N*H* spectral region. Further anion additions did not induce any further observable changes, either in the N*H* region, or in the spectrum as a whole (Figure 3.4). Similar observations were seen in the case of ^{1}H NMR titrations of **70** with bromide anion (Figure 3.5).

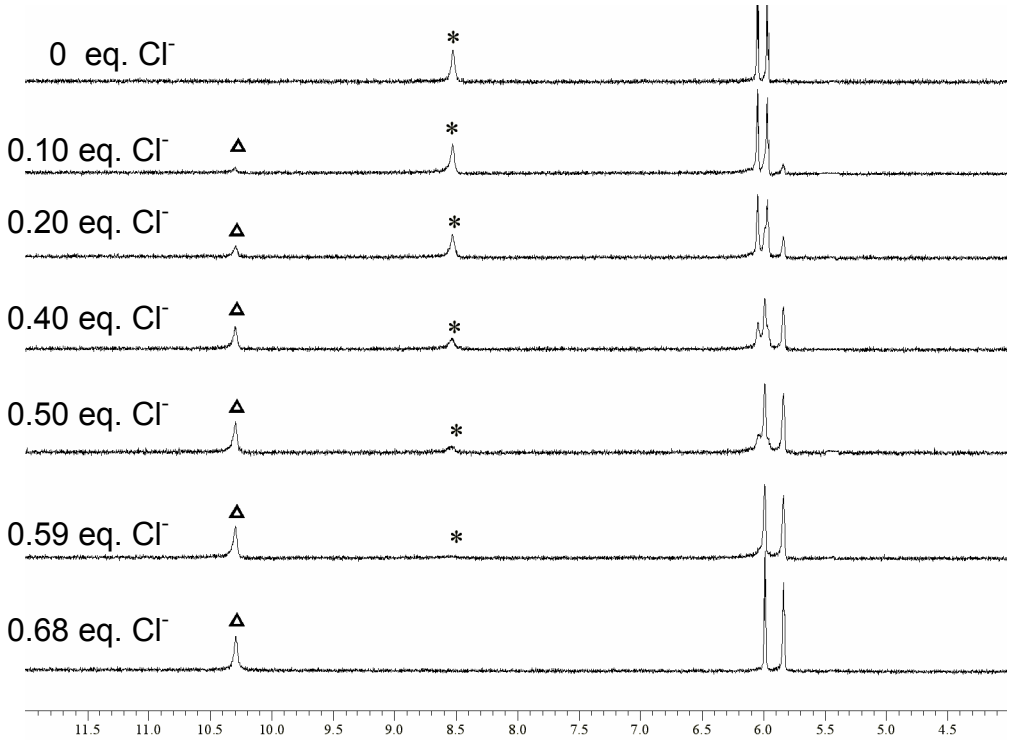

Figure 3.4 ^{1}H NMR titration of calix[3]bipyrrole **70** (2×10^{-3} mol/L) with TBACl in CD_3CN (*: chemical shift of the NH protons of the free ligand; Δ: chemical shift of the NH protons of the ligand bound with chloride anion)

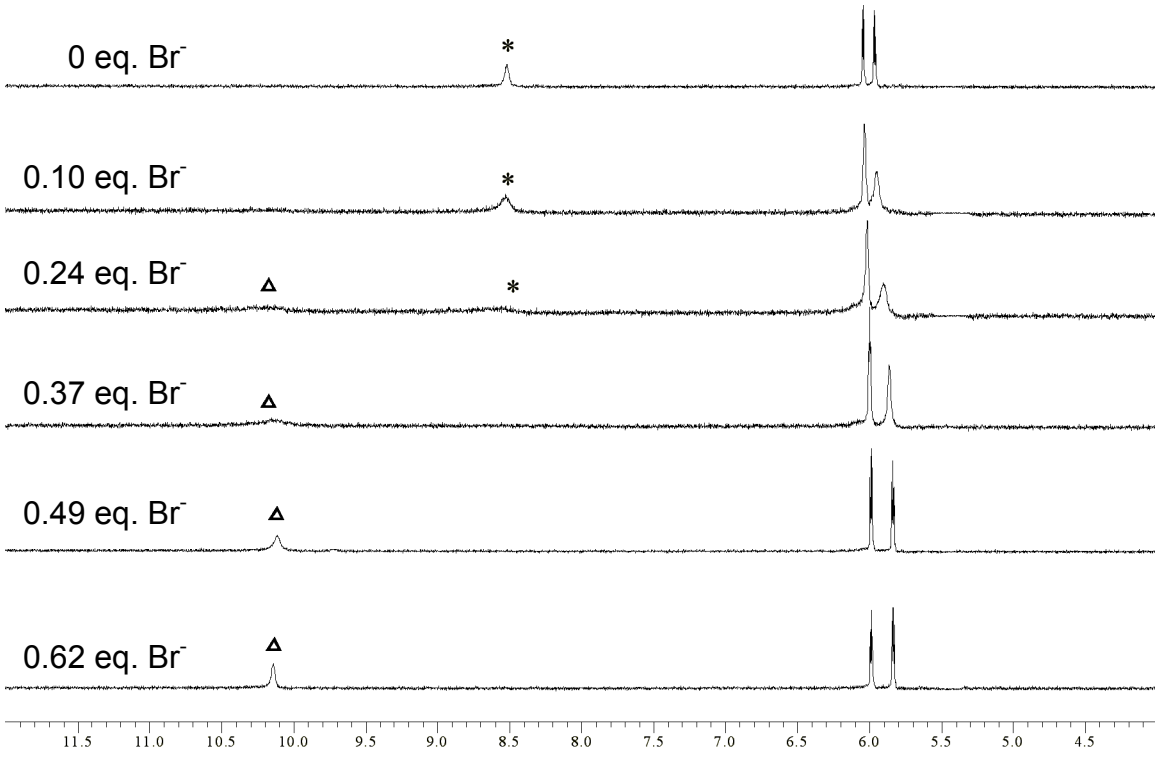

Figure 3.5 1H NMR titration of calix[3]bipyrrole 70 (2 × 10-3 mol/L) with TBABr in CD3CN (*: chemical shift of the NH protons of the free ligand; Δ: chemical shift of the NH protons of the ligand bound with bromide anion).

As in the case of chloride anion the observed slow exchange process precluded an accurate determination of either the binding stoichiometry or the corresponding receptor-anion association constants. However, the fact that slow exchange was seen was considered to be an indication that calix[3]bipyrrole **70** binds chloride and bromide anions strongly in acetonitrile. Consistent with this supposition was the finding that fast exchange was seen in the case of iodide anion, a substrate that based on analogy to what is seen with calix[4]pyrrole **1** (K_a = 17 M^{-1}; acetonitrile-d_3), was expected to be bound less well than Cl^- or Br^-. In this case, ^{1}H NMR spectroscopic titrations revealed that

calix[3]bipyrrole **70** binds iodide anion with a stability constant of 9300 M^{-1} in acetonitrile-d_3 (Figure 3.6, Table 3.1). Relative to **1**, this represents an affinity enhancement factor of over 500.

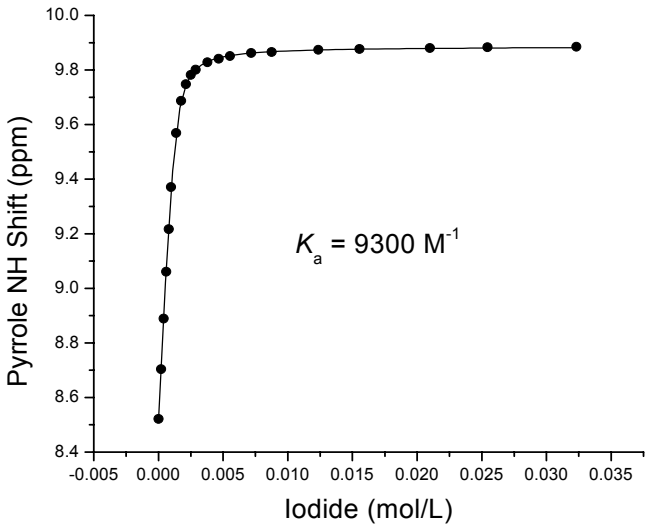

Figure 3.6 Binding profile derived from a ^{1}H NMR spectroscopic titration of calix[3]bipyrrole **70** (2×10^{-3} mol/L) with iodide anion in CD_3CN. The curve shows the fit of the experiment data to a 1:1 binding profile.

DMSO-d_6 was also used as solvent for the ^{1}H NMR anion binding studies of compound **70**. Here, in contrast to the slow exchange seen in the titrations of **70** with chloride or bromide anion in acetonitrile-d_3, fast exchange was observed with the NH signal moving to lower field in a monotonic manner upon the addition of increasing quantities of anion. Good fits to 1:1 binding profiles could be made in the case of both chloride and bromide anions, thus allowing association constants to be calculated in the usual way (Table 3.1). The resulting values support the conclusion that receptor **70** displays higher affinities for larger anions, such as bromide anion, as compared to the

parent system **1**. The effect is not small with the enhancement factors being over an order of magnitude or more in the most favorable of cases.

Table 3.1 Association constants (M^{-1}) for calix[3]bipyrrole **70** and calix[4]pyrrole **1** with halide anions in acetonitrile and DMSO.[a]

Anion	Solvent	Calix[3]bipyrrole **70**	Calix[4]pyrrole **1**	K_{rel}[e]
Cl^-	CH_3CN	110,000[b]	140 000[b]	0.79
	DMSO	9 600[b]	1 300[b]	
	DMSO-d_6	15 000[c]	1 025[d]	14.6
Br^-	CH_3CN	100 000[b]	3 400[b]	29.4
	DMSO	440[b]	N.D.	
	DMSO-d_6	450[c]	17[c]	26.5
I^-	CH_3CN	[f]	N.D.	
	CH_3CN-d_3	9 300[c]	17[c]	547
	DMSO-d_6	N.D.	N.D.	

[a] Anions used in this assay were in the form of their tetrabutylammonium salts; values are the average of at least three separate measurements and are considered reproducible to ± 15%; N.D.: not determined. [b] Value obtained from ITC titrations at 30 ˚C. [c] Determined from ^{1}H-NMR titrations carried out at 25˚ C. [d] From ref. 63. [e] Represents the ratio of the association constants for **70** and **1**, respectively, recorded under identical conditions. [f] No reliable fit could be obtained.

Due to our inability to obtain accurate association constants for compound **70** in the case of Cl^- and Br^- in CD_3CN, we turned to ITC titration methods in an effort to assess these values. As above, the studies were carried out in both dry CH_3CN (Figure

3.7) and DMSO (Figure 3.8). Good fits to 1:1 host-guest binding profile were obtained, allowing the association constants to be determined for both anions in both solvents. As such, these studies provided an independent confirmation of a representative subset of the K_a values originally determined *via* ^{1}H-NMR spectroscopic titrations as described above (Table 3.1). The fact that nearly coincident values were seen bolsters confidence in the conclusion that calix[3]bipyrrole **70** is a good receptor for Br^- and I^-, both in absolute terms and when considered in comparison to calix[4]pyrrole **1**. Such a finding, in turn, provides support for the notion that receptors, such as **70**, that provide a better size- and geometry-based matching towards their targeted substrates, in this case larger anions, as well as a greater number of hydrogen bond donor sites, will, in fact, display higher affinities than analogous systems with a lower level of host-guest optimization.

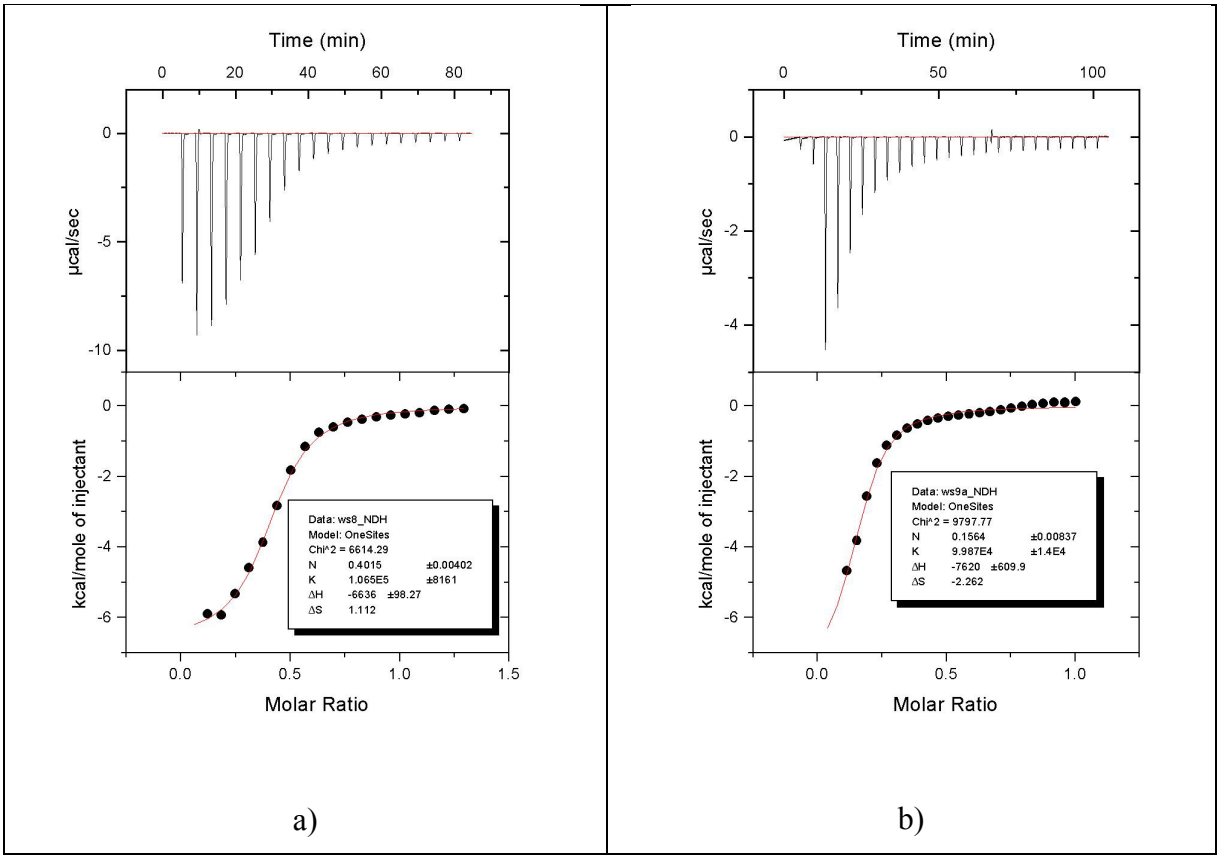

Figure 3.7 Curves obtained from ITC titrations of calix[3]bipyrrole **70** with a) TBACl and b) TBABr in CH_3CN. The inset shows that **70** binds Cl^- and Br^- in acetonitrile with comparable affinities.

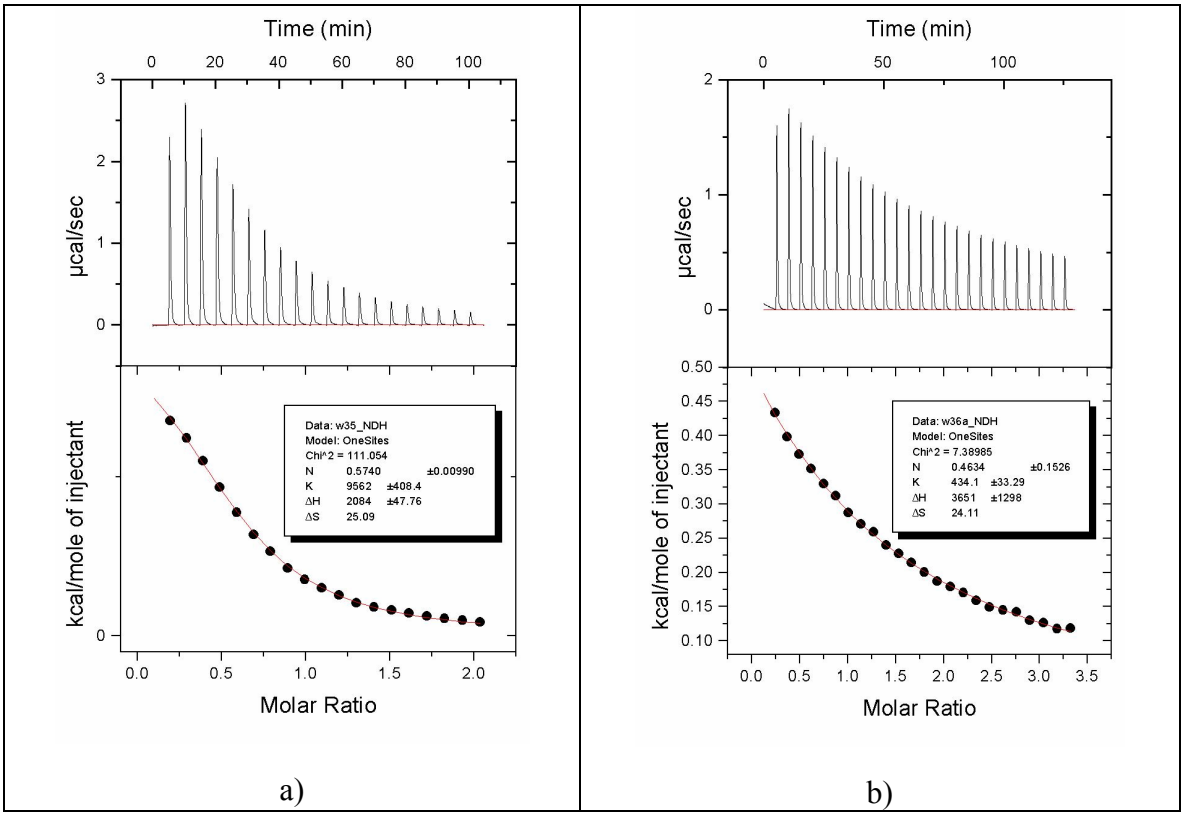

Figure 3.8 Curves obtained from ITC titrations of calix[3]bipyrrole **70** with a) TBACl and b) TBABr in DMSO. The inset shows that **70** binds Cl^- over Br^- in DMSO with a selectivity factor of more than 20.

Interestingly, detailed analysis of the ITC curves for **70** leads to the inference that the binding processes in acetonitrile are enthalpy-driven, while those in DMSO are entropy-driven. This difference is rationalized in terms of what are assumed to be strong interactions between the anion receptor and solvent molecules in DMSO solution but not to an appreciable extent in acetonitrile solution.

It is of interest to note that the chloride anion affinity of calix[3]bipyrrole **70** is actually lower than that of calix[4]pyrrole **1** in acetonitrile, in spite of the greater number of potential NH donor sites in receptor **70** than in **1**. We attribute this difference to the

poor size match between receptor **70** and Cl^-, as revealed by both the unfavorable nitrogen-hydrogen-chloride angles and the nitrogen-to-chloride hydrogen bond lengths seen in the solid state structure of [**70**·Cl]$^-$ compared to those of [**1**·Cl]$^-$. This incommensurate binding geometry, we think, partially neuturalize the binding advantage that an increased number of hydrogen bonds would be expected to impart, at least in this relatively less polar solvent. However, this is not the case in polar solvent such as DMSO. Instead, the increased number of hydrogen bond donor groups plays a more important role that serves to overcome competition from the solvent, resulting in the relatively stronger chloride anion binding for **70** as compared to **1**.

3.5.2 Calix[4]bipyrrole 71

During the initial studies of calix[3]bipyrrole **70**, its larger homologue, calix[4]bipyrrole **71**, was excluded since it appeared to us that it might be too large and too flexible to complex various anions of interest. Behind this negative assessment regarding potential interest, however, was an inference drawn from the crystal structure of **71**·4THF. In this structure, the calix[4]bipyrrole molecule was found to be complexed to four tetrahydrofuran molecules, adopting a square-like conformation with the two bipyrroles at the 1,3- (or 2,4-) positions being parallel to each other and in *cis*-like orientations. Inspired by this structure, we thought to assemble this macrocycle into a column-containing structure in the solid state *via* the use of a linear bidentate hydrogen bond acceptor moiety, for example, 4,4'-bipyrridyl.

While attempts to obtain such column-containing structures have so far failed, we did succeed in solving the structure of a new adduct of **71**, namely, **71**·2$C_{10}H_8N_2$ (Figure 3.9). As in the previous structure, macrocycle **71** was found to adopt a square-like conformation in the case of this newer adduct. However, in contrast to what is seen in the solid state structure of **71**·4C_4H_8O, in **71**·2$C_{10}H_8N_2$ only two of the four bipyrrole subunits, at the opposite sides of the square (sides "1" and "3") were found to interact with the two 4,4'-bipyrridyl "substrate" molecules. These latter entities lie parallel to one other but are oriented in opposite directions. The nitrogen-to-nitrogen distances are 2.991(3) Å and 3.040(3) Å, respectively. The nitrogen-hydrogen-nitrogen angles are 165(3)º and 173(2)º, respectively. The two bipyrroles that define sides "2" and "4" are likewise parallel to one another. However, as noted above, they do not interact with the 4,4'-bipyrridyl "substrate" and both are present in their respective trans conformations.

a)

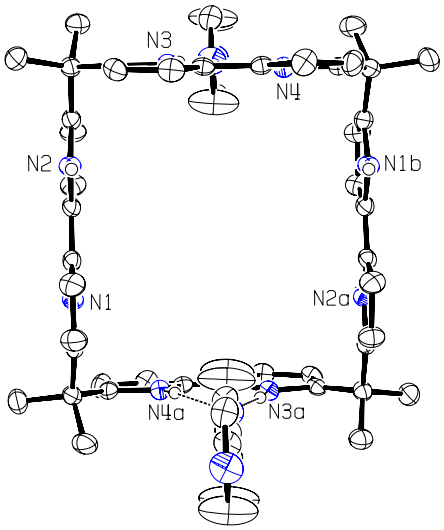

b)

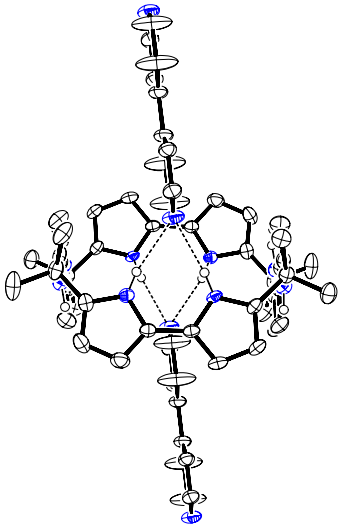

c)

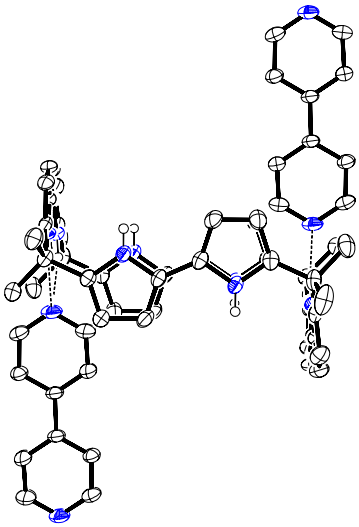

Figure 3.9 Ortep view of the molecular structure of the **71**·2$C_{10}H_8N_2$. a) Top view; b), c) side views. Displacement ellipsoids are scaled to the 50% probability level. Most hydrogen atoms have been removed for clarity. Dashed lines are indicative of N-H---N hydrogen bonding interactions.

The presence of hydrogen bonding interactions in the solid states of both **71**·$4C_4H_8O$ and **71**·$2C_{10}H_8N_2$, led us consider that this system, in spite of earlier considerations to the contrary, might act as an effective anion receptor. Consistent with this proposition were the findings from X-ray diffraction analyses of single crystals of [**71**·Cl]$^-$ and [**71**·Br]$^-$, which provided prima facie evidence of anion binding in the solid state, as discussed below.

Diffraction-grade crystals of [**71**·Cl]$^-$ were grown by allowing diethyl ether vapor diffuse slowly into a dichloromethane solution containing a 1:1 mixture of **71** and tetrabutylammonium chloride. X-ray diffraction analysis revealed the presence of a bound chloride anion that is nested within the binding "cavity" as opposed to perched above it, as seen in the case of [**1**·Cl]$^-$ and, to a lesser extent, [**70**·Cl]$^-$ (Figure 3.10). In [**71**·Cl]$^-$, the macrocycle adopts a V-shaped (D_{2d}) conformation with the chloride ion sitting in the center and bound to all eight pyrrole units *via* eight separate NH---Cl$^-$ hydrogen bond interactions. The nitrogen-to-chloride distances are in the range of 3.422(4) - 3.572(4) Å; the NH proton-to-chloride distances (Å) are in the range of 2.53 - 2.70 Å; and the nitrogen-to-chloride angles are in the range of 161.7° - 173.9°.

a)

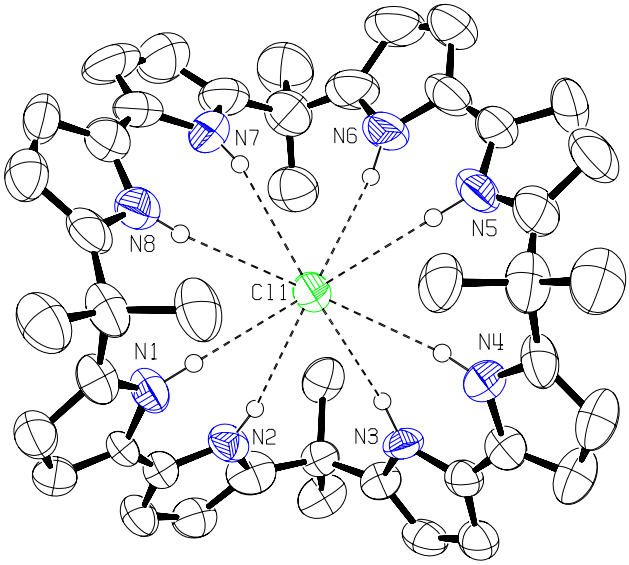

b)

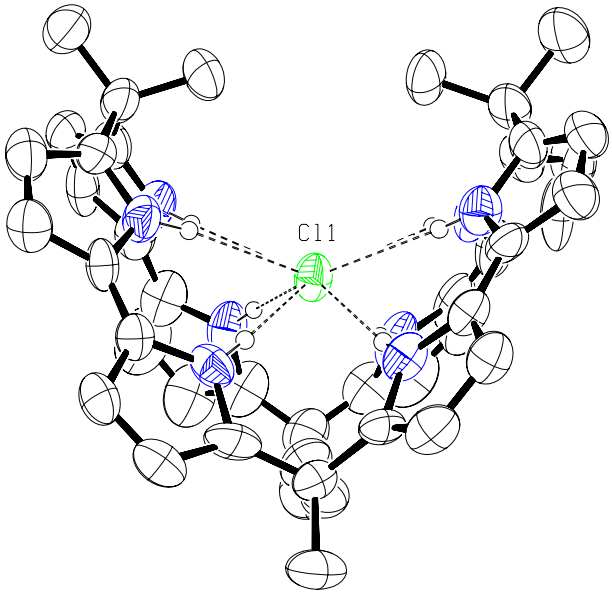

Figure 3.10 Ortep view of the molecular structure of the [**71**·Cl]$^-$. a) Top view; b), c) side views. Displacement ellipsoids are scaled to the 30% probability level. Most hydrogen atoms have been removed for clarity. Dashed lines are indicative of N-H---Cl$^-$ hydrogen bonding interactions.

Diffraction-grade crystals of [**71**·Br]$^-$ were grown by allowing a dichloromethane solution containing a 1:1 mixture of **71** and tetraethylammonium bromide to undergo slow evaporation in an atmosphere saturated with hexanes vapor. X-ray diffraction analysis revealed the existence of two structurally-similar macrocycles in the unit cell, both of which displayed, in analogy to what was seen in the case of [**71**·Cl]$^-$, the presence of a bound bromide anion nested within the binding "cavity" (Figure 3.11). As in the case of [**71**·Cl]$^-$, the macrocycles in [**71**·Br]$^-$ adopts a V-shaped (D_{2d}) conformation with the bromide ion sitting in the center, being bound there *via* eight NH---Br$^-$ hydrogen bond interactions. In molecular structure 1, the nitrogen-to-bromide distances are in the range of 3.492(4) - 3.608(3) Å; the NH proton-to-chloride distances are in the range of 2.60 – 2.73 Å; and the nitrogen-to-bromide angles are in the range of 154.7° - 174.6°. In molecular structure 2, the nitrogen-to-bromide distances are in the range of 3.430(3) - 3.583(4) Å; the NH proton-to-chloride distances (Å) are in the range of 2.54 - 2.73 Å; and the nitrogen-to-bromide angles are in the range of 158.5° - 177.2°. Figure 3.12 shows the unit cell packing diagram of these two molecular structures.

a)

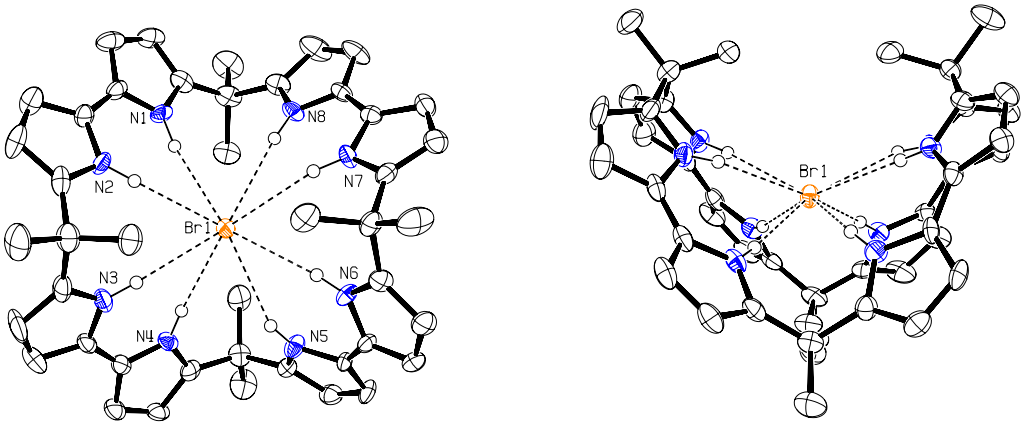

top view side view

b)

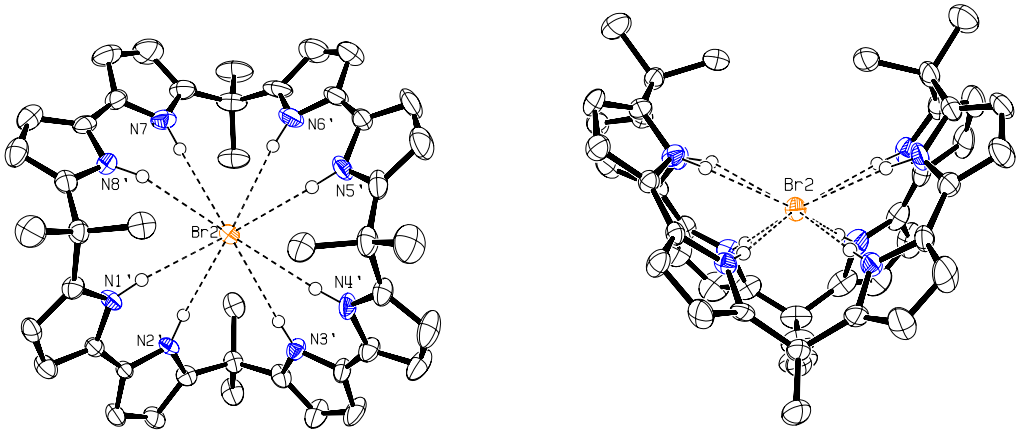

top view side view

Figure 3.11 Ortep view of the molecular structures of the [**71**·Br]$^-$. a) Molecular structure 1; b) molecular structure 2. Displacement ellipsoids are scaled to the 50% probability level. Most hydrogen atoms have been removed for clarity. Dashed lines are indicative of N-H---Br H-bonding interactions.

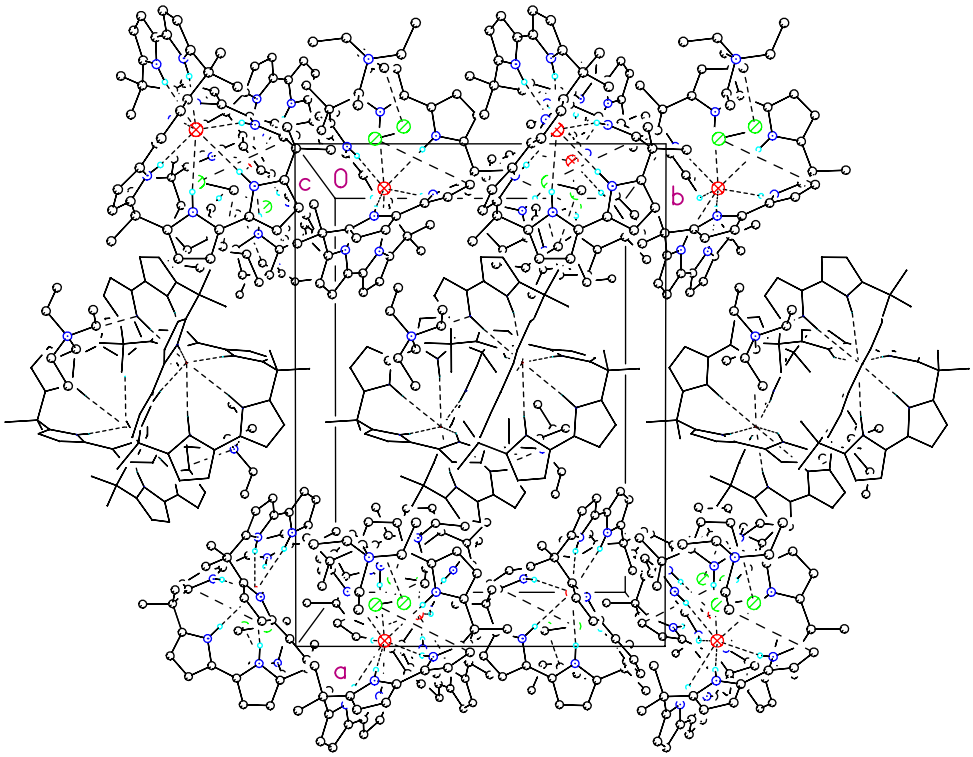

Figure 3.12 Unit cell packing diagram for [**71**·Br]$^-$. The view is approximately down the **c** axis. Macrocycle 2 is displayed in wireframe form (near x = ½) while macrocycle 1 is shown in ball-and-stick form.

The finding that **71** stabilizes the formation of what appear to be well-encapsulated chloride and bromide anion complexes in the solid state that are characterized by a greater number of hydrogen bonding interactions (eight) than seen in any other calixpyrrole or calixpyrrole-like anion complex, led us to consider that system **71**, in spite of its large size and expected conformational mobility might prove to be a highly effective chloride anion receptor in organic solution. As a test of this consideration, the binding of selected anions was studied in acetonitrile-d_3 solution using ^{1}H NMR spectroscopic titration and ITC titration methods. The results of these studies are summarized in Table 3.2.

Table 3.2 Association constants (K_a, M^{-1}) for the interaction of receptors **71, 70** and **1** with different anions in acetonitrile.[a]

Anions	**71**	**70**	**1**
Cl^-	2 940 000[b]	110 000[d]	140 000[d]
Br^-	112 000[b]	100 000[d]	3 400[d]
I^-	56[c]	9 300[d]	17[d]
NO_3^-	453[c]	11 060[c]	52[c]

[a] Anions were studied in the form of their corresponding tetrabutylammonium salts; values are the average of at least three measurements and are considered reproducible to ± 15%; [b] Value obtained from ITC titrations in dry CH_3CN at 30 ºC. [c] Value obtained from ^1H NMR titrations carried out in CD_3CN at 25 ºC. [d] From ref. 60.

Inspection of Table 3.2 reveals that, compared to **70** and **1**, the octapyrrolic macrocycle **71** displays an enhanced affinity for chloride anion, binding this species over 20 times more effectively than either **70** or **1**. In the case of bromide, receptor **71** shows an affinity that is substantially increased, by a factor of roughly 33, compared to **1**, but which is essentially similar to that displayed by **70**. For the larger anions, nitrate and iodide, it is actually the latter species, not **71**, that displays the highest affinity, although the absolute K_a values are low.

The crystal structures of [**71**·Cl]$^-$, to the extent it provides a model for the dominant species present in solution, helps provide a rationale for the high chloride anion affinity seen in the case of this larger system, namely an ability to adopt a conformation wherein eight pyrrole NH hydrogen bond donor groups can interact with the anionic center. The deep "walls" of the receptor "cavity" are expected to provide greater protection from solvation than in the chloride anion complexes of **1** and **70**. Similar

arguments, however, are not likely to hold for the other larger anions considered in this study, namely iodide and nitrate, thus accounting for a degree of selectivity for **71** that is remarkable for such a large, flexible receptor system.

When DMSO was used as a solvent, compound **71** failed to show any appreciable interaction with either chloride or bromide anion. This stands in marked contrast to what is true for its smaller homologue, calix[3]bipyrrole **70**; this latter more rigid anion receptor displays K_a values of 9600 and 440 M^{-1} for these two anions, respectively.[60] The reduced level of preorganization present in **71** is expected to allow this system to be highly solvated by DMSO and other competitive solvents. In fact, the lack of observed anion binding is most easily rationalized in terms of anion-receptor interactions that are not capable to compete with this solvation and the associated strong DMSO to NH interactions.

3.6 CONCLUSION

Two bipyrrole-based anion receptors, calix[3]bipyrrole **70** and calix[4]bipyrrole **71**, were successfully synthesized.

As proved true for the solid-state structure of [**1**·Cl]$^-$, in [**70**·Cl]$^-$ the macrocyclic molecule adopts a cone-like conformation, with a chloride anion perched on the cavity. Solution-phase studies revealed that compound **70** binds large halide anions (e.g., Br$^-$) with affinities that are substantially enhanced relative to those of calix[4]pyrrole **1**.

In contrast to what is seen in the solid-state structures of both **[1**·Cl]$^-$ and [**70**·Cl]$^-$, single crystal X-ray structural analysis of [**71**·Cl]$^-$ and [**71**·Br]$^-$ reveals the macrocyclic complex geometries wherein adopts V-shaped conformations, with a chloride or bromide anion nested within the cavity. In spite of being both large and conformationally flexible, the octapyrrolic system **71** was found to bind chloride anions well and with high selectivity in acetonitrile. On the other hand, no appreciable anion binding is seen in the more polar solvent, like DMSO. This latter lack of observable binding is attributed to the high degree of solvation allowed by the large, flexible octapyrrolic structure.

3.7 FUTURE DEVELOPMENTS

The fact that calix[4]bipyrrole **71** displays no appreciable anion binding in DMSO reflects the poor structural preorganization of this macrocycle. On the other hand, in the case of the chloride and bromide complexes this same molecule adopts a beautiful "nesting" conformation in the solid state that allows these anions to be "caught" within the cavity. These findings, as a whole, inspire us to propose that future work could entail the design of modified calix[4]bipyrroles that are structurally "locked" into a preorganized nesting conformation. This "locking" could be achieved through the use of certain linkers bridged across the 1,3-*meso* carbons (Figure 3.13). CPK models show that such kind of molecules, in contrast to **71**, would be preorganized and provide a targeted anion with a binding cavity that could surround it with eight pyrrole units. Even in polar solvent like DMSO, such molecules are predicted to behave as strong anion receptors. Due to their structural similarity to the strapped calix[4]pyrroles,[35-37] these molecules could be named as "strapped" calix[4]bipyrroles.

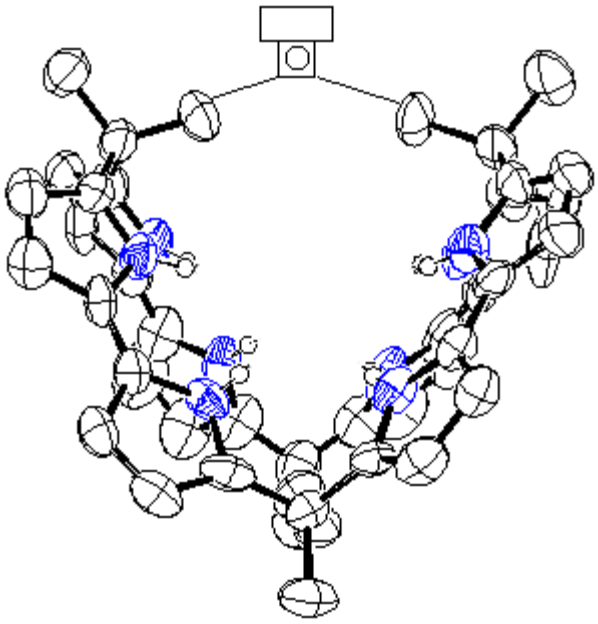

Figure 3.13 Schematic view of a proposed structurally "locked" calix[4]bipyrrole.

Based on the above assumption, compounds **79-81** have been designed as specific targets for synthetic consideration. Here, the length of the strap is expected to play an important role in regulating the binding and conferring success on this strategy. If they are too long or too flexible, they will not serve to lock the structure into the desired "nesting" conformation. On the other hand, straps that are too short will complicate the synthesis. Considering this balance, straps containing 1,3-phenylene-diyl structures were chosen as the best first set of proposed candidates.

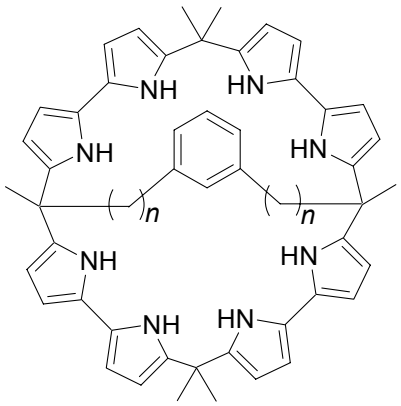

79 n = 0

80 n = 1

81 n = 2

It is suggested that the synthetic methodology used to prepare the strapped calix[4]pyrroles **31-34** can be readily applied to the synthesis of strapped calix[4]bipyroles **79-81**. Specifically, the reaction of diketones **82-84** with excess bipyrrole in acetonitrile in the presence of a catalytic amount of acid is expected to afford intermediates **85-87**. Follow-up condensation with acetone is then expected to give target compounds **79-81**. These strapped calix[4]bipyrroles, once made, would provide a correlated set of calixpyrrole-based macrocycles endowed with pocket-like cavities that should allow this critical preorganization vs. solvation hypothesis to be tested accurately *via* direct experimental analysis. Correlating the findings to higher level theoretical predictions, beyond the scope of this dissertation, would also be interesting.

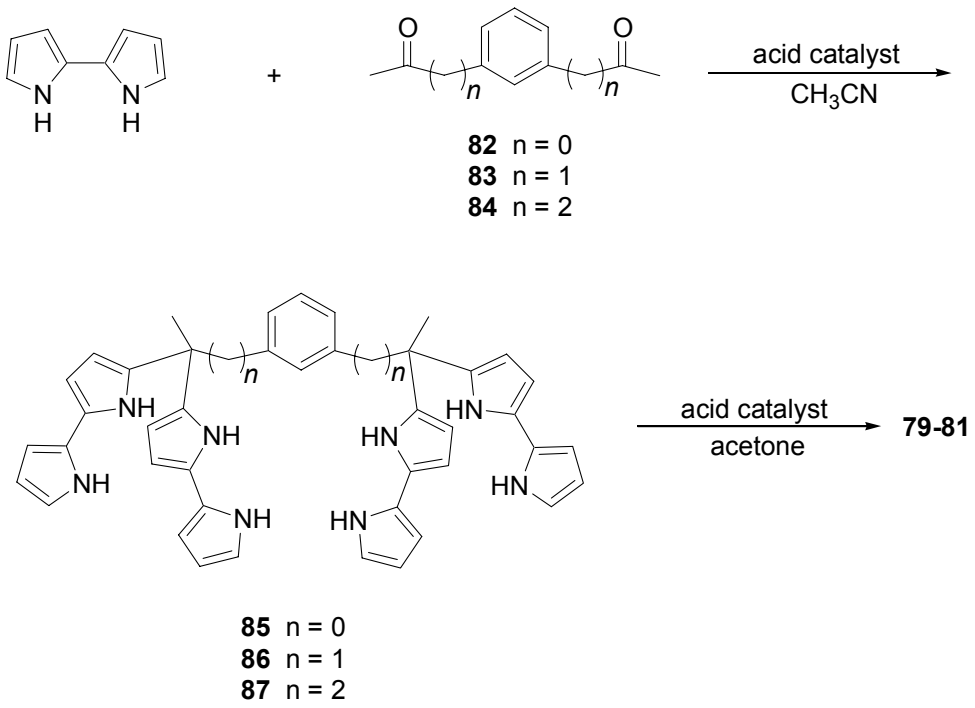

Scheme 3.7 Proposed synthesis of target compounds **79**-**81**.

Chapter 4: Calix[2]bipyrrole[*m*]furan[*n*]thiophene (*m* + *n* = 2): Synthesis, Characterization, and Anion Binding Studies

4.1 INTRODUCTION

In addition to being the sole building blocks for rosarins and their higher order homologues, bipyrroles are also co-building blocks for expanded porphyrins such as sapphyrins[64] and rubyrins.[65] Rubyrin-like macrocycles include heterorubyrins;[66] these systems are composed of bifuran or bithiophene with pyrrole. The macrocyclic structures and synthesis methodologies used to prepare these expanded porphyrins provide an important inspiration for the design and synthesis of new, larger calixpyrrole analogues. As detailed elsewhere in this dissertation, there has been considerable effort devoted of late towards the synthesis and study of so-called higher order calixpyrroles. The specific thought therefore, was that the use of bipyrroles and related analogues might provide a new entry into such systems. Here, an ancillary objective was to create novel receptors that might display different anion selectivities than seen for other, previously reported calixpyrrole systems.

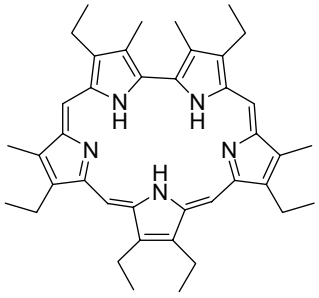

Sapphyrin

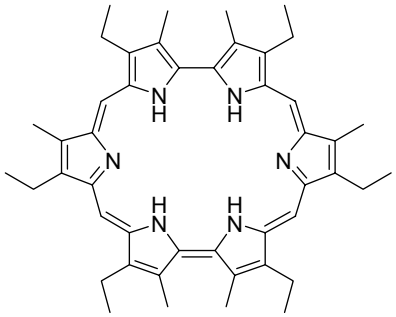

Rubyrin

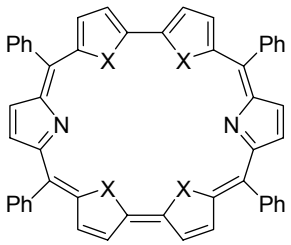

X = O, S

Hetereorubyrins

"Y-shaped" carboxylates are important elements in many biological and synthetic organic molecules. As introduced in Chapter 1, Gale and coworkers demonstrated that a

calix[4]pyrrole **25** bearing a fifth pyrrole in one of the *meso* positions bound carboxylate anions (acetate and benzoate) selectively relative to chloride anion. This stands in contrast to the poor selectivity seen in the case of **1**. In fact, no evidence of selective carboxylate anion binding has so far been observed in other simple, unfunctionalized calix[*n*]pyrroles (n ≥ 4).

These findings, coupled with a desire to use bipyrrole as a building block, triggered our interest in designing novel calixpyrrole-like receptors for carboxylate anions. Molecular model (CPK) analyses led us to believe that calixpyrrole systems such as **88** would be good candidates as carboxylate anion receptors. This structure is geometrically commensurate with carboxylate anion binding, which should lead to good host-guest interactions. Unfortunately, all efforts to obtain system **88** have so far proved unsuccessful. Therefore, the use of heteroatom analogues was considered.

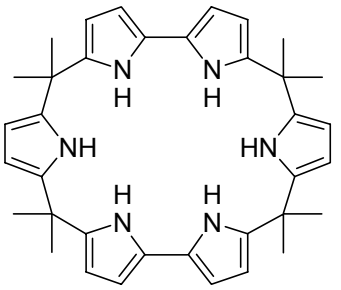

88

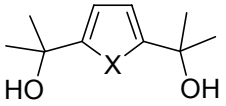

89 X = O
90 X = S

In recent years, Lee and coworkers have synthesized a series of calix[*n*]pyrrole (*n* ≥ 4) analogues containing heterocycles, such as furan, thiophene, and bithiophene, in addition to pyrroles.[67] Two useful precursor units, namely **89** and **90**, were broadly applied in the synthesis of these calixpyrrole hybrids.[68] We expect that this strategy, *via* appropriate modification, could be used to synthesize various target molecules analogous to structure **88**.

4.2 RESEARCH GOAL

The above considerations lead us to propose **91-93** as a first set of synthetic targets. Such systems, when conformationally preorganized, may behave as good receptors for carboxylate anions. Here, it was considered likely that the two bipyrrole units would act as bidentate carboxylate binding ligands, whereas the two heterocycle subunits (furan or thiophene) would act either as simple linkers, or possibly as hydrogen bonding acceptors when the targeted substrates consisted of anions that contain hydrogen bonding donor subunits.

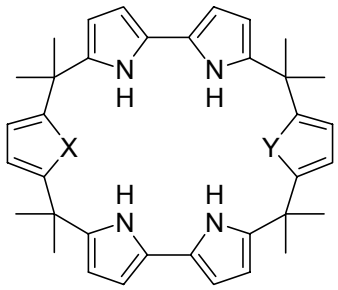

91 X = Y = O
92 X = Y = S
93 X = O, Y = S

As in the past, it was expected that the anion binding properties of these novel macrocycle would be studied using both solution-phase techniques, such as ^{1}H NMR spectroscopic and ITC titrations, and solid-phase technique, such as X-ray diffraction analysis. These measurements made, the anion binding properties of **91**-**93** could then be evaluated relative to the parent system **1**, as well as the precursor bipyrrole **72**.

4.3 SYNTHESIS

The synthesis of **91-93** is shown in Scheme 4.1.[69] Precursors **89** and **90** were synthesized according to literature.[68] Efforts to obtain **91** and **92** in one step by condensing bipyrrole **72** directly with **89** and **90** proved fruitless, producing a hard-to-separate mixture of compounds. Accordingly, we modified Lee's stepwise procedure in an effort to obtain these targets.

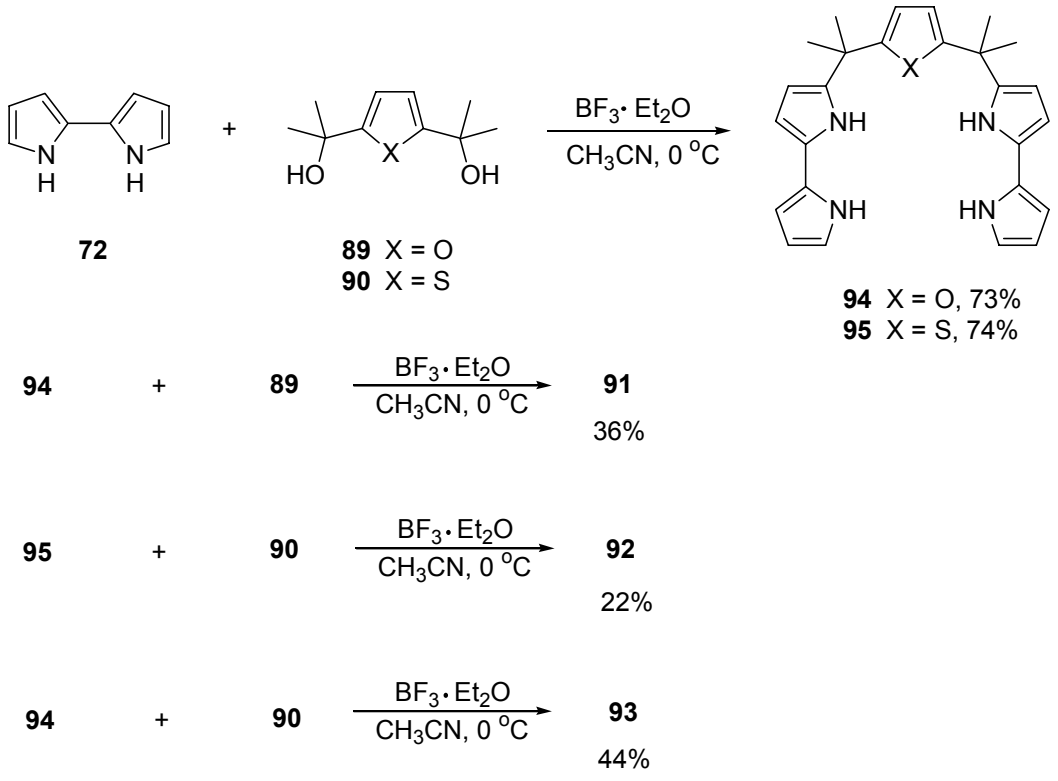

Scheme 4.1 Stepwise synthesis of target macrocycles **91-93**.

Reacting **89** with excess **72** (10 equiv. or more) in acetonitrile in the presence of a catalytic amount of $BF_3 \cdot Et_2O$ at 0 ºC afforded **94** in 73% yield. Condensation of **94** with **89** in a 1:1 ratio, under the same reaction conditions as above, produced target compound

91 in 38% yield. Using an analogous procedure, compound **92** was synthesized from **72** and **90** in two steps in 74% and 22% yield, respectively. Compound **93** was synthesized from the condensation of **90** with **94,** an intermediate synthesized from **89**, in 44% yield.

4.4 CHARACTERIZATION

All new compounds were characterized by standard spectroscopic techniques including ^{1}H NMR, ^{13}C NMR, and HR-MS. Compounds **91-93** were also characterized by X-ray diffraction analysis.

Diffraction-grade crystals of **91** were grown by slow evaporation of a chloroform solution of **91** under an atmosphere saturated with hexanes vapor. X-ray structural analysis revealed that no solvent molecules are trapped in the lattice, and that the two pyrroles in each bipyrrole unit are orientated in opposite directions relative to each other. The two furan rings are also oriented in opposite directions (Figure 4.1).

Diffraction-grade crystals of **92** were grown from a tetrahydrofuran solution of the macrocycle layered with water on the bottom and methanol on the top. X-ray structural analysis revealed two crystallographically unique hydrogen bound complexes per asymmetric. In the more complex structure, the thiophene ring was found to be disordered. Thus, only one complex of the two in the unit cell was described in detail (Figure 4.2). For this structure, in contrast to what proved true in the case of **91**, the two pyrroles in each bipyrrole unit face in the same direction. Also, each bipyrrole unit is bound to a tetrahydrofuran molecule *via* two NH (pyrrole)---O (THF) hydrogen bonding interactions. The nitrogen-to-oxygen distances are between 2.981(4) and 3.094(4) Å; the nitrogen-hydrogen-oxygen bond angles are in the range of 162.4-172.2 º.

a)

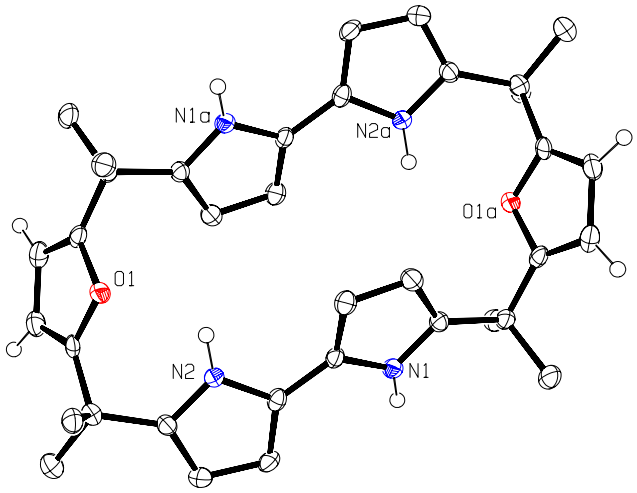

b)

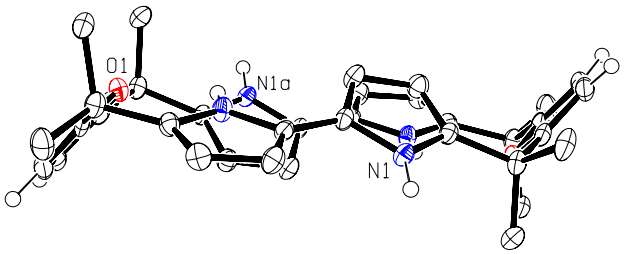

Figure 4.1 Ortep view of the molecular structure of **91**. a) Top view; b) side view. Thermal ellipsoids are scaled to the 50% probability level. Most hydrogen atoms have been removed for clarity.

a)

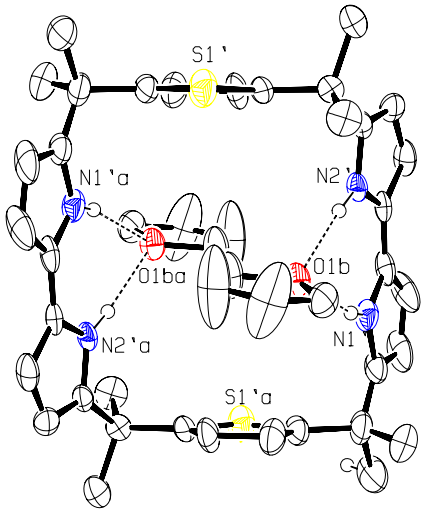

b)

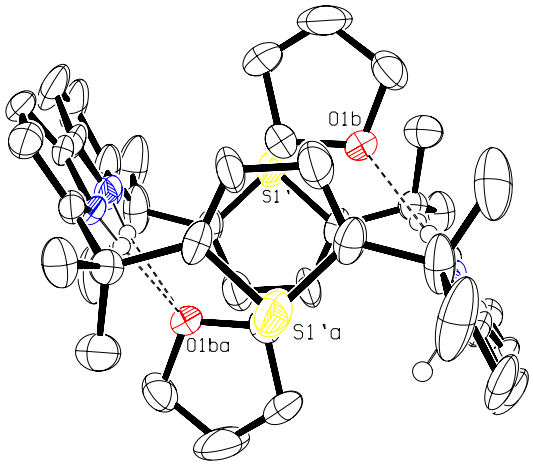

Figure 4.2 Ortep view of the molecular structure of the **92**·2C_4H_8O. a) Top view; b) side view. Displacement ellipsoids are scaled to the 30% probability level. Most hydrogen atoms have been removed for clarity. Dashed lines are indicative of N-H---O hydrogen bonding interactions.

Diffraction-grade crystals of **93** were grown by slow evaporation of a dichloromethane solution of **93** in an atmosphere saturated with hexanes. X-ray structural analysis revealed that two dichloromethane molecules are included in the unit cell, and the positions of the oxygen atom and the sulfur atom are disordered about the center of symmetry. This disorder is not shown in Figure 4.3, which gives a representation of the structure. The two pyrroles in each bipyrrole unit are orientated in opposite directions. The two pyrroles linked to the same heterocyclic linker (furan or thiophene) are orientated in the same directions, with both NH protons bound to one chlorine atom from a dichloromethane molecule *via* two NH---Cl hydrogen bonding interactions. Each of the pyrrole rings is also bound to one hydrogen atom present on a different dichloromethane molecule *via* one π---H-C hydrogen bonding interaction. The nitrogen-to-chlorine distances are 3.430(2) and 3.486(2) Å, respectively; the NH proton-to-chlorine distances are 2.83(2) Å and 2.90(2) Å, respectively; the nitrogen-hydrogen-chlorine bond angles are 128(2) ° and 129(2) °, respectively. These hydrogen bond distances are within the ranges expected for effective hydrogen bonding interactions, although the bond angles are less than ideal. Interestingly, the hydrogen atoms on the solvent molecule are in close contact with the ring center of the pyrrole rings. The bond lengths for the proposed CH---π type interactions involving the solvent (CH) hydrogen and pyrrole ring of 2.55(3) Å and 2.53(2) Å, respectively, are also in the range of what is expected for these kinds of motifs.

a)

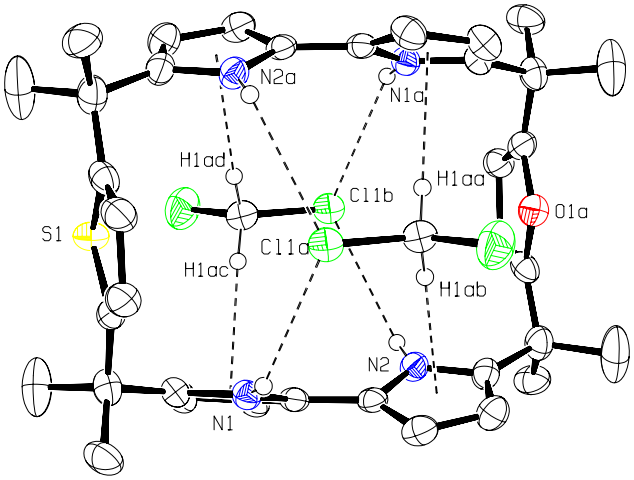

b)

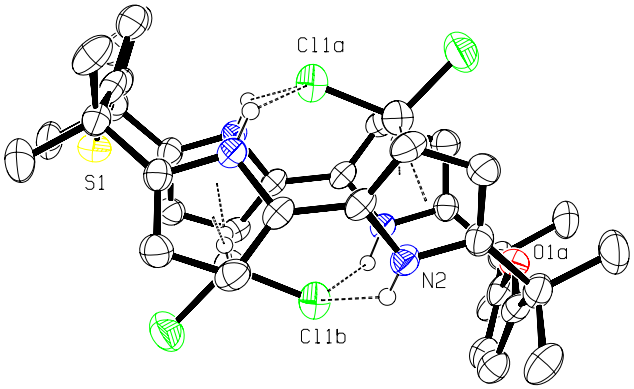

Figure 4.3 Ortep view of the molecular structure of **93**·2CH_2Cl_2. a) Top view; b) side view. Displacement ellipsoids are scaled to the 30% probability level. Most hydrogen atoms have been removed for clarity. Dashed lines are indicative of N-H---Cl and (dichloromethane) C-H---π (pyrrole ring) hydrogen bonding interactions.

4.5 ANION BINDING STUDIES

Crystal structures of **92**·$2C_4H_8O$ and **93**·$2CH_2Cl_2$ display bound solvent molecules contained in the unit cells and hydrogen bonded to the macrocycles, revealing that such molecules may act as novel anion receptors. Solution-phase anion binding studies were carried out using standard ^{1}H NMR spectroscopic titrations in dry CD_3CN, and ITC titrations carried out in dry CH_3CN. X-ray structural analysis was also performed to study the solid-phase anion coordinating properties of these receptors. While there is not necessarily a direct correspondence, it was expected that the solid-state structural data would be helpful for understanding the corresponding solution-phase behavior.

4.5.1 ^{1}H NMR and ITC Titration Studies

As shown in Table 4.1, standard ^{1}H NMR spectroscopic titrations confirmed that compounds **91**-**93** bind chloride, bromide, and hydrogen sulfate anions only weakly. Such a lack of strong binding was expected given the size and geometry mismatch between the anions and the receptor binding cavities. By contrast, the tetrahedral anion, dihydrogen phosphate was found to be bound well by **92**, whereas compound **91** displays only a weak affinity for this anion. Unfortunately, no binding constant could be determined for **93** due to the lost NH proton signals upon addition of the dihydrogen phosphate anion.

We ascribe the differences in $H_2PO_4^-$ binding displayed by **91** and **92** to the different degree of geometry matching between the anion and the macrocyclic receptor in question. Specifically, the C_{meso} - C_{meso} and C_α - C_α distances in the furan case are shorter than those in the thiophene case (Figure 4.4). The different lengths of the linkers (furan or thiophene) in compounds **91** and **92** serve to define two different bipyrrole separations,

which, in turn, regulates the possible macrocycle-anion interactions and hence the anion affinities.

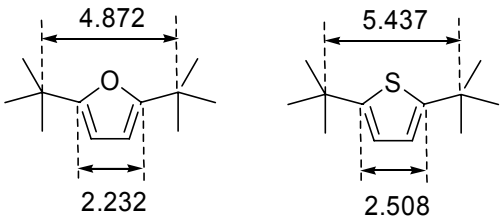

Figure 4.4 Different carbon-carbon distances (Å) as determined from the crystal structures of compounds **91** and **92**.

Similar ^{1}H NMR spectroscopic titration methods were also used to study the binding of benzoate and acetate anions. In this case it was found that the interactions were so strong that the exact binding constants could not be determined. We thus resorted to ITC methods to quantify the binding interactions.

In order to ensure that the binding constants obtained from the two methods are comparable, the binding of chloride anion was also studied *via* ITC for compounds **91** and **92**. As shown in Table 4.1, there is no substantial difference between the affinity values obtained using these two methods. The affinity constants for benzoate binding to **91-93** were thus determined by ITC and found to be 63,000, 99,600, and 670,000 M^{-1}, respectively. These values are 15, 20, and 160 times higher than those displayed by bipyrrole **72** (as a control compound). Acetate, a close "structural relative" of benzoate, was found to be bound even more strongly by receptors **91-93**.

Table 4.1 Stability constants (K_a, M^{-1}) for the interaction of anion receptors with different anions in acetonitrile using ^1H NMR and ITC titration methods.[a]

Anions	**91**	**92**	**93**	**72**	**1**
Cl^-	1 100[b]	940[b]	N.D.	250[b]	140 000[d]
	960[c]	1 500[c]	6 400[c]		
Br^-	37[c]	100[c]	150[c]	53[c]	3 400[d]
HSO_4^-	130[c]	28[c]	36[c]	35[c]	N.D.
$H_2PO_4^-$	240[c]	> 10,000[c]	N.D.	850[c]	-
$PhCO_2^-$	63 000[b]	100 000[b]	670 000[b]	4 100[b]	120 000[b]
$MeCO_2^-$	78 000[b]	140 000[b]	710 000[b]	3 700[b]	290 000[b]

[a] Anions used in this assay were studied in the form of their tetrabutylammonium salts; values are the average of at least three separate measurements and are considered reproducible to ±15%; N.D.: not determined. [b] Values obtained from ITC titrations at 30 ºC. [c] Value obtained from ^1H NMR titrations at 25 ºC. [d] From ref. 60.

A surprising result is how the minor structural difference associated with using **93** rather than **91** or **92**, gave rise to a rather significant change in anion binding ability. Specifically, relative to compounds **91** and **92**, compound **93** shows affinities for chloride, benzoate, and acetate anions that are enhanced by five to ten folds, while it only shows comparable affinities to bromide and hydrogen sulfate anions. As a result, relative to **91** and **92**, compound **93** displays enhanced selectivity for carboxylate anions over bromide and hydrogen sulfate, but no improved selectivity for carboxylates over chloride anion.

In contrast to the selective carboxylate anion binding behavior displayed by receptors **91-93**, calix[4]pyrrole **1** shows no carboxylate-chloride anion selectivity. Taken in concert, these findings support the notion that "fine-tuning" of the internal cavity size and overall shape of calixpyrrole-type receptors can lead to systems whose selectivities are optimized for certain classes of anions. The present findings are also noteworthy because they illustrate how changes in calix[*n*]pyrrole core design, as opposed to external ring functionalization, may be used to generate receptors for species that are relatively weak hydrogen bonding acceptors. This perturbation in inherent selectivities is also important in a more general sense since it shows how appropriate receptor design may be used to generate neutral receptors for carboxylate anions

The finding that compounds **91-93** selectively bind carboxylate anions over other anions revealed possible geometry matching between the hosts and the guests. Based on an analysis of the geometries of both the carboxylate anions and these receptors, we propose three possible binding modes that might contribute largely to host-guest interactions in solution (Figure 4.5). One such interaction involves a "one point binding" mode, in which only one oxygen atom of the carboxylate anion interacts with the macrocycles *via* four NH---O Hydrogen bonds. This kind of binding mode was seen in the crystal structure of calix[4]pyrrole carboxylate dimers.[70] The other two proposed interactions can be considered as "two point binding" modes, where both oxygen atoms of the carboxylate anion interact with the macrocycle *via* four NH---O hydrogen bonds. Here, both "cross binding" and "parallel binding" modes can be defined. In the "cross binding" mode, the carboxylate anion plane is perpendicular to the bipyrrole plane, with each oxygen atom bound to one bipyrrole unit. By contrast, in the "parallel binding" mode, the carboxylate anion plane is parallel to the two bipyrrole subunits, with each of the latter being bound to the two carboxylate oxygen atoms simultaneously. However,

other than the three extreme binding modes described above, there are also large amounts of intermediate binding modes that might contribute to the overall binding interactions. Unfortunately, few solution-phase methods proved effective to probe the distribution of these binding modes within the overall binding interactions.

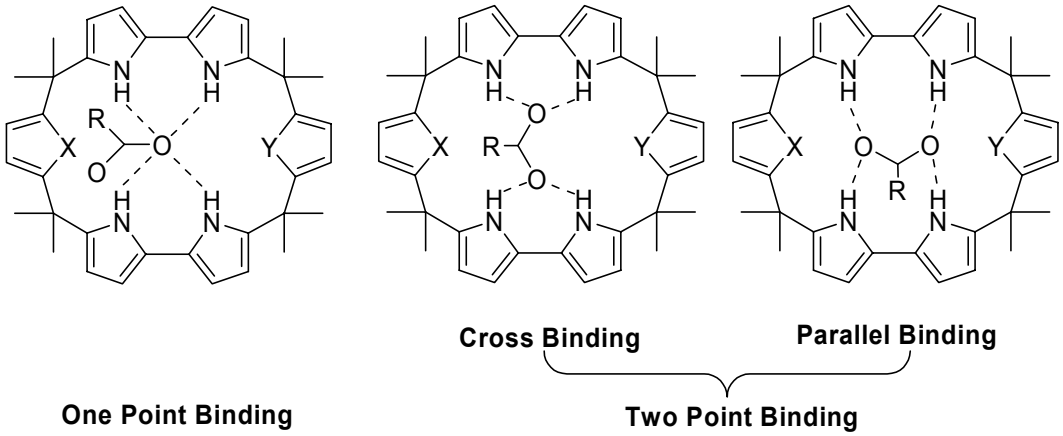

Figure 4.5 Three possible binding modes proposed for the interactions of receptors **91-93** with carboxylate anions.

4.5.2 X-ray Diffraction Analysis

Insights into the binding modes in the solid state came from X-ray structural analyses. Such analyses are often used to obtain useful information that is supplementary to that derived from solution-phase studies. Several diffraction-grade crystals of macrocycle **92**-anion complexes were successfully obtained and studied *via* X-ray diffraction analysis. The crystals were grown by the author and the structures were elucidated by Dr. Vincent Lynch of this department.

Diffraction grade crystals of $[\mathbf{92}\cdot PhCO_2]^-$ were grown by slow evaporation of a dichloromethane solution containing **92** and tetrabutylammonium benzoate (1:1 molar ratio) in an atmosphere saturated with hexanes. X-ray structural analysis revealed that the macrocycle adopts a cone-like conformation, with each bipyrrole unit bound to one oxygen atom of a benzoate anion *via* NH---O hydrogen bonding interactions (Figure 4.6). The two thiophene planes are nearly parallel to each other, pointing towards outside from the parallel positions with small angles. The nitrogen-to-oxygen distances are in the range of 2.840(3)-2.854(4) Å; and the nitrogen-hydrogen-oxygen angles are in the range of 161(3)-172(4)º. As a result, the planar benzoate anion is perpendicular to the bipyrrole plane, bisecting the macrocycle into two mirror parts across the midpoints of the two bipyrrole units. The anion is thus bound in a "cross binding", and not in a "parallel binding" or "one point binding" mode, at least in this solid-phase structure. However, the side view shows that the axis of the benzoate anion is not perpendicular to the macrocyclic plane (defined by N_4 root-mean-square). Rather, a small deviation is seen. As a consequence, two different sets of hydrogen bonding interactions are defined between the two bipyrrole units and the two oxygen atoms of the benzoate anion.

a)

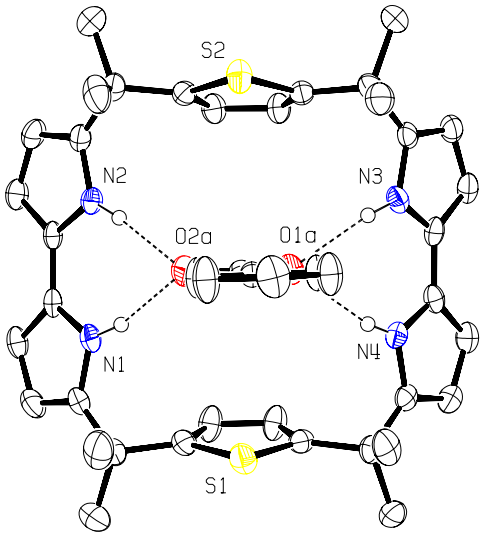

b)

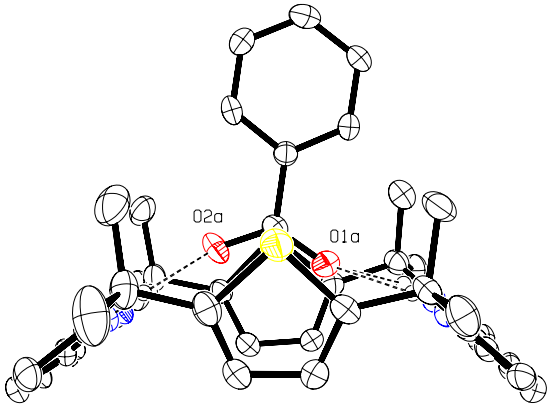

Figure 4.6 Ortep view of the molecular structure of [**92**·$PhCO_2$]$^-$. a) Top view; b) side view. Displacement ellipsoids are scaled to the 30% probability level. Most hydrogen atoms have been removed for clarity. Dashed lines are indicative of N-H---O hydrogen bonding interactions.

The cross binding mode displayed by the solid-state structure of [**92**·$PhCO_2$]$^-$ is further supported by the crystal structure of the acetate anion complex, [**92**·CH_3CO_2]$^-$. X-ray structural analysis revealed a molecular structure for [**92**·CH_3CO_2]$^-$ that is quite similar to that of [**92**·$PhCO_2$]$^-$ (Figure 4.7). The nitrogen-to-oxygen distances are in the range of 2.855(4)-2.869(3) Å, and the nitrogen-hydrogen-oxygen angles are in the range of 167(2)-169(3)º. One difference between the two crystal structures is that the methyl group of the acetate anion is buried within the cone-like cavity of the macrocycle, while the benzyl group of the benzoate anion resides outside the cavity. As reflected by both the shorter hydrogen bond distances involved and more dramatically the associated hydrogen bond angles, the crystal structure in the case of [**92**·CH_3CO_2]$^-$ reveals more effective host-guest hydrogen bonding interactions in the case of this complex than in [**92**·$PhCO_2$]$^-$. This difference in solid-state binding is also consistent with the binding constant values shown in Table 4.1.

Another difference between the two crystal structures is that the axis of the acetate anion is perpendicular to the macrocycle plane, while the axis of benzoate anion deviates from the perpendicular position to a small degree. To explain this phenomenon, the geometry of the electron orbitals of the oxygen atoms should be taken into account. The electron orbitals of the oxygen atoms (carboxylate anions) are sp^2 hybridized, with the three electron orbitals coplanar and separated by angles that are close to 120º. When hydrogen bonding to the pyrrolic protons, one electron orbital would be oriented towards the electron orbital of the hydrogen bonding donor (refers to pyrrolic hydrogen atoms) so as to maximize the electron orbital overlap. In the case of [**92**·CH_3CO_2]$^-$, when the acetate anion is oriented perpendicular relative to the macrocycle plane, one orbital of each oxygen atom is oriented towards the spherical electron orbital of the hydrogen. In the case of [**92**·$PhCO_2$]$^-$, with the benzoate anion oriented perpendicular to the

a)

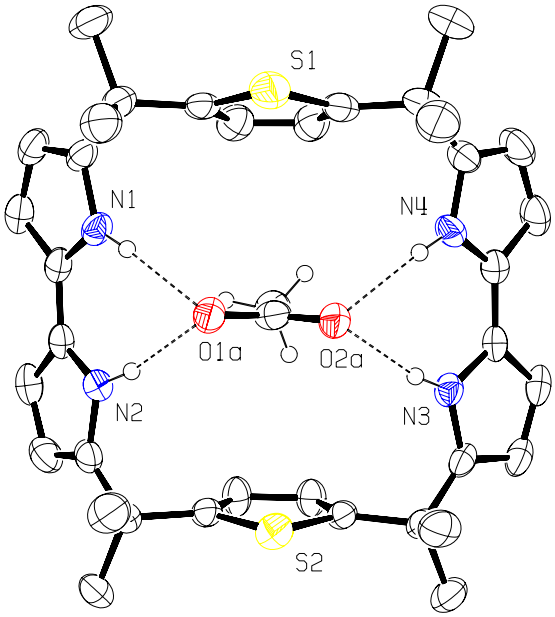

b)

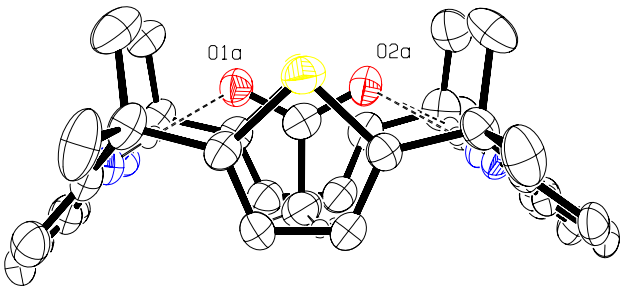

Figure 4.7 Ortep view of the molecular structure of the [**92**·CH_3CO_2]$^-$. a) Top view; b) side view. Displacement ellipsoids are scaled to the 50% probability level. Most hydrogen atoms have been removed for clarity. Dashed lines are indicative of N-H---O hydrogen bonding interactions.

macrocycle plane but out of the cavity, effective overlap with the hydrogen atom orbitals is precluded. Therefore such a positioning does not support good hydrogen bonding interactions. However, once the benzoate anion begins to deviate from its initial perpendicular position, the hydrogen bonding interactions are expected to increase due to the improved electron orbital overlap between the oxygen and the hydrogen atoms (Scheme 4.2).

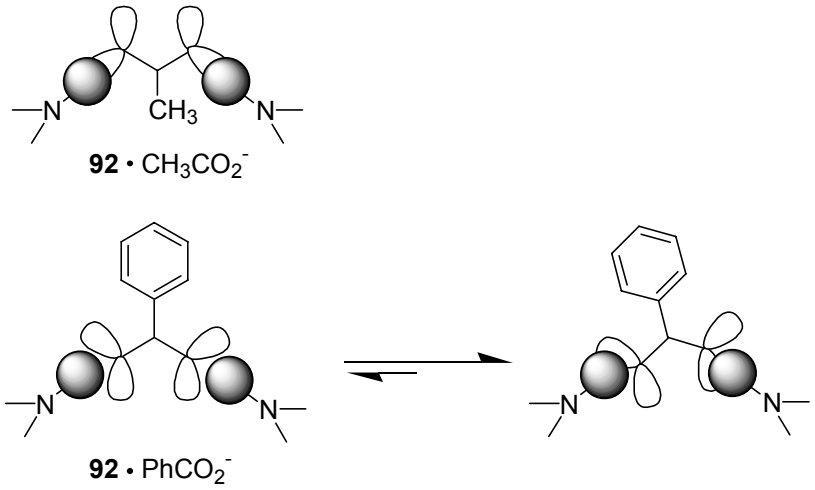

Scheme 4.2 Electron orbital overlap between the pyrrole NH protons and the oxygen atoms of two different carboxylate anions bound by receptor **92**.

In spite of the above "fine tuning" details, it is important to appreciate that both crystal structures reflect the geometry match between **92** and carboxylate anions. Given this nice fit, we ascribe the poor anion affinities displayed by compound **92** (or **91** and **93**) for other anions, such as chloride, to a geometry mismatch between the host and guest. To provide support for this latter explanation, efforts were made to obtain diffraction grade crystals of [**92**·Cl]$^-$ so as to permit an X-ray structural analysis.

Diffraction-grade crystals of the chloride anion complex of **92** were obtained by vapor diffusion of pentane into a dichloromethane solution containing **92** and tetrabutylammonium chloride (1:1 molar ratio). X-ray structural analysis of [**92**·Cl]$^-$ revealed that one of the thiophene rings of the macrocycle was disordered by rotation about the *meso* carbons to which the ring is attached to the macrocycle (the disorder is removed from Figure 4.8 for clarity). The macrocycle adopts a 1,3-alternate conformation in the solid state, with the two bipyrrole units oriented in one direction and the two thiophene units oriented in the opposite direction. One bipyrrole unit is bound to a chloride anion *via* two NH---Cl hydrogen bonds, while another bipyrrole unit is bound to a water molecule *via* two NH---O hydrogen bonding interactions. The bound chloride simutaneously interacts with the bound water molecule *via* one OH---Cl hydrogen bond. Interestingly, two adjacent macrocycles dimerize through a unique hydrogen bond anion-water bridge. A chloride anion hydrogen bonded to one macrocycle is also hydrogen bonded to a water molecule, which is, in turn, hydrogen bonded to the adjacent macrocycle (Figure 4.9). The nitrogen-to-oxygen distances are 2.939(5) and 3.032(5) Å, respectively; the nitrogen-to-chloride distances are 3.207(4) and 3.330(4), respectively; and the oxygen-to-chloride distances are 3.125(5) and 3.312(6). The nitrogen-hydrogen-oxygen angles are 162.8º and 164.3º; the nitrogen-hydrogen-chloride angles are 161.9º and 171.5º; and the oxygen-hydrogen-chloride angles are 143.5º and 156.8º.

a)

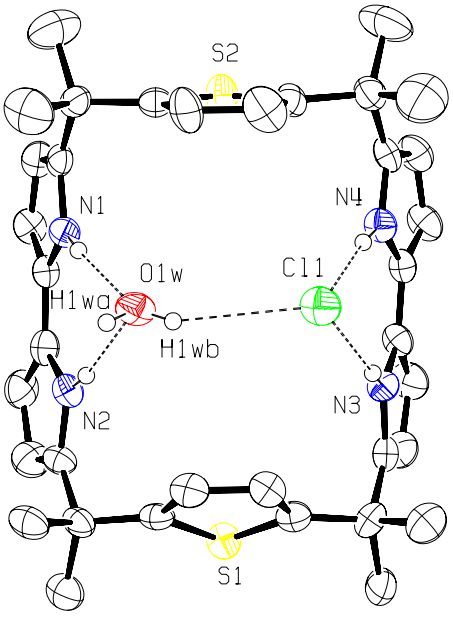

b)

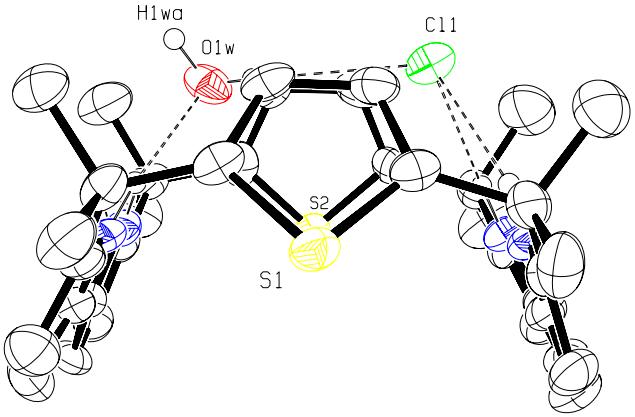

Figure 4.8 Ortep view of the molecular structure of [**92**·Cl]$^-$. a) Top view; b) side view. Displacement ellipsoids are scaled to the 40% probability level. Most hydrogen atoms have been removed for clarity. A disorder involving one of the thiophene rings is also not shown for clarity. Dashed lines are indicative of hydrogen bonding interactions.

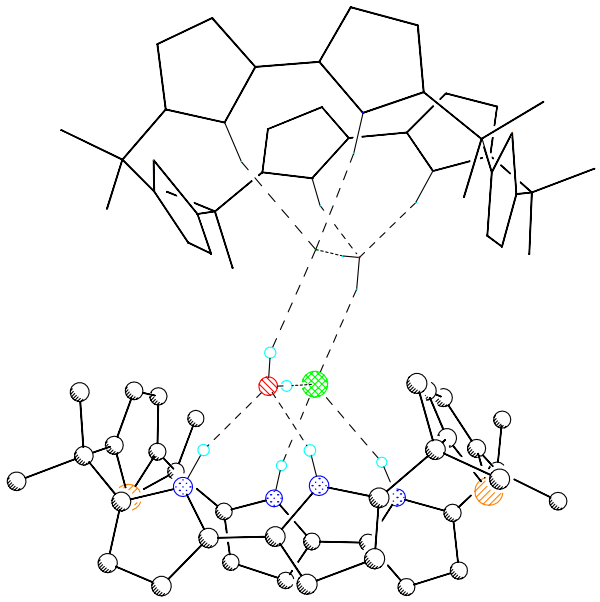

Figure 4.9 View of the molecular structure of [**92**·Cl]$^-$ illustrating the hydrogen bonding interactions between the macrocycle, the chloride anions, and the water molecules. The hydrogen bound complex lies around a crystallographic inversion center at ½, ½, 0. Dashed lines are indicative of hydrogen bonding interactions.

Figure 4.8 and 4.9 highlight the fact that, at least in the solid state, the size and geometry of **92** and chloride anion are poorly matched. This finding, together with the good match seen in the X-ray structures of [**92**·$PhCO_2$]$^-$ and [**92**·CH_3CO_2]$^-$, provide an attractive rationale for the selectivities seen in the solution-phase studies (cf. Table 4.1).

4.6 CONCLUSION

Novel anion receptors **91-93** were successfully synthesized using bipyrrole, furan, and thiophene as novel building blocks. All these new structures were successfully characterized by both standard spectroscopic techniques and X-ray diffraction analysis.

The solution-phase anion binding affinities, as determined by using ^{1}H NMR and ITC titration methods, revealed that compounds **91-93** selectively bind carboxylate anions, such as acetate and benzoate, over other anions such as chloride, bromide, and hydrogen sulfate in acetonitrile. An additional significant finding is that the minor structural perturbation embodied in compound **93** leads to remarkably enhanced anion affinities for chloride, acetate, and benzoate relative to **91** and **92**.

X-ray structural analyses of crystals of the anion complexes [**92**·$PhCO_2$]$^-$, [**92**·$MeCO_2$]$^-$, and [**92**·Cl]$^-$, revealed good size and geometry matching between the receptor (**92**) and the carboxylate anion substrates but poor matching in the case of chloride anion. It also shows that the carboxylate anions are bound to this macrocycle *via* a "cross binding" structural mode, at least in the solid state. Such findings provide a basis for understanding the solution-phase behavior of these macrocyclic anion receptors.

4.7 FUTURE DEVELOPMENTS

The finding that compounds **91-93** selectively bind carboxylate anions has triggered our interest in the design of additional bipyrrole-based macrocycles. Two targets that are similar to molecules **91-93** are systems **94** and **95**. They both use benzene units in place of the furan or thiophene linkers found in **91-93** (Scheme 4.3). As revealed by the anion binding studies detailed earlier in this Chapter, small changes in the structure of a receptor may cause rather big changes in the anion binding properties. We expect that the replacement of the furan (thiophene) linkers in **91-93** by benzene units might bring some interesting results. Furthermore, these benzene units are easy to functionalize (e.g., at the 4 position), which, in turn, may help modify the anion binding properties of the macrocycles. We thus feel that **94** and **95** represent worthwhile targets. A possible approach to their synthesis is shown in Scheme 4.3. Briefly, it is proposed that methods analogous to those used to prepare **91-93** could be exploited to access **94** and **95**. Thus, it is expected that **94** and **95** could be synthesized from bipyrrole and tetramethyl-1,3-phenylenedimethanol **96** and **97**[71] in two steps.

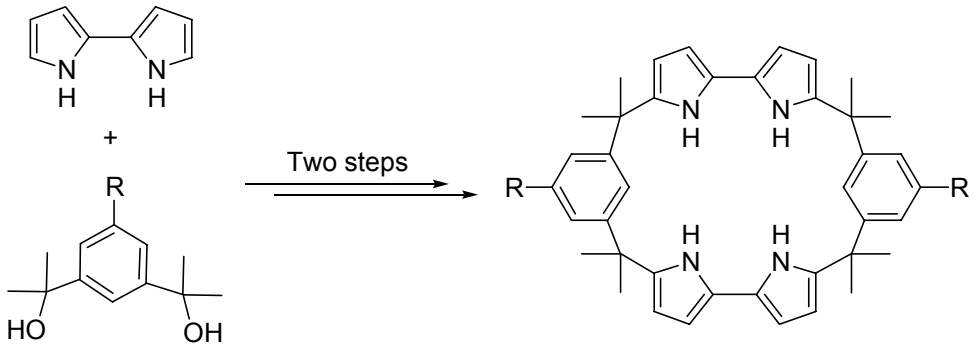

96 R = H

97 R = OCH_3

94 R = H

95 R = OCH_3

Scheme 4.3 Proposed synthesis of target compounds **94** and **95**.

Compound **88** represents another target of interest. Although we have so far not succeeded in synthesizing this compound, its similarity to **91**-**93** means that further effort devoted to its synthesis is justified. The fact that it contains two pyrrole units means that additional NH-based anion binding sites would be available for substrate reconnition. To the extent these pyrroles participate in anion recognition, enhanced binding relative to the corresponding furan or thiophene systems **91**-**93** would be expected.

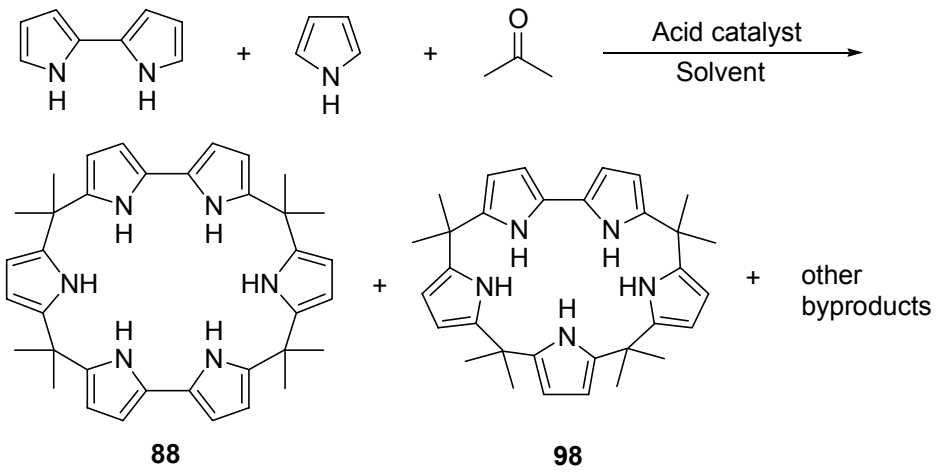

Scheme 4.4 Proposed synthesis of target compounds **88** and **98**.

For the same reason **88** is attractive, we are interested in another target compound, namely **98**, a system that bears structural analogy to sapphyrin. Since the stepwise synthesis of **88** and **98** proved to be difficult (see section 4.1), it is proposed that a mixed condensation between acetone, bipyrrole, and pyrrole might provide a convenient means of synthesizing both compounds *via* a one-pot procedure (Scheme 4.4). Recently, we attempted this mixed condensation reaction in methanol in the presence of methanesulfonic acid. We were able to observe both products *via* mass spectrometric analysis. However, TLC analysis indicated that the yield was very low. Nonetheless, it

is hoped that upon optimization of the reaction conditions, including reactant ratio, catalyst, and solvent, one or both of these targets may be obtained in reasonable yield.

A final target molecule of interest is compound **99**. Again, it is structurally similar to **91-93** but differs from these systems in that it is the product of a formal desulfurization procedure. The desulfurization could potentially be achieved *via* many hydrodesulfurization (HDS) process, such as the use of organometallic clusters under biphasic conditions (Scheme 4.5).[72]

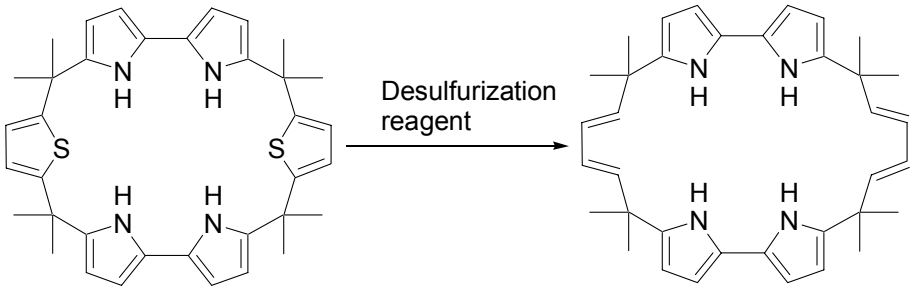

92 **99**

Scheme 4.5 Proposed synthesis of compound **99** from **92** by desulfurization.

Chapter 5: Calix[*n*]bispyrrolylbenzene (*n* = 2, 3, 4): Synthesis, Characterization, and Anion Binding Studies

5.1 INTRODUCTION

In Chapters 3 and 4 we introduced a series of novel calixpyrroles: **70** and **71** based on bipyrrole **72** as the sole building block; and **91-93** based on a mixture of several building blocks, including bipyrrole, furan, and thiophene. The finding that these systems act as highly effective anion binding agents led us to consider the next logical step, namely the use of terpyrrole, **100**[73], as the key pyrrole-containing building block.

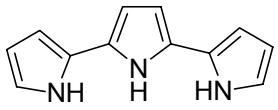

100

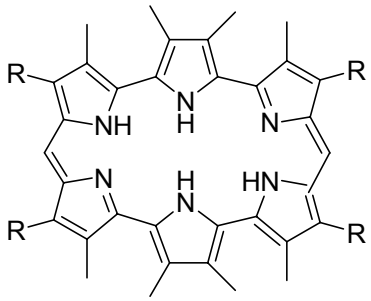

101 R = Et
102 R = Me

Terpyrroles have been used as precursors for the syntheses of amethyrins **101** and **102**.[74] Therefore, our initial thought was that it should be possible to synthesize calix[*n*]terpyrroles (n ≥ 2) from terpyrrole **100** *via* simple condensation with acetone. Unfortunately, to date we have been unable to isolate any stable products from condensation reactions involving terpyrrole **100** and various ketones (e.g., acetone). We thus turned our attention to an alternative precursor **103** that has been used in the synthesis of a fused benzene-containing bisvinylogous porphyrin **104**.[75,76] This building block, or its analogues, were expected to be more stable than terpyrrole **100**. Thus, these

species should represent good precursors for the design and synthesis of novel calixpyrrole systems.

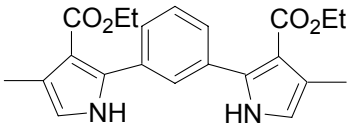

103

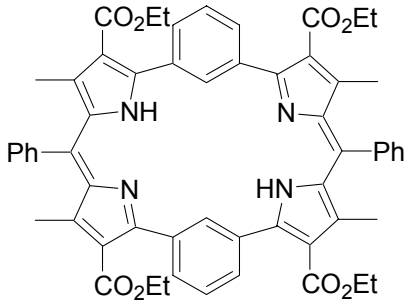

104

5.2 RESEARCH GOAL

Given the above considerations, a series of building blocks **105a-c**, 1,3-bis(pyrrol-2-yl)benzenes (BPBs) were designed based upon precursor **103**. These precursors differ from **103** in that they possess different peripheral substituents. In point of fact, targets **105a-c** bear no substituents on the β-pyrrolic positions other than hydrogen. This choice reflects our experience that the synthesis of calixpyrrole systems from β-substituted pyrrolic precursors is always met with difficulties due to steric effects. On the other hand, the absence of such substituents can lead to problems associated with low solubility in organic media. Therefore, in addition to **105a**, efforts were made to prepare **105b** and **105c** that contain additional solubilizing groups on the 4 position of the phenyl ring.

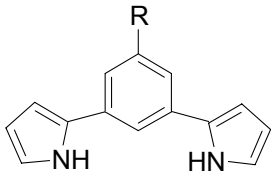

105a R = H
105b R = t-butyl
105c R = n-hexyloxy

With precursors **105a-c** in hand, it was considered likely that calix[*n*]BPBs (*n* = 2-4) **106a-c – 108a-c** could be synthesized *via* a one-pot condensation of **105a-c** with acetone in the presence of an acid catalyst. Macrocyclic homologues with different cavity sizes could then be separated, characterized, and studied for their anion binding potential using the standard techniques described in previous Chapters.

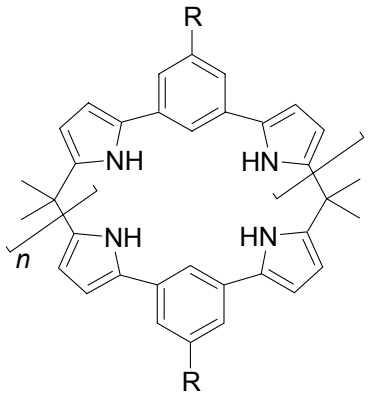

106a-c *n* = 1
107a-c *n* = 2
108a-c *n* = 3

a R = H
b R = t-Butyl
c R = n-Hexyloxy

5.3 SYNTHESIS

5.3.1 Syntheses of Precursors 105a-c

The key 1,3-bis(pyrrol-2-yl)benzene precursors, **105a-c**, were synthesized using a modification of a literature method used to prepare 1,4-bis(pyrrol-2-yl)benzene.[77] Intermediates **109a-b** were obtained from the reaction of the corresponding isophthaloyl chlorides, **110** and **111**, with allylamine and triethylamine in dichloromethane. The ether functionalized system **109c** was obtained *via* the aminolysis of dimethyl-5-hexyloxyisophthalate **112** in the presence of allylamine. Reaction of **109a-c** with phosgene (to give the presumed imino chloride derivatives), followed by immediate reaction with potassium *tert*-butoxide in THF afforded **105a-c** in yields of 29%, 43%, and 96%, respectively. The electron donating groups at the 5-position of the benzene rings are expected to stabilize the intermediate carbocations formed during the reaction, thus accounting for the increased yields observed on passing from **105a** to **105c**.

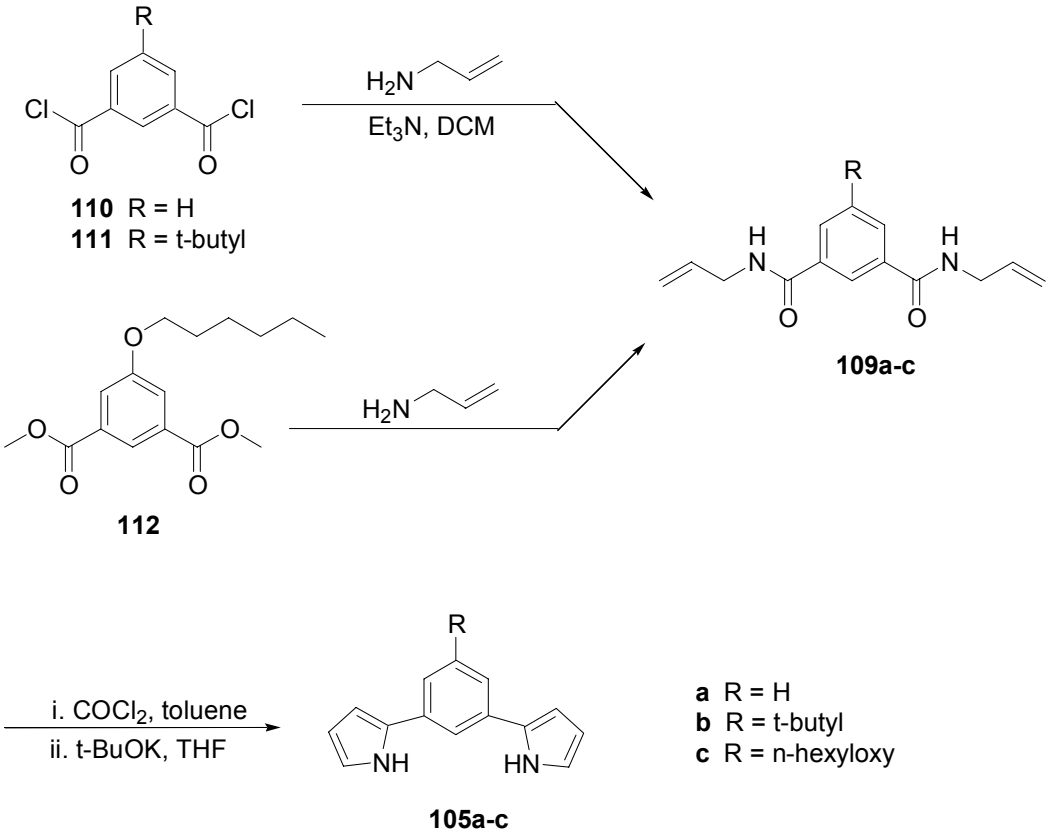

Scheme 5.1 Synthesis of precursor **105a-c**.

5.3.2 Syntheses of Calix[*n*]BPBs (*n* = 2 - 4) 106-108

Our initial goal was to synthesize small-sized calix[2]BPBs **106a-c** without producing the larger homologues **107a-c** and **108a-c**. However, BPBs **105a-c** proved to be less reactive than pyrrole and bipyrrole **72**. Thus condensation of **105a-c** with acetone in methanol in the presence of methanesulfonic acid gave rise to a low yield of **106a-c** even after a long reaction time. When thus resorted to stirring intermediates **105a-c** in acetone overnight in the presence of one equivalent of trifluoroacetic acid, using this procedure we were able to isolate products **106a-c**, **107a-c**, and **108a-c**. Under these reaction conditions, the smaller macrocycles **106a-c** precipitated out of the reaction solution, which may account for their being isolated in higher yield than when methanol is used as a solvent. However, even under these conditions, the larger calix[3]BPBs **107a-**c are the reaction products produced in the highest yield.

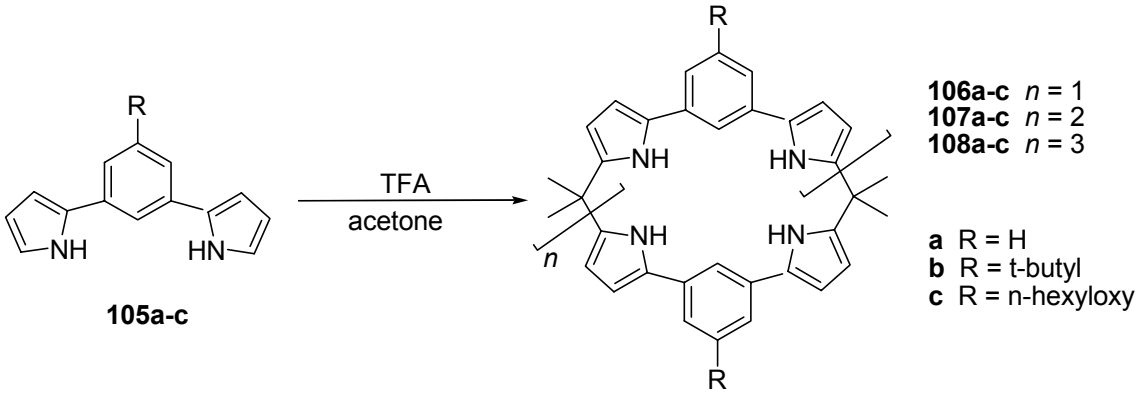

Scheme 5.2 Syntheses of **106a-c – 108a-c** from **105a-c** using a one-pot condensation procedure.

5.4 CHARACTERIZATION

All compounds were characterized by standard spectroscopic techniques including ^{1}H NMR, ^{13}C NMR, and HR-MS. Compounds **105a**-**108a** were also characterized by X-ray diffraction analysis.

Diffraction-grade crystals of **105a** were obtained by slow evaporation of a solution of **105a** in dichloromethane under an atmosphere saturated with hexanes vapor. An X-ray structural analysis of **105a** revealed that the molecule adopts a "*cis*-" conformation in the solid state and contains an internal symmetry plane. Both pyrrole NH donor groups point in towards the center of the resulting cleft (Figure 5.1a) but are twisted out of the plane defined by the benzene ring with N1-C4-C5-C6 torsion angles of 23.48° (c.f., Figure 5.1b). No evidence of π stacking is observed in the packing diagram. However, the possibility of intermolecular NH-π type hydrogen bonding interactions involving the pyrrole-NH protons of one molecule and the benzene π electrons of another can be inferred from this same packing profile (Figure 5.2)

a)

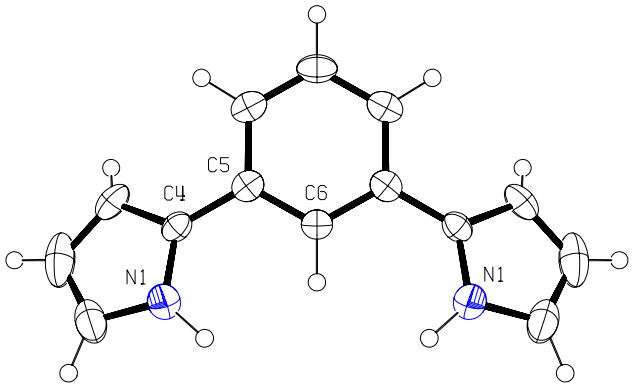

b)

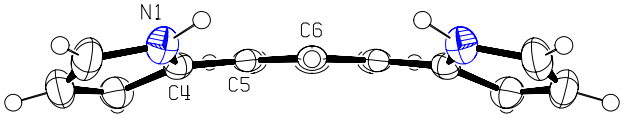

Figure 5.1 Ortep view of the molecular structure of the **105a**. a) Top view; b) side view. Displacement ellipsoids are scaled to the 50% probability level.

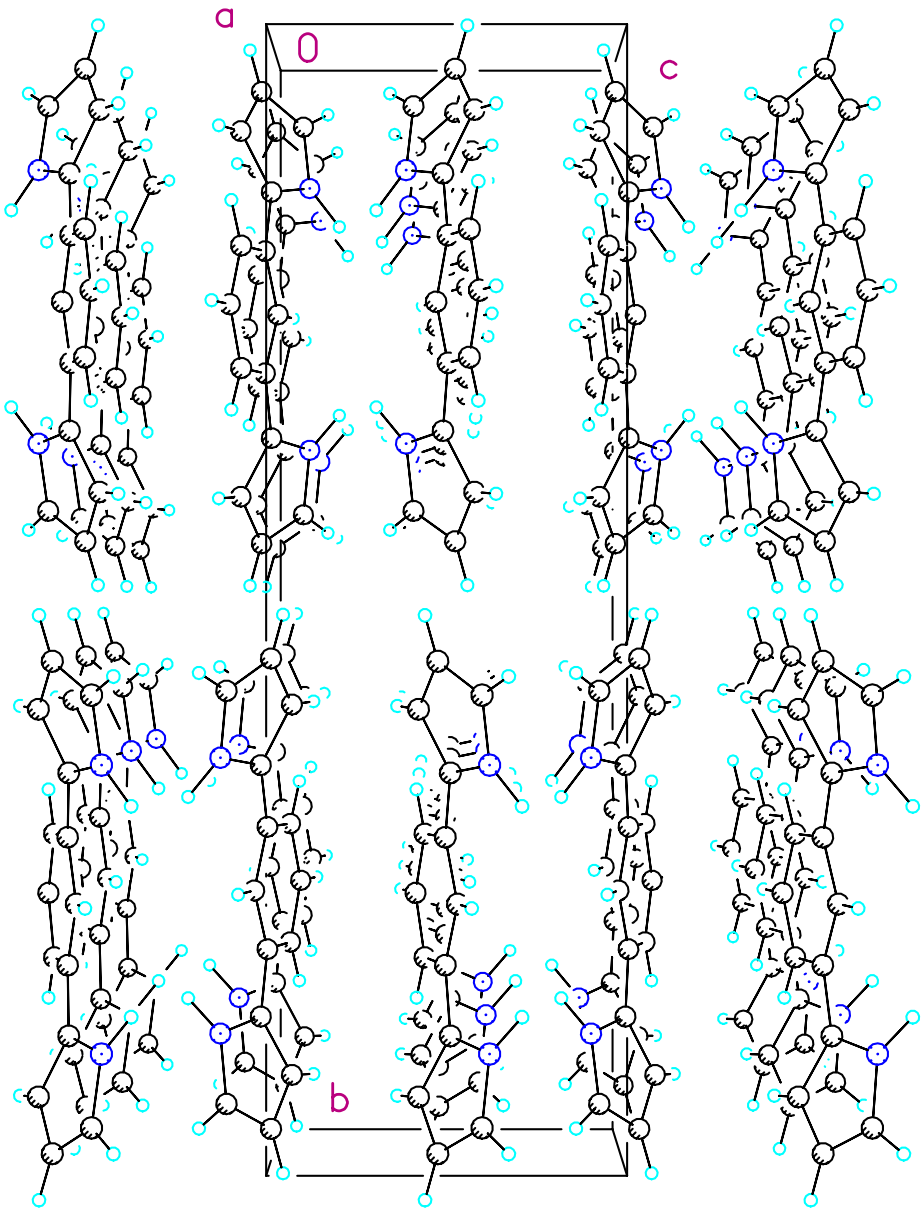

Figure 5.2 Unit cell packing diagram for **105a**. The view is approximately down the **a** axis.

Diffraction grade crystals of **106a**·$2C_3H_6O$ were obtained by slow evaporation of a solution of **106a** in dichloromethane and acetone under an atmosphere saturated with hexanes vapor. X-ray analysis revealed that the molecule adopts a 1,2-alternate (C_{2h}) conformation (Figure 5.3). The two benzene rings, although on opposite sides of the molecule, are nearly coplanar. By contrast, the pyrrolic subunits connected to each of the two *meso*-carbon atoms are tilted out of the plane defined by the benzene rings, hydrogen bonding to one acetone molecule *via* two NH-O hydrogen bonds. Each of the two pyrroles around the bridging *meso*-carbon atoms is hydrogen bonded to one acetone molecule and each pair points to a different side of the plane. The nitrogen-to-oxygen distances are in the range of 3.033(3)-3.122(3) Å, the NH hydrogen-to-chloride distances are in the range of 2.12(3)-2.16(3) Å, and the nitrogen-hydrogen-anion angles are in the range of 167(2)-177(3)º. The X-ray analysis also revealed that this macrocyclic host molecule uses the two sets of pyrroles bound to the two *meso*-carbon atoms, or more precisely, their NH donor subunits, to interact with the bound acetone "guests", rather than the alternative pairing of the pyrrole subunits attached to the two benzene rings.

a)

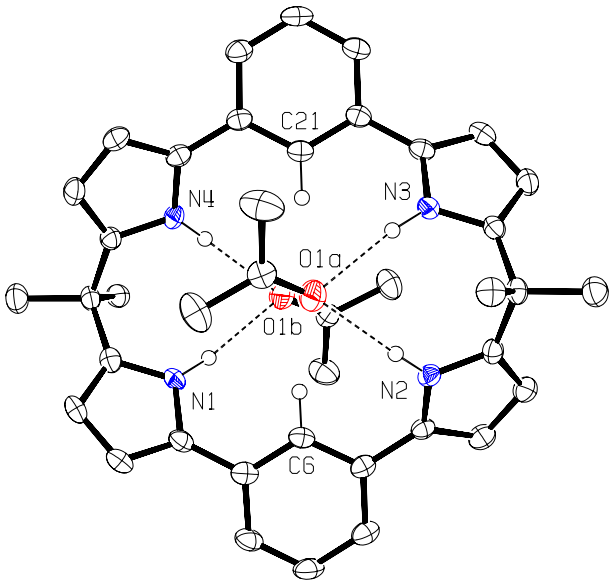

b)

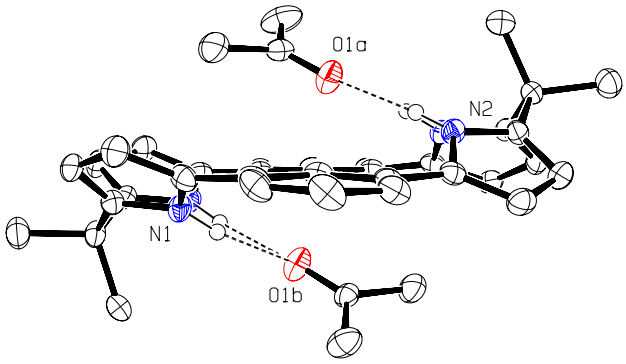

Figure 5.3 Ortep view of the molecular structure of **106a**·$2C_3H_6O$. a) Top view; b) side view. Displacement ellipsoids are scaled to the 50% probability level. Most hydrogen atoms have been removed for clarity. Dashed lines are indicative of NH---O hydrogen bonding interactions.

To date, efforts to obtain diffraction-grade crystals of free **107a** have proved unsuccessful. However, good-quality crystals of [**107a**·PF_6]$^-$ were obtained by slow evaporation of a dichloromethane solution containing **107a** and tetrabutylammomium hexafluorophosphate ($TBAPF_6$) in a 1:1 stoichiometric ratio. The corresponding X-ray analysis revealed a structure without any obvious symmetry (Figure 5.4). However, it also revealed that the PF_6^- anion is bound *via* five major hydrogen bonding interactions. These involve five out of the six possible pyrrole NH donor groups and three out of the six possible fluorine atoms, as determined from the respective hydrogen binding parameters. In particular, these latter nitrogen-to-fluoride bond distances are in the range of 3.263(12)-3.523(12) Å; the NH hydrogen-to-fluorine bond distances are in the range of 2.38-2.63 Å; and the nitrogen-hydrogen-fluorine bond angles are in the range of 165.5-173.8 º. There are two more hydrogen bonds involved in host-guest interactions (N6-H---F6 and N4-H---F1); they show good nitrogen-to-fluorine bond lengths of 3.049(12) Å and 3.318(11) Å, respectively, but poor bond angles of 116.7º and 138.1º, respectively. In contrast to what is seen in the structure of **106a**·2(acetone), in the case of [**107a**·PF_6]$^-$, the two fluoride atoms participating in the hydrogen bonding interact pair-wise with the pyrroles attached to the two benzene rings, as opposed to those attached to the bridging, *meso*-like carbon atoms.

a)

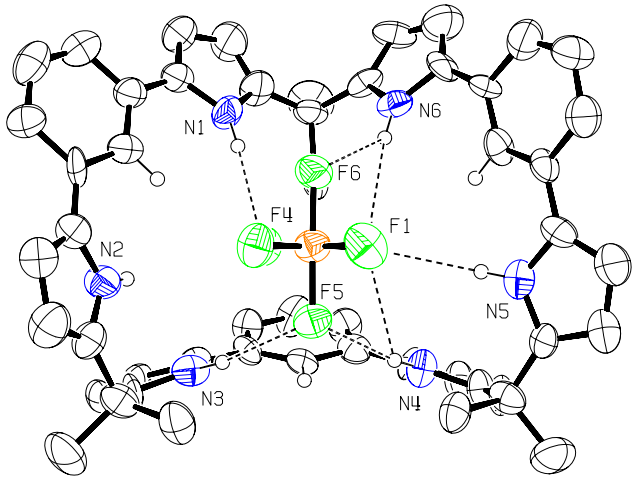

b)

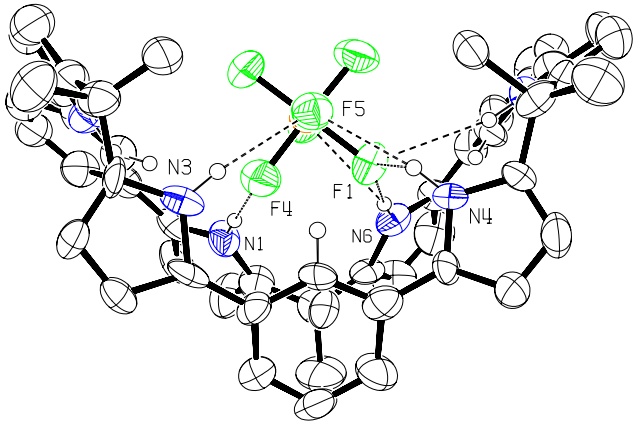

Figure 5.4 Ortep view of the molecular structure of [**107a**·PF_6]$^-$. a) Top view; b) side view. Displacement ellipsoids are scaled to the 30% probability level. Most hydrogen atoms have been removed for clarity. Dashed lines are indicative of NH---F hydrogen bonding interactions.

An X-ray structural analysis of **108a**, studied as **108a**·$(C_4H_8O_2)_4$, revealed that this larger macrocycle adopts a square-shaped conformation (Figure 5.5). In contrast to the conformation of BPB shown in Figure 5.1, in **108a** each BPB adopts a "trans" conformation with both pyrroles pointing away from the center. The four ethyl acetate molecules interact with the macrocycle *via* NH---O (carbonyl) hydrogen bonds. Interestingly, the two pyrroles attached to the *meso* carbon C15 (and C15a) are bound to one ethyl acetate molecule *via* two NH---O hydrogen bonds, while each of the pyrroles attached to the *meso* carbon C30 (and C30a) hydrogen-bond to one ethyl acetate molecule. The latter are also bound to a second pyrrole from another macrocycle. As the result of these interactions, the unit cell packing diagram displays a column-like assembly, as can be seen from an inspection of Figure 5.6.

a)

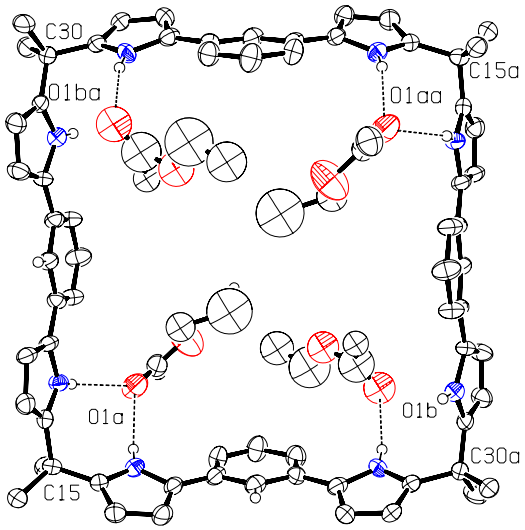

b)

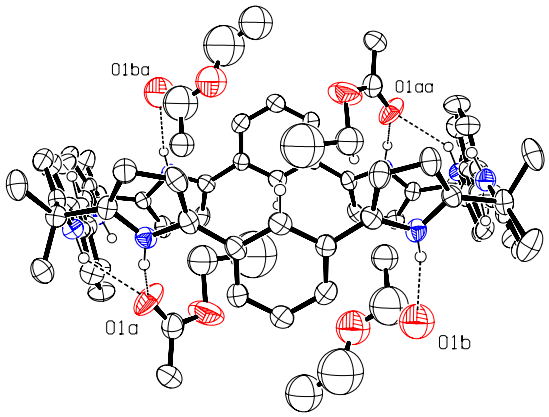

Figure 5.5 Ortep view of the molecular structure of **108a**·$4C_4H_8O_2$. a) Top view; b) side view. Displacement ellipsoids are scaled to the 30% probability level. Most hydrogen atoms have been removed for clarity. Dashed lines are indicative of NH---O hydrogen bonding interactions.

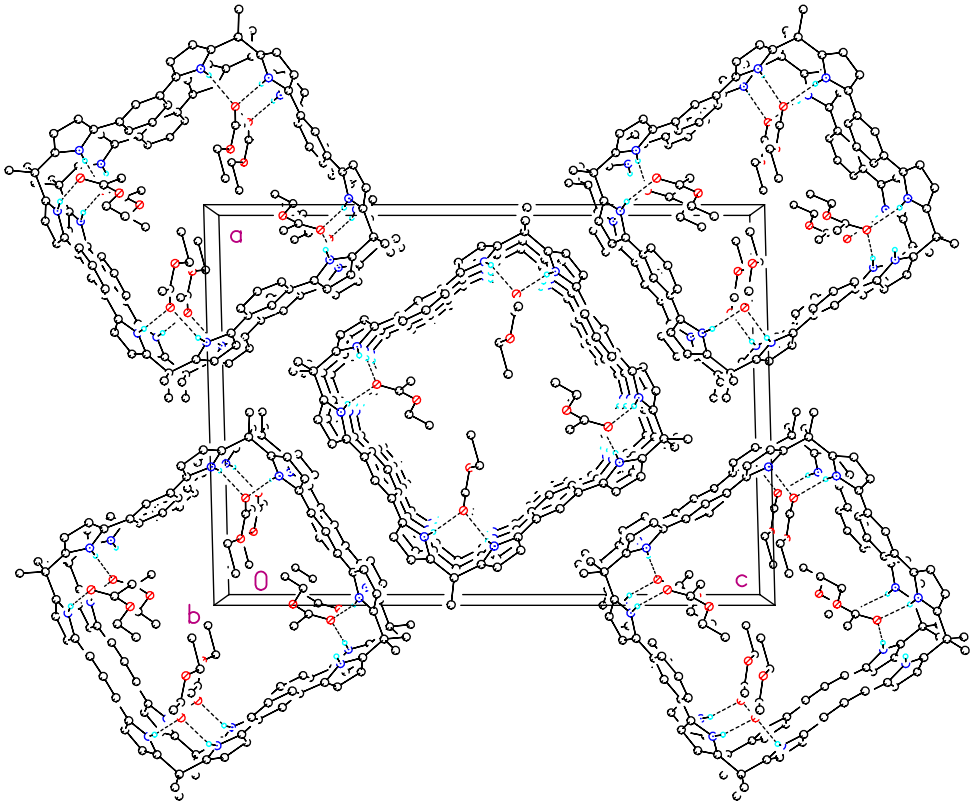

Figure 5.6 Unit cell packing diagram for **108a**·$4C_4H_8O_2$. The view is approximately down the **b** axis.

5.5 ANION BINDING STUDIES

Anion binding studies for compounds **106a-108a** were carried out using standard ^{1}H NMR spectroscopic titrations as well as ITC titrations. These results were then evaluated relative to the parent system **1**. Also, the building block for **106a-108a**, compound **105a**, was used as a control compound for assessing the anion binding properties of these novel anion receptors. The anion binding properties of dimethyl dipyrromethane **113**,[78] which may be considered as the building block for calix[4]pyrrole **1** that is formally analogous to **106a**, were also determined and used to evaluate the performance of **105a**. Diffraction-grade crystals of two anion complexes of compound **106a** and one anion complex of compound **107a** were obtained and studied using X-ray diffraction analysis.

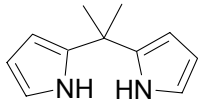

113

5.5.1 ^{1}H NMR and ITC Titration Studies

Due to the poor solubility of compound **106a** in acetonitrile and DMSO, anion binding studies involving compounds **105a-108a**, **1**, and **113** were all carried out in CD_2Cl_2 using standard ^{1}H NMR titration methods. The binding of chloride, hydrogen sulfate, and nitrate anions was also studied in 1,2-dichloroethane (DCE) using ITC titration method.

In the case of the ^{1}H NMR titration studies involving **106a**, the pyrrole NH signals were initially found to broaden beyond the point of clear identification upon the addition of small amounts (~0.1 equiv.) of various halide anions and dihydrogen phosphate anion. The signals then became sharp in the presence of excess anion. Such

broadening was also observed for the benzene 2-CH signal in the case of the halide anions. It was not observed for either signal in the case of HSO_4^-, NO_3^-, and ClO_4^-. However, in all cases, substantial shifts in the CH proton signal corresponding to the 2 position of the BPB benzene ring in **106a** were seen over the full course of the titration, with downfield shifts of between 0.52 and 2.05 ppm being seen, depending on the choice of anion.

Table 5.1 Anion binding constants (M^{-1}) determined by ^1H NMR spectroscopic titrations in CD_2Cl_2.[a]

Anions	**106a**	**107a**	**108a**	**1**	**105a**	**113**
F^-	> 10 000[b]	> 10 000[b]	N.D.	17 000[c]	2 300[b]	2 100
Cl^-	> 10 000	3 100	> 10 000	350[c]	4 300	110
Br^-	> 10 000	390	> 10 000	10[c]	1 100	20
I^-	> 10 000	150	N.D.	< 10[c]	190	< 10
HSO_4^-	> 10 000	780	N.D.	< 10[c]	290	< 10
$H_2PO_4^-$	6 300	1 700	N.D.	97[c]	1 300	310
NO_3^-	> 10 000	5 100	> 10 000	< 10	280	11
ClO_4^-	8 400	30	110	N.D.	30	< 10

[a] Anion used in the assay were in the form of their tetrabutylammonium salts; values are the average of at least three separate measurements and are considered reproducible to ±15%; N.D. not determinable. [b] Tetrabutylammonium fluoride trihydrate was used as the anion source. [c] From ref. 14.

In light of the above observations, the change in chemical shift of the pyrrolic NH resonance of **106a** as a function of anion concentration was used to determine the K_a in

the case of HSO_4^-, NO_3^-, and ClO_4^- (Table 5.1). By contrast, the changes in either the *β*-pyrrolic CH or benzene 2-CH resonances were used to follow the binding process in the case of the halides and dihydrogen phosphate, respectively. In all cases, curve fitting was carried out using standard curve fitting methods (Wilcox 1:1 or Connor 1:1 curve fitting equations, see Appendix A).

The anion binding constants determined for macrocycle **106a** and open-chain control **105a** are given in Table 5.1, along with those recorded previously for **1**. As might be inferred from the broadening of the NH peaks seen in many of the NMR titrations, compound **106a** was found to be a very effective anion receptor. In fact, with the exception of dihydrogen phosphate and perchlorate, for which K_a values of 6,300 and 8,400 M^{-1}, respectively, were recorded, in all cases the anion affinities proved too large to measure accurately by ^1H NMR spectroscopic methods. This stands in marked contrast to what is seen in the case of **1**, where strong binding is seen only in the case of fluoride anion and no appreciable binding is seen in the case of perchlorate. Interestingly, the open-chain control system **105a** was also found, as a general rule, to be a more effective anion receptor than both **1** and its building block **113**, although in most cases it is far less selective.

Table 5.1 also shows that, compared to **106a**, the larger macrocyclic receptor **107a** is overall a less effective anion receptor, at least for all the anions included in this study. Presumably, this finding reflects the overly large nature of the cavity, as well as its relatively rigid structure. Based on simple CPK model studies the large cavity size is not compatible, in terms of size, with most of the anions of interest. Likewise, the rather rigid structure (close to triangular shape) limits its ability to adopt different conformations, as might be necessary to coordinate anions of different sizes and shapes. Interestingly, in spite of such considerations, **107a** shows the highest binding affinity for

nitrate, an anion that is traditionally a weak hydrogen bonding acceptor. This selectivity, we believe, reflects the better size and geometry matching between receptor **107a** and this triangular anion relative to other anions.

Proton NMR spectroscopic titration studies of compound **108a** failed to give reliable binding constants for F^-, I^-, HSO_4^-, and $H_2PO_4^-$ due either to a broadening of the signals used to trace the anion binding process (F^-, HSO_4^-, and $H_2PO_4^-$) or difficulties in fitting of the binding curve (I^-). On the other hand, except for the weak binding affinity seen for perchlorate anion, macrocycle **108a** binds the remaining anions of interest (Cl^-, Br^-, and NO_3^-) more strongly than **107a**. Compared to **107a**, compound **108a** has a larger macrocyclic size, which should be even less compatible with most anions. However, like calix[4]bipyrrole **71**, the square-shaped macrocycle **108a** is more flexible than the triangle-shaped macrocycle **107a**; this conformational flexibility may permit the macrocycle to adopt conformations that are better suited for accommodating the targeted anions, particularly in less polar solvents such as dichloromethane.

Because of the limitations inherent in the NMR spectroscopy-based titration methods, efforts were made to determine the anion affinities of these compounds *via* other, more sensitive means. Unfortunately, the lack of a spectroscopic "handle" in **105a-108a** meant that no useful binding information could be obtained from UV-vis or fluorescence titration experiments. On the other hand, it was found that reliable isothermal titration calorimetry (ITC) measurements could be carried out in 1,2-dichloroethane.

Table 5.2 tabulates the binding constants for compounds **105a-108a**, **113**, and **1** and several anions, including Cl^-, HSO_4^-, and NO_3^-. Compound **106a** shows the highest anion affinities for all three anions compared to the other anion receptors. However, it does not display good anion selectivity. Compound **107a** displays selective binding to

Cl^- over HSO_4^- and NO_3^- in DCE; this differs from the selectivity towards NO_3^- observed in dichloromethane. This exemplifies how the selectivity of an anion receptor can change as the result of a change in the solvent. It also stresses the importance specifying the solvent system when discussing the anion selectivity of a given receptor. Compound **108a** shows higher anion affinities compared to **107a**, albeit ones that are lower than those of **106a**. Compounds **106a-108a** all display higher anion affinities than does **1**. Likewise, the building block from which they are constructed, **105a**, also binds chloride anion more strongly than the building block for **1**, **113**. These findings are consistent with the results from the ^1H NMR titration studies.

Table 5.2 Anion binding constants derived from ITC titrations carried out in 1,2-dichloroethane.[a]

Anions	**106a**	**107a**	**108a**	**1**	**105a**	**113**
Cl^-	5 600 000	82 000	240 000	18 000	6 800	[b]
HSO_4^-	1 200 000	11 000	76 000	[b]	[b]	[b]
NO_3^-	2 500 000	3 800	220 000	[b]	b	[b]

[a] Anion used in the assay were in the form of their tetrabutylammonium salts; values are the average of at least three separate measurements and are considered reproducible to ±15%. [b] Value too low to be determined reliably.

5.5.2 X-ray Diffraction Analysis

Solution-phase studies showed that compound **106a** binds most anions strongly in both dichloromethane-d_2 (^{1}H NMR) and 1,2-dichloroethane (ITC). Compound **107a** displays the highest affinity for nitrate in dichloromethane-d_2, albeit not in 1,2-dichloroethane. These and other selectivity issues were difficult to rationalize a prior. Therefore, like in chapters 3 and 4, we sought to carry out solid-phase structural studies to shed light on the host-guest interactions.

Diffraction-grade crystals of the chloride anion complex of **106a** were grown by slow evaporation of a dichloromethane solution containing **106a** and tetrabutylammonium chloride in a 1:1 stoichiometric ratio. X-ray structural analysis revealed that **106a** adopts a cone-shaped (or V-shaped, C_{2v}) conformation in the solid state, with the four pyrrole NH protons involved in hydrogen bonding interactions to the chloride ion (Figure 5.7). The nitrogen-to-chloride bond distances are in the range of 3.306(3)-3.401(3) Å, while the corresponding NH hydrogen-to-chloride distances range between 2.37(3) and 2.58(2) Å. The nitrogen-hydrogen-chloride angles are in the range of 169-177º. As a result, the chloride ion resides 1.377(4) Å above the N_4 root-mean-square plane of the core of **106a**. The distances between the CH protons (C6*H* and C21*H* of benzene rings) and the bound chloride anion are 2.588 Å and 2.721 Å, respectively, while the corresponding carbon-hydrogen-chloride angles are 157.88º and 162.60º. These parameters are within the range expected for hydrogen bonding interactions, leading to the consideration that these CH protons may also be acting to stabilize the bound chloride anion. This proposal leads, in turn, to the suggestion that these CH protons could be used to trace the anion binding properties of this receptor *via* solution-based ^{1}H NMR titration means.

a)

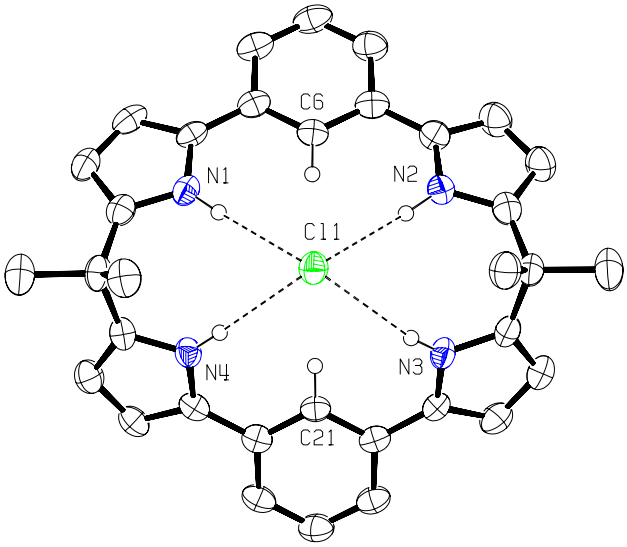

b)

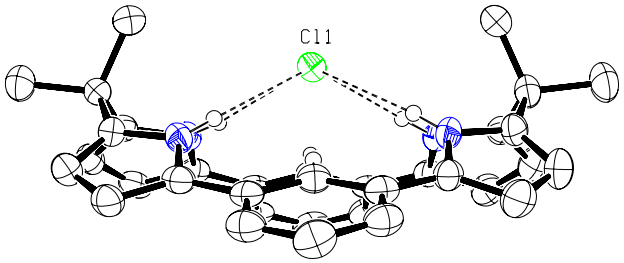

Figure 5.7 Ortep view of the molecular structure of [**106a**·Cl]$^-$. a) Top view; b) side view. Displacement ellipsoids are scaled to the 50% probability level. Most hydrogen atoms have been removed for clarity. Dashed lines are indicative of NH---Cl$^-$ hydrogen bonding interactions.

In order to understand why compound **106a** binds some weak hydrogen bond acceptors, such as nitrate anion, so strongly in dichloromethane-d_2 and 1,2-dichloroethane, efforts were made to obtain single crystals of the nitrate anion complex of **106a**. Such crystals were also obtained *via* slow evaporation of a dichloromethane

solution containing **106a** and tetrabutylammonium nitrate (1:1 molar ratio). Again, the macrocycle adopts a cone-like conformation in the solid state with the nitrate anion being bound through four NH---O hydrogen bonds (Figure 5.8). In contrast to what is seen in the crystal structure of [**106a**·Cl]$^-$, where the four pyrrolic NH protons are hydrogen bonded to the single bound chloride anion, in the crystal structure of [**106a**·NO_3]$^-$ two of the three nitrate anion oxygen atoms are involved in hydrogen bonding interactions: one oxygen (O2a) is bound to three NH protons (N1*H*, N2*H*, and N4*H*); another oxygen (O1a) is bound to one NH proton (N3*H*). The nitrogen-to-oxygen distances are in the range of 2.956(2) – 3.405(3) Å; the NH proton-to-oxygen distances are in the range of 2.09(3) – 2.56(3) Å; and the nitrogen-hydrogen-oxygen bond angles are in the range of 159(2) – 175(2)º. This "two point" binding mode, rather than the "one-point" binding mode displayed in the crystal structure of [**106a**·Cl]$^-$, provides an appealing rationale for the finding that compound **106a** binds nitrate anion, a weak hydrogen bonding acceptor, and chloride, a strong hydrogen bonding acceptor, with comparable affinities in both dichloromethane and 1,2-dichloroethane. A similar explanation may be invoked to rationalize the relatively high binding affinity that **106a** displays towards perchlorate anion, an even weaker hydrogen bonding acceptor in dichloromethane. The same kind of binding behavior as displayed by **106a** is not likely to occur in the case of the smaller calix[4]pyrroles such as **1**, and, in fact, there is no evidence of such binding modes in the large number of solid-state structures reported for these latter systems.

a)

b)

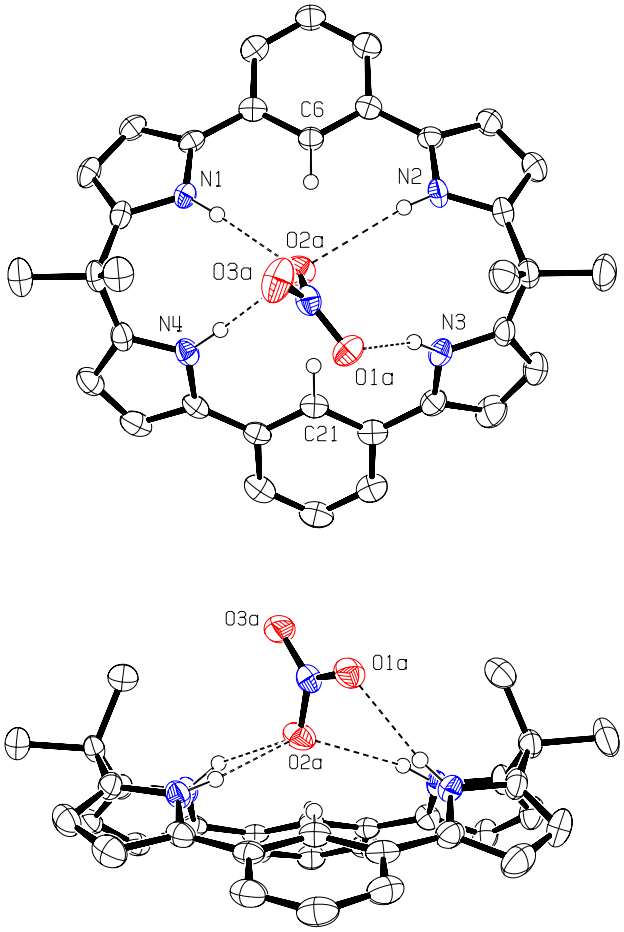

Figure 5.8 Ortep view of the molecular structure of [**106a**·NO_3]$^-$. a) Top view; b) side view. Displacement ellipsoids are scaled to the 50% probability level. Most hydrogen atoms have been removed for clarity. Dashed lines are indicative of NH---O hydrogen bonding interactions.

The crystal structures of these anion complexes of **106a**, in conjunction with that for **106a**·2(acetone), confirm that macrocycle **106a** can adopt different conformations in the solid state and display different binding modes when interacting with different substrates. This leads us to suggest that it could be a versatile host and one that might be

endowed with a degree of inherent selectivity based, precisely because different substrates, solvents, etc. could serve to modulate this conformational flexibility.

Solid-state studies on the anion complexes of **106a** inspired us to try growing crystals of **107a** complexed with different anions, such as nitrate, chloride, and perchlorate. Diffraction-grade crystals of [**107a**·NO_3]$^-$ were successful grown using methods analogous to those used to obtain crystals of [**106a**·NO_3]$^-$. Resulting structure reveals that the macrocycle adopts a V-shaped conformation (C_s), with four out of its six pyrrole NH protons bound to a nitrate anion *via* four NH---O hydrogen bonds (Figure 5.9). In contrast to what may seen for [**106a**·NO_3]$^-$, in [**107a**·NO_3]$^-$ all three oxygen atoms of the nitrate anion are involved in hydrogen bonding interactions with the receptor in the solid state. These hydrogen bonds include N1-H---O3b, N3-H---O1b, N4-H---O1b, and N6-H---O2b interactions. The two remaining pyrrole units are not involved in any hydrogen bonding interactions with the bound anion. The nitrogen-to-oxygen distances are in the range of 3.107(4) – 3.304(3) Å; the NH proton-to-oxygen distances are in the range of 2.32(3) – 2.51(2) Å; and the nitrogen-hydrogen-oxygen bond angles are in the range of 167(3) - 172(3) º.

a)

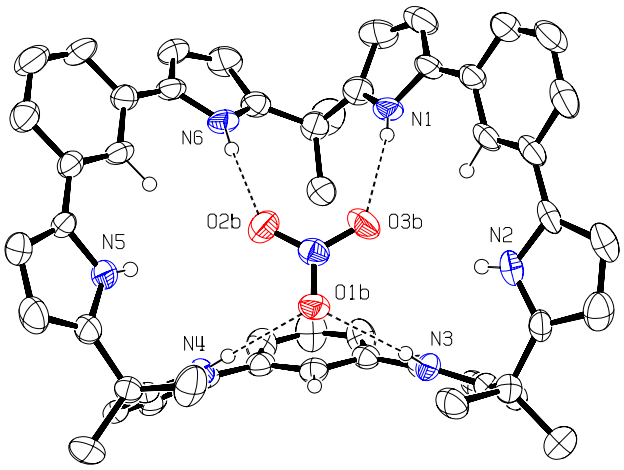

b)

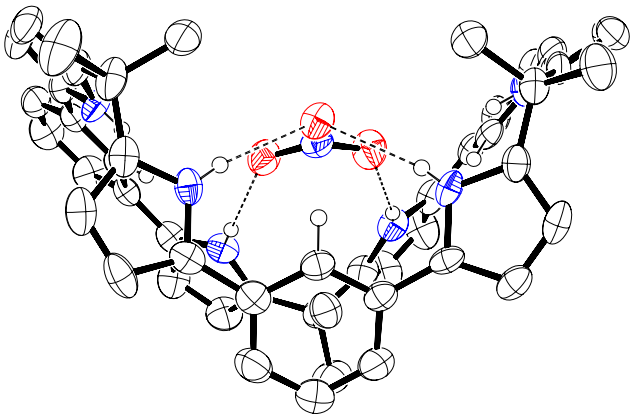

Figure 5.9 Ortep view of the molecular structure of [**107a**·NO_3]$^-$. a) Top view; b) side view. Displacement ellipsoids are scaled to the 50% probability level. Most hydrogen atoms have been removed for clarity. Dashed lines are indicative of NH---O hydrogen bonding interactions.

Further comparison of the crystal structure of [**107a**·NO_3]$^-$ with that of [**107a**·PF_6]$^-$, reveals that in both cases not all of the pyrrole units are involved in hydrogen bonding interactions with the bound anions. This finding is consistent with the results from the solution-phase studies, which show that **107a** is a less effective anion receptor than **106a**. This binding behavior, as previously discussed, may be ascribed to the relative large, less flexible cavity revealed by the solid-state structure of **107a**.

5.6 CONCLUSION

BPBs **105a-c** were successfully applied as building blocks for the synthesis of a series of novel calixpyrrole-like anion receptors. Compound **106a** shows high binding affinities for many anions of interest, a finding that was further supported by ITC studies carried out in 1,2-dichloroethane. Compound **107a** shows selective binding to nitrate in dichloromethane-d_2, while ITC studies in DCE revealed selective chloride anion binding. Proton NMR spectroscopic titrations carried out in dichloromethane-d_2 proved to be an ineffective means of probing the anion binding properties of **108a**. However, ITC studies carried out in DCE revealed that **108a** displays anion affinities that are larger than those of **107a** but smaller than those of **106a**.

X-ray structural analysis on several anion complexes of **106a** and **107a** strongly supported the solution-phase results that these novel anion receptors could adopt different conformations in the solid state to accommodate anions bound within the molecular cavities. Presumably, this ability accounts for the stronger anion affinities seen for most anions of interest compared to the parent system **1**.

A further comparison between **105a**, the building block for **106a-108a**, and **113**, the building block for **1**, revealed that the former shows higher anion affinities to all anions than does the latter, revealing that the inherent anion binding properties of **105a** play an important role in defining the higher anion binding abilities shown by **106a-108a** relative to **1**.

5.7 FUTURE DEVELOPMENTS

Future studies in this area could focus on several logical extensions based on the present target molecules. Here, one goal would be to improve the solubility of the basic structure of **106a** in solvents other than the chlorinated ones used to date. This could be done by introducing more solubilizing groups to the benzene rings, as shown by structures **114** and **115**. Anion binding properties of these "soluble" receptors could be studied in more polar solvents, such as acetonitrile and DMSO. Anion transport studies would also be of interest since these kinds of anion receptors are expected to be effective anion transporting agents.

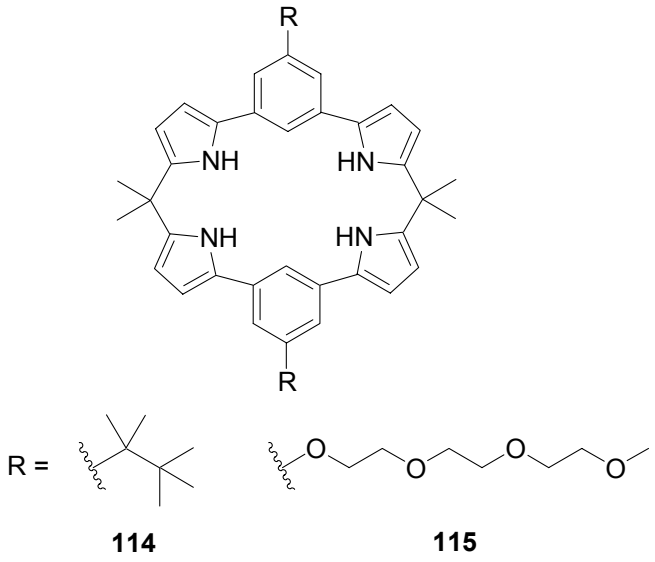

114 **115**

Another goal is to understand the binding behavior of **108a** in the solid state, which may help us understand why such a big, flexible molecule displays high anion affinities to small anions such as chloride anion. Crystals of anion complexes of **108a**, which have so far unattainable, may be accessible using different derivatives and different crystal growing techniques. To the extent this objective can be attained, follow-

up X-ray diffraction analysis is expected to provide useful information about anion binding in the solid state.

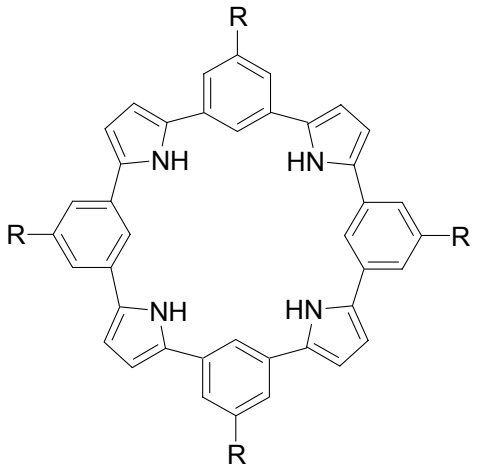

116 R = t-Butyl
117 R = n-Hexyl

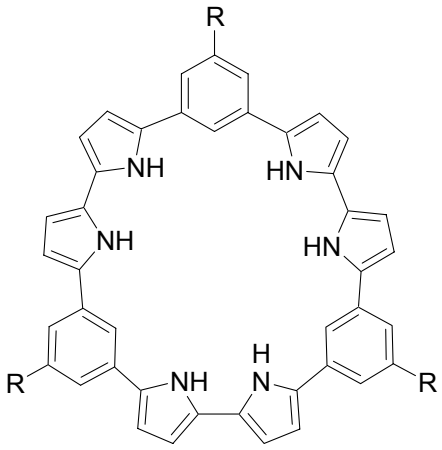

118 R = t-Butyl
119 R = n-Hexyl

The strong anion binding abilities shown by **106a-108a** provide an inspiration to design additional macrocyclic anion receptors. Systems **116-119**, based on building blocks **105b-c**, look particularly attractive. Here, building on what we have learned to date, we propose to exclude **105a** from consideration as a possible building block, due to solubility concerns. Target compounds **116** and **117** bear analogy to the cyclo[*n*]pyrrole,[79,80] but unlike these latter species cannot exist in a fully conjugated form. Nonetheless, the neutral, nearly planar core structure of **116** and **117** might allow these macrocycles to display special anion binding properties, provided, of course, that they can be prepared. Target compounds **118** and **119** are also neutral macrocycles with even larger core sizes than **116** and **117**. Interestingly, their core structures contain two different kinds of anion binding units, specifically bipyrroles and BPBs; this might lead

to interesting anion binding properties. Needless to say, synthesis of these novel macrocycles will be a great challenge.

The retro synthesis of compound **116** (also applicable to **117)** shows two possible synthetic methodologies for the target compound (Scheme 5.3). The direct approach shown on the left of Scheme 5.3 includes a Suzuki coupling of the bisbromo-BPB precursor **120**, a key intermediate that can be synthesized from **105b**, and diboronic acid **121**, which could be obtained from the corresponding dibromobenzene. The masked strategy shown on the right of Scheme 5.3 relies on an approach analogous to that used by Kohnke for the synthesis of calix[*n*]pyrroles.[49,50] Specifically, the corresponding macrocycle **122**, which contains four furanyl and four phenyl rings connected in an alternating manner, will be synthesized first using either Suzuki coupling or Stille coupling methods. Compound **116** will then be synthesized from **122** in three steps following Kohnke's methodology.

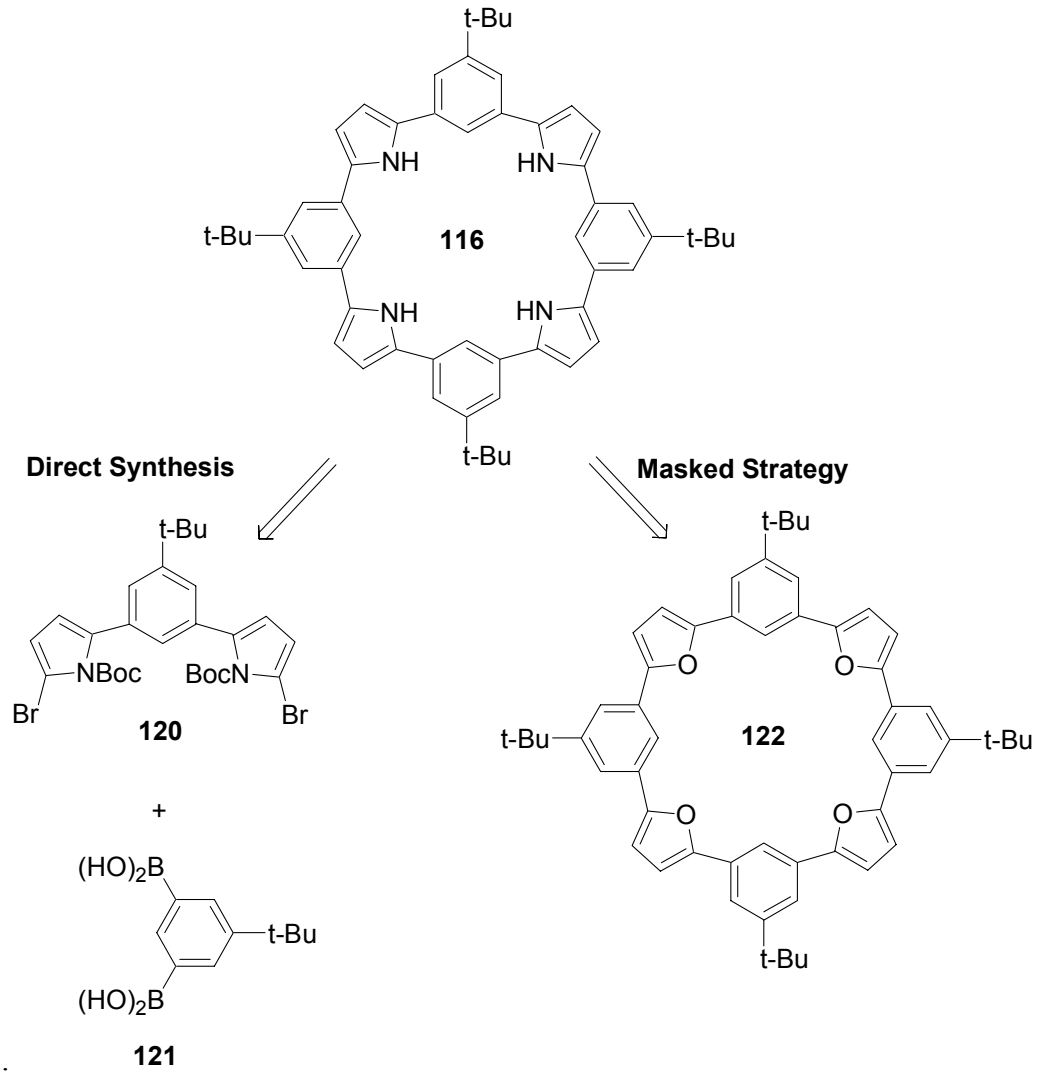

Scheme 5.3 Retro synthesis of target compound **116**.

The retro synthesis of **118** is shown in Scheme 5.4. In analogy to what is expected to be true for **116**, target compound **118** (as well as **119**) might be synthesized using two coupling strategies: Suzuki coupling and oxidative coupling. The former is expected to rely on the Suzuki coupling of the Boc-protected bisbromo-bipyrrole precursor, **123**, an intermediate that can be synthesized from bipyrrole **72**, and diboronic

acid **121**. By contrast, the oxidation-based strategy relies on oxidative coupling of **105a** using the same metal salt-based approach used to prepare cyclo[8]pyrrole and its congeners.

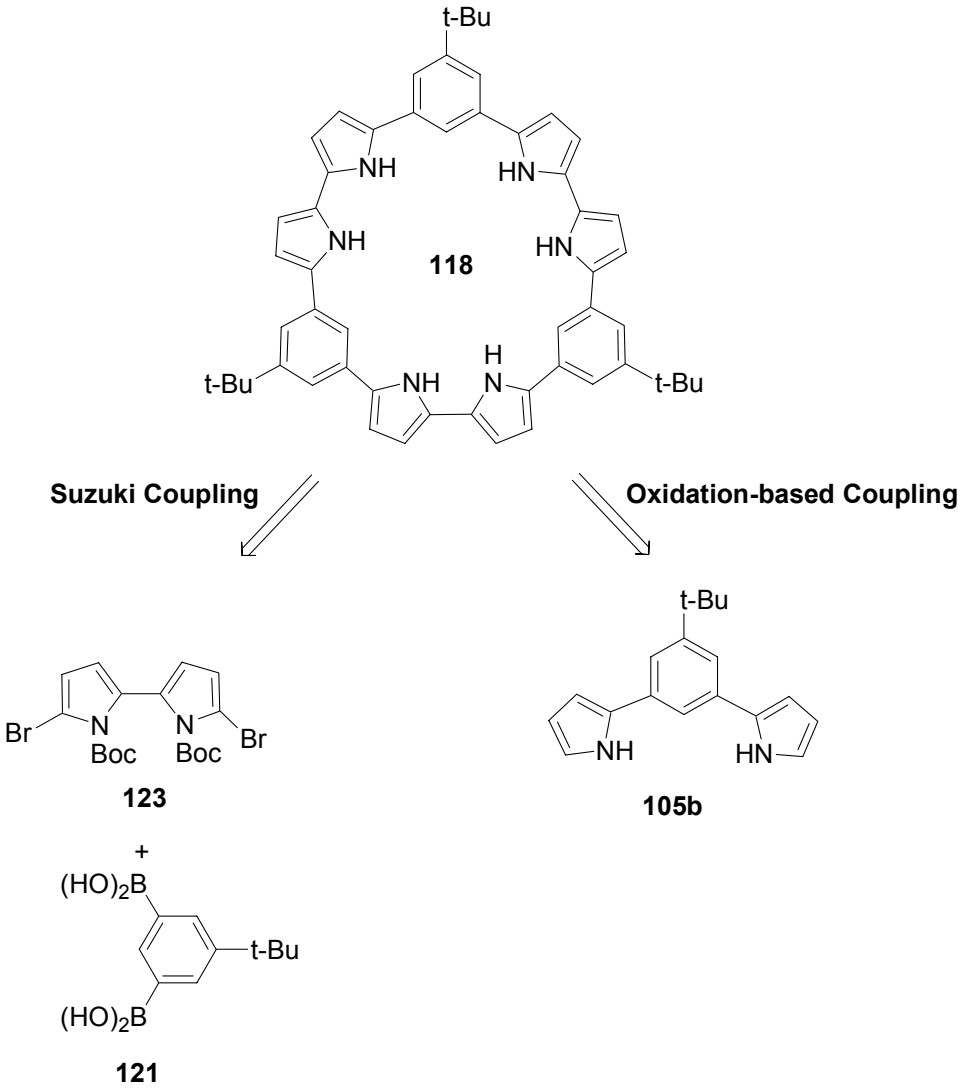

Scheme 5.4 Retro synthesis of target compound **118**.

5.8 SUMMARY AND GENERAL OUTLOOK

In this dissertation, a series of novel calixpyrrole-like anion receptors were introduced. Similar to calix[*n*]pyrrole-based (n ≥ 4) anion receptor, these macrocyclic receptors bind anionic substrates based on the use of acidic pyrrole NH protons as hydrogen bonding donors. However, different from the former ones, these receptors were constructed using heterocycles other than pyrroles as building blocks, such as bipyrrole, bispyrrolylbenzenes, furan, and thiophene. Furthermore, they bear cavities of larger sizes and different shapes than calix[4]pyrroles, thus leading to their different anion binding properties than the latter species. These worthwhile explorations expand the territory of normal calix[*n*]pyrrole anion binding chemistry.

Future developments of thses kinds of anion receptors have been discussed in each Chapter, and therefore the details will not be included here. Generally, further research need to focus on two directions. One is to continue designing and synthesizing new macrocyclic receptors based on new construction units or a combination of several building blocks that have already been used in this area. The other is to improve the anion binding properties of the already-made anion receptors, using the methods that have been introduced in Chapter 1, or newer methods. The ultimate goal is to put these macrocyclic anion receptors to practical uses, which is being pursued hard in this group presently.

Chapter 6: Experimental Section

6.1 GENERAL EXPERIMENTAL

6.1.1 Solvents

Solvent for reaction: Acetonitrile was dried by passage through two columns of molecular sieve. Dichloromethane was dried by distillation under argon over calcium hydride. Methanol was dried by passage through two columns of molecular sieve. Tetrahydrofuran (THF) was dried by passage through two columns of activated alumina.

NMR solvents: Acetonitrile-d_3 was purchased in bottles from Cambridge Isotope Inc. and dried by molecular sieve (4A). Chloroform-d_1 was purchased in bottles from Cambridge Isotope Inc., and used after passage through a small column of basic alumina to remove the small amount of acid contained in solvent. Dichloromethane-d_2 was purchased in individual ampules from Cambridge Isotope Inc., and used after passage through a small column of basic alumina to remove the small amount of acid contained in solvent.

ITC solvents: Acetonitrile (HPLC grade, water% 0.002), 1,2-dichloroethane (DCE, Certified ACS grade, water% 0.003) and DMSO (Certified ACS grade, water% 0.03) were purchase from Fisher Scientific International Inc. and used as received.

6.1.2 Reagents

Tetrabutylammonium chloride was purchased from Fluka, Inc. and dried under vacuum at 40°C for 24 h before use. All other reagents were obtained from commercial sources and used as received. Thin layer chromatography was performed on silica TLC plates (Sorbent Technologies; layer thickness 200μm). Column chromatography was carried out on silica gel (Scientific Adsorbents Inc.; particle size 32-63 μm).

6.1.3 Instruments

Melting points were measured on a Mel-Temp II device and not corrected. ^{1}H and ^{13}C NMR spectra used in the characterization of product and titration studies were recorded on Varian Unity 400 MHz or 500 MHz spectrometers. Low resolution FAB and CI mass spectra were obtained on a Finningan MAT TSQ 70 mass spectrometer. High resolution FAB and CI mass spectra were obtained on a VG ZAB2-E mass spectrometer. Microcalorimetric titration studies were performed using an Isothermal Titration Calorimeter (ITC) purchased from Microcal Inc., MA.

6.2 EXPERIMENTAL DETAILS

β-Octachloro-*meso*-octamethylcalix[4]pyrrole 65

3, 4-Dichloropyrrole 69 (0.5 g, 3.7 mmol) was dissolved in dry dichloromethane (100mL), and the solution was degassed with Ar for 10 minutes. After acetone (0.22 g, 3.7 mmol) was added and the reaction mixture was stirred for another 10 minutes, boron trifluoride diethyl etherate (0.26g, 1.8 mmol) was added, and the reaction mixture was left stirring overnight at room temperature. After the reaction was quenched with saturated aqueous sodium bicarbonate, the organic layer was washed with water and brine, and dried over magnesium sulfate. Evaporation of the solvent under reduced pressure yielded a white solid. Flash chromatography (silica gel, dichloromethane-hexanes 3:7 v/v) afforded 65 as a white solid (0.36 g, 56%). ^{1}H NMR (500 MHz, $CDCl_3$, 25˚C) δ 1.80 (s, 24H, CH_3), 7.14 (s, 4H, NH). ^{13}C NMR (125 MHz, $CDCl_3$, 25˚C) δ 25.14, 37.29, 109.45, 127.54. HRMS (CI^+) *m*/*z* (M^+) calcd for $C_{28}H_{28}Cl_8N_4$: 699.9822, found: 699.9811.

β-Monofluoro-*meso*-octamethylcalix[4]pyrrole 66

Calix[4]pyrrole **1** (100 mg, 0.23 mmol) was dissolved in dry THF (20 mL). N-fluoropyridinum triflate (70 mg, 0.28 mmol) was then added to the solution. The reaction mixture was stirred for 0.5 h at 60 ˚C under Ar. The solvent was then evaporated off. The residue was purified by column chromatography (silica gel, dichloromethane-hexane 1:1). The fraction displaying an R_f value of 0.53 on TLC (silica, eluent: dichloromethane-hexane 1:1 v/v; the starting material **1** has an R_f = 0.50.) was isolated (15 mg, 15%). ^{1}H NMR (500 MHz, CD_2Cl_2, 25˚C) δ 1.45 (s, 6H, CH_3), 1.51 (s, 12H, CH_3), 1.54 (s, 6H, CH_3), 5.71 (d, 1H, pyrrole CH), 5.92-5.86 (m, 6H, pyrrole CH), 6.41

(s, 1H, NH), 6.99 (s, 1H, NH), 7.16 (s, 1H, NH), 7.25 (s, 1H, NH). ^{13}C NMR (125 MHz, CD_2Cl_2, 25˚C) δ 28.35, 28.37, 28.83, 29.05, 30.05, 35.38, 35.46, 35.49, 35.61, 93.41, 93.56, 102.67, 102.96, 103.20, 103.50, 103.72, 104.16, 118.31, 118.47, 134.15, 134.19, 137.55, 138.15, 138.62, 138.95, 138.97, 139.15, 146.10, 147.99. HR-MS (CI^+) *m*/*z* (M^+) calcd for $C_{28}H_{35}FN_4$: 447.2924, found: 447.2935. Anal. Calcd for $C_{28}H_{35}FN_4$: C, 75.30; H, 7.90; N, 12.55. Found: C, 74.98; H, 7.97; N, 12.35.

β-Monochloro-*meso*-octamethylcalix[4]pyrrole 67

Calix[4]pyrrole **1** (100 mg, 0.23 mmol) was dissolved in dry THF (10 mL). N-chlorosuccinimide (NCS; 45 mg, 0.34 mmol) was then added to the solution. The reaction mixture was stirred for 3 h at 60 ˚C under Ar. The solvent was then evaporated off. The residue was purified by column chromatography (silica gel, eluent: dichloromethane/hexane 1:1 v/v). The fraction displaying an R_f = 0.54 on TLC (silica, eluent: dichloromethane-hexane 1:1 v/v) was isolated (35 mg, 33%). ^{1}H NMR (500 MHz, CD_2Cl_2, 25˚C) δ 1.45 (s, 6H, CH_3), 1.51 (s, 12H, CH_3), 1.64 (s, 6H, CH_3), 5.96 - 5.83 (m, 7H, pyrrole CH), 6.73 (s, 1H, NH), 6.94 (s, 1H, NH), 7.27 (s, 1H, NH), 7.30 (s, 1H, NH). ^{13}C NMR (125 MHz, CD_2Cl_2, 25˚C) δ 27.87, 28.66, 28.75, 29.41, 35.33, 35.42, 35.62, 36.64, 102.14, 103.03, 103.16, 103.91, 104.14, 104.45, 106.03, 106.57, 131.30, 136.57, 137.42, 137.60, 138.07, 138.68, 139.24, 139.40. HRMS (CI^+) *m*/*z* (M^+) calcd for $C_{28}H_{35}ClN_4$: 463.2628, found: 463.2619. Anal. Calcd for $C_{28}H_{35}ClN_4$-0.5H_2O: C, 71.24; H, 7.69; N, 11.87. Found: C, 71.46; H, 7.60; N, 11.81.

β-Monobromo-*meso*-octamethylcalix[4]pyrrole 68

Calix[4]pyrrole **1** (100 mg, 0.23 mmol) was dissolved in dry THF (10 mL). N-bromosuccinimide (NBS; 50 mg, 0.28 mmol) was then added to the solution. The

reaction mixture was stirred for 5 h at 60 ˚C under Ar. The solvent was evaporated off using a rotary evaporator. The residue was then purified by column chromatography (silica gel, eluent: dichloromethane/hexane 1:1 v/v). The fraction displaying an R_f value of 0.54 on TLC (silica, eluent: dichloromethane/hexane 1:1 v/v) was isolated (25 mg, 21%). ^{1}H NMR (500 MHz, CD_2Cl_2, 25˚C) δ 1.45 (s, 6H, CH_3), 1.51 (s, 12H, CH_3), 1.64 (s, 6H, CH_3), 5.96 - 5.82 (m, 7H, pyrrole CH), 6.83 (s, 1H, NH), 6.94 (s, 1H, NH), 7.29 (s, 2H, NH). ^{13}C NMR (125 MHz, CD_2Cl_2, 25˚C) δ 28.00, 28.64, 28.73, 29.48, 35.33, 35.43, 35.60, 36.88, 90.92, 102.07, 103.06, 103.15, 103.96, 104.22, 104.49, 108.75, 132.95, 137.42, 137.45, 137.48, 137.97, 138.65, 139.28, 139.43. HRMS (CI^+) *m*/*z* (M^+) calcd. for $C_{28}H_{35}BrN_4$: 506.2045, found: 506.2049. Anal. Calcd for $C_{28}H_{35}BrN_4$-0.5H_2O: C, 65.11; H, 7.03; N, 10.85. Found: C, 65.20; H, 6.90; N, 10.72.

β-Monoiodo-*meso*-octamethylcalix[4]pyrrole 18

Calix[4]pyrrole **1** (100 mg, 0.23 mmol) was dissolved in dry dichloromethane (10 mL). Bis(trifluoroacetoxy)iodobenzene (83 mg, 0.19 mmol) and iodine (40 mg, 0.16 mmol) were then added to the solution. The reaction mixture was stirred for 10 minutes at room temperature under Ar. After passing through a small amount of silica gel (eluent: CH_2Cl_2), the solvent was evaporated off using a rotary evaporator. The residue was purified by column chromatography (silica gel, eluent: dichloromethane-hexane 1:1 v/v). The fraction displaying an R_f = 0.55 on TLC (silica gel, eluent: dichloromethane-hexane 1:1 v/v) was isolated (26 mg, 20%). ^{1}H NMR (500 MHz, CD_2Cl_2, 25˚C) δ 1.45 (s, 6H, CH_3), 1.52 (s, 12H, CH_3), 1.67 (s, 6H, CH_3), 5.97 - 5.82 (m, 6H, pyrrole-CH), 6.06 (d, 1H, pyrrole CH), 6.93 (s, 2H, NH), 7.28 (s, 2H, NH). ^{13}C NMR (125 MHz, CD_2Cl_2, 25˚C) δ 28.47, 28.68, 28.76, 29.52, 35.38, 35.49, 35.55, 37.06, 54.87, 102.09, 103.14, 103.20, 104.01, 104.28, 104.48, 114.35, 136.14, 137.55, 137.94, 138.66, 138.84, 139.12,

139.33, 139.46. HRMS (CI^+) *m*/*z* (M^+) calcd for $C_{28}H_{35}IN_4$: 554.1906, found: 554.1896. Anal. Calcd for $C_{28}H_{35}IN_4$: C, 60.65; H, 6.36; N, 10.10. Found: C, 60.65; H, 6.35; N, 9.90.

General Synthetic Procedure for Calix[*n*]bipyrroles

2,2'-Bipyrrole was dissolved in methanol (100 mM) and the mixture was degassed by bubbling with Ar for 10 minutes. Ketone (1 equiv.) was added and the mixture was stirred for another 5 minutes at room temperature. Methanesulfonic acid (0.5 equiv.) was added, with the resulting mixture stirred at room temperature for 2 hours. Saturated sodium bicarbonate (aq) was added to quench the reaction, followed by extraction with dichloromethane. The organic phase was washed with water, dried over anhydrous sodium sulfate, filtered, and evaporated to dryness. The residue obtained was then purified by column chromatography.

***Meso*-hexamethylcalix[3]bipyrrole 70 and *meso*-octamethylcalix[4]bipyrrole 71**

2,2'-Bipyrrole **72** (0.2 g, 1.5 mmol) and acetone (88 mg, 1.5 mmol) was reacted according to the general procedure. The residue obtained was then purified by column chromatography (silica gel, eluent: dichloromethane for **70**, followed by dichloromethane-ethyl acetate 98:2 v/v for **71**) to afford **70** and **71**:

70: Pale green solid (63 mg, 24%). M.p. > 200 °C (decomp.). ^{1}H NMR (400 MHz, CD_3CN, 25 °C) δ 1.61(s, 18 H, *meso*-CH_3), 5.95 (t, 6H, β-pyrrole CH), 6.03 (t, 6H, β-pyrrole CH), 8.52 (s, 6H, pyrrole-NH). ^{13}C NMR (100MHz, CD_3CN, 25 °C) δ 29.5, 36.1, 104.0, 104.7, 125.4, 138.9. HR-MS (CI^+) *m*/*z* ($M + H^+$) calcd for $C_{33}H_{37}N_6$: 517.3079, found: 517.3069.

71: Pale green solid (75 mg, 29%). M.p. > 200 °C (decomp.). ^{1}H NMR (400 MHz, CD_3CN, 25 °C) δ 1.56 (s, 24 H, *meso*-CH_3), 5.91 (t, 8H, β-pyrrole CH), 5.99 (t, 8H, β-pyrrole CH), 8.42 (s, 8H, pyrrole-NH). ^{13}C-NMR (100MHz, CD_3CN, 25 °C) δ 29.1, 35.7, 102.5, 104.8, 125.6, 138.4. HR-MS (CI^+) *m*/*z* (M^+) calcd for $C_{44}H_{48}N_8$: 688.4001, found: 688.3998.

***Meso*-tris(cyclohyxendiyl)-calix[3]bipyrrole 75**

2,2'-Bipyrrole **72** (0.132 g, 1 mmol) and cyclohexanone (98 mg, 1 mmol) was reacted for 5 h according to the general procedure. The residue obtained was then purified by column chromatography (silica gel, eluent: dichloromethane) to afford **75** (30 mg, 14%). ^{1}H NMR (400 MHz, $CDCl_3$, 25 °C) δ 1.49 (m, 6 H, CH_2), 1.62 (m, 12H, CH_2), 2.07 (t, 12H, CH_2), 5.98 (t, 6H, β-pyrrole CH), 6.06 (t, 6H, β-pyrrole CH), 7.45 (s, 6H, pyrrole-NH). ^{13}C NMR (100MHz, $CDCl_3$, 25 °C) δ 22.81, 26.01, 36.68, 40.03, 104.66, 105.38, 124.98, 138.34. MS (CI^+) *m*/*z* (M^+) 637.

***Meso*-tris(9,9-fluorene-diyl)calix[3]bipyrrole 77 and *meso*-tetra(9,9-fluorene-diyl) calix[4]bipyrrole 78**

2,2'-Bipyrrole **72** (0.132 g, 1 mmol) and 9,9-fluorenone (0.18 g, 1 mmol) was reacted for 2 h according to the general procedure. The residue obtained was then purified by column chromatography (silica gel, eluent: dichloromethane-hexanes 4:1 v/v) to afford **77** and **78**.

77: Dark red solid (20 mg, 7%). ^{1}H NMR (400 MHz, $CDCl_3$, 25 °C) δ 5.69 (t, 6H, β-pyrrole CH), 6.08 (t, 6H, β-pyrrole CH), 7.33-7.43 (m, 12H, Benzene CH), 7.63 (d, 6H,

benzene-CH), 7.77 (d, 6H, benzene CH), 8.59 (s, 6H, pyrrole NH). ^{13}C-NMR (100MHz, $CDCl_3$, 25 °C) δ 55.55, 105.07, 108.49, 120.44, 124.93, 126.34, 127.59, 128.02, 133.60, 139.71, 148.26. HR-MS (CI^+) *m*/*z* ($M + H^+$) calcd for $C_{63}H_{43}N_6$: 883.3549, found: 883.3586.

78: Dark red solid (50 mg, 17%). ^{1}H NMR (400 MHz, $CDCl_3$, 25 °C) δ 5.81 (t, 8H, β-pyrrole CH), 6.01 (t, 8H, β-pyrrole CH), 7.27-7.40 (m, 16H, Benzene CH), 7.54 (d, 8H, benzene-CH), 7.73 (d, 8H, benzene CH), 8.43 (s, 8H, pyrrole NH). ^{13}C-NMR (100MHz, $CDCl_3$, 25 °C) δ 55.73, 104.23, 108.33, 120.49, 124.99, 125.87, 127.78, 128.13, 133.05, 139.66, 148.47. HR-MS (CI^+) *m*/*z* (M^+) calcd for $C_{84}H_{56}N_8$: 1176.4628, found: 1176.4581.

1-Aza-6,6-diphenyl-2-(pyrrol-2-yl)fulvene 76

2,2'-Bipyrrole **72** (0.132 g, 1 mmol) and benzophenone (0.182 g, 1 mmol) was reacted for 26 h according to the general procedure. The residue obtained was then purified by column chromatography (silica gel, eluent: dichloromethane-methanol 97:3 v/v) to afford **76** as a red solid (0.144 g, 48%). ^{1}H NMR (400 MHz, $CDCl_3$, 25 °C) δ 6.24 (m, 1H, α-pyrrole CH), 6.01 (dd, J = 1.2 Hz and 4.0 Hz, 1H, β-pyrrole CH), 6.87 (q, J = 1.2 Hz, 1H, β-pyrrole CH), 7.05 (d, J = 4.8 Hz, 1H, β-pyrrole CH), 7.12 (d, J = 4.8 Hz, 1H, β-pyrrole CH), 7.32-7.45 (m, 8H, benzene CH), 7.62-7.65 (m, 2H, benzene CH). ^{13}C-NMR (100MHz, $CDCl_3$, 25 °C) δ 110.07, 113.64, 123.51, 126.94, 127.43, 127.73, 127.85, 128.81, 128.85, 132.13, 133.36, 137.14, 139.65, 140.94, 146.44, 154.90, 163.48. HR-MS (CI^+) *m*/*z* ($M + H^+$) calcd for $C_{21}H_{17}N_2$: 297.1392, found: 297.1379.

2,5-Bis[(α-(1H, 1'H-[2,2']bipyrro-5-yl)-α,α-dimethyl)methyl]furan 94

2,2'-Bipyrrole **72** (1.32 g, 10 mmol) and 2,5-bis[(α-hydroxy-α,α-dimethyl)methyl]furan **89** (0.184 g, 1 mmol) were dissolved in dry acetonitrile (100 mL), and the mixture was degassed by bubbling Ar through the solution for 10 min. The mixture, kept under Ar, was then cooled to 0 ºC using an ice-water bath. $BF_3{\cdot}Et_2O$ (0.14 g, 1 mmol) was added, and the mixture was stirred at 0 ºC for 40 min. The reaction was quenched with triethylamine, and the solvent was evaporated under reduced pressure. The residue was purified by column chromatography (silica gel, dichloromethane-hexanes 3:2 v/v) to afford **94** as a green solid (0.30 g, 73%). ^{1}H NMR (400 MHz, $CDCl_3$, 25 °C) δ 1.66 (s, 12H, *meso*-CH_3), 5.99-6.06 (m, 8H, *β*-pyrrole CH), 6.19 (q, 2H, *α*-pyrrole CH), 6.65 (s, 2H, *β*-furan CH), 7.96 (s, 4H, pyrrole-NH). ^{13}C NMR (100 MHz, $CDCl_3$, 25 °C) δ 27.57, 36.17, 103.60, 103.63, 104.01, 104.23, 109.11, 117.30, 124.85, 125.85, 137.91, 159.61. HR-MS (CI^+) *m/z* (M^+) calcd for $C_{26}H_{28}N_4O$: 412.2263, found: 412.2260.

2,5-Bis[(α-(1H, 1'H-[2,2']bipyrro-5-yl)-α,α-dimethyl)methyl]thiophene 95

2,2'-Bipyrrole **72** (1.32 g, 10 mmol) and 2,5-bis[(α-hydroxy-α,α-dimethyl)-methyl]thiophene **90** (0.20 g, 1 mmol) were dissolved in dry acetonitrile (100 mL) and subject to reaction and purification using exactly the same procedure used to prepare **94**. Compound **95** was obtained as a white solid (0.32 g, 74%). ^{1}H NMR (400 MHz, $CDCl_3$, 25 °C) δ 1.70 (s, 12H, *meso*-CH_3), 6.04 (t, 2H, *β*-pyrrole CH), 6.07 (t, 2H, *β*-pyrrole CH), 6.09 (m, 2H, *β*-pyrrole CH), 6.19 (q, 2H, *β*-pyrrole CH), 6.58 (s, 2H, *β*-thiophene CH), 6.72 (m, 2H, *α*-pyrrole CH), 7.82 (s, 2H, pyrrole-NH), 8.15 (s, 2H, pyrrole-NH). ^{13}C NMR (100 MHz, $CDCl_3$, 25 °C) δ 31.08, 37.97, 103.18, 103.35, 104.87, 109.33, 117.44, 122.29, 124.99, 125.98, 139.54, 152.72. HR-MS (CI^+) *m/z* ($M + H^+$) calcd for $C_{26}H_{29}N_4S$: 429.2113, found: 429.2102.

***Meso*-octamethylcalix[2]bipyrrole[2]furan 91**

2,5-Bis[(α-(1H, 1'H-[2,2']bipyrro-5-yl)-α,α-dimethyl)methyl]furan **94** (83 mg, 0.2 mmol) and 2,5-bis[(α-hydroxy-α,α-dimethyl)methyl]furan **89** (37 mg, 0.2 mmol) were dissolved in dry acetonitrile (200 mL), and the mixture was degassed by bubbling Ar through the solution for 10 min. The mixture, kept under Ar, was then cooled to 0 ºC using an ice-water bath. $BF_3 \cdot Et_2O$ (29 mg, 0.2 mmol) was added, and the mixture was stirred at 0 ºC for 2 h. The reaction was quenched with triethylamine, and the solvent was evaporated under reduced pressure. The residue was purified by column chromatography (silica gel, dichloromethane-hexanes 4:1 v/v) to afford **91** as a white solid (43 mg, 38%). ^{1}H NMR (400 MHz, $CDCl_3$, 25 °C) δ 1.61 (s, 24H, *meso*-CH_3), 5.76 (t, 4H, *β*-pyrrole CH), 5.95 (m, 8H, 4 *β*-pyrrole CH + 4 *β*-furan CH), 7.68 (s, 4H, pyrrole-NH). ^{13}C NMR (100 MHz, $CDCl_3$, 25 °C) δ 27.16, 35.88, 102.84, 103.06, 103.57, 125.26, 137.22, 159.75. HR-MS (CI^+) *m/z* (M^+) calcd for $C_{36}H_{40}N_4O_2$: 560.3151, found: 560.3149.

***Meso*-octamethylcalix[2]bipyrrole[2]thiophene 92**

2,5-Bis[(α-(1H, 1'H-[2,2']bipyrro-5-yl)-α,α-dimethyl)methyl]thiophene **95** (86 mg, 0.2 mmol) and 2,5-bis[(α-hydroxy-α,α-dimethyl)methyl]thiophene **90** (40 mg, 0.2 mmol) were dissolved in dry acetonitrile (200 mL) and subject to reaction and purification using exactly the same procedure used to prepare **91**. Compound **92** was obtained as a white solid (28 mg, 22%). ^{1}H NMR (400 MHz, $CDCl_3$, 25 °C) δ 1.67 (s, 24H, *meso*-CH_3), 5.96-6.00 (overlapping triplets, 8H, *β*-pyrrole CH), 6.66 (s, 4H, *β*-thiophene CH), 7.66 (s, 4H, pyrrole NH). ^{13}C NMR (100 MHz, $CDCl_3$, 25 °C) δ 30.45, 37.59, 104.25, 104.57, 121.35, 125.32, 139.67, 153.52. HR-MS (CI^+) *m/z* ($M + H^+$) calcd for $C_{36}H_{41}N_4S_2$: 593.2773, found: 593.2757.

***Meso*-octamethylcalix[2]bipyrrole[1]furan[1]thiophene 93**

2,5-Bis[(α-(1H, 1'H-[2,2']bipyrro-5-yl)-α,α-dimethyl)methyl]furan **94** (0.13 g, 0.3 mmol) and 2,5-bis[(α-hydroxy-α,α-dimethyl)methyl]thiophene **90** (60 mg, 0.3 mmol) were dissolved in dry acetonitrile (300 mL) and subject to reaction and purification using exactly the same procedure used to prepare **91**. Compound **93** was obtained as a white solid (77 mg, 44%). ^{1}H NMR (400 MHz, $CDCl_3$, 25 °C) δ 1.62 (s, 12H, *meso*-CH_3), 1.71 (s, 12H, *meso*-CH_3), 5.88 (t, 2H, *β*-pyrrole CH), 5.95-5.96 (m, 8H, 6 *β*-pyrrole CH + 2 *β*-furan CH), 6.71 (s, 2H, *β*-thiophene CH), 7.65 (s, 2H, pyrrole NH), 7.86 (s, 2H, pyrrole NH). ^{13}C NMR (100 MHz, $CDCl_3$, 25 °C) δ 27.24, 30.06, 36.03, 37.75, 103.68. 103.89, 104.03, 104.26, 109.71, 121.28, 124.94, 137.78, 139.71, 153.43, 159.66. HR-MS (CI^+) *m/z* ($M + H^+$) calcd for $C_{36}H_{41}N_4OS$: 577.3001, found: 577.2991.

N,N'-Diallylisophthaldiamide 109a

Allylamine (12.56 g, 0.22 mol) and triethylamine (30.36 g, 0.3 mol) were dissolved in dichloromethane (100 mL) in a 500 mL round bottom flask equipped with a 250 mL additional funnel and cooled with an ice-water bath. To the amine solution was then added isophthaloyl chloride (**110**; 20.30 g, 0.1 mol) dissolved in dichloromethane (100 mL) dropwise *via* an additional funnel. Once the addition was complete, the cooling bath was removed and the reaction was stirred at room temperature overnight. The reaction mixture was washed with water (3 × 100 mL) and brine (100 mL), and dried with sodium sulfate. The volatile components were removed using a rotary evaporator and the residue was dried under vacuum. The resulting pale yellow solid (23.15 g, 95%) was used for the next step without further purification. M.p. 115 °C. ^{1}H NMR (400 MHz, $CDCl_3$, 25 °C): δ 4.08 (m, 4 H, NH*C*H_2), 5.19 (dd, 2 H, J 1.2 and 10 Hz, C=CH*H* cis), 5.26 (dd, 2 H, J = 1.2 and 17.2 Hz, C=C*H*H trans), 5.92 (m, 2 H, C*H*=CH_2), 6.47 (s, 2 H, NH), 7.51 (t, 1 H,

J 8 Hz, benzene CH), 7.94 (dd, 2 H, J = 2 and 8 Hz, benzene CH), 8.22 (t, 1 H, J 2 Hz, benzene CH). ^{13}C NMR (100 MHz, $CDCl_3$, 25 °C) δ 42.53, 116.92, 125.33, 128.95, 130.02, 133.74, 134.65, 166.50. HRMS (CI^+) *m*/*z* (M + H^+) calcd for $C_{14}H_{17}N_2O_2$: 245.1290, found: 245.1292.

N,N'-Diallyl-5-(tert-butyl)isophthaldiamide 109b

A mixture of 5-(*tert*-butyl)isophthalic acid (**111**; 11.10 g, 50 mmol), thionyl chloride (150 mL), and 10 drops of DMF was heated under refulx for 5 h. Excess thionyl chloride was removed under vacuum. The residue was used for the next step directly without purification. Allylamine (6.28 g, 0.11 mol) and triethylamine (12.12 g, 0.12 mol) were dissolved in dichloromethane (100 mL) in a 500 mL round bottom flask equipped with a 250 mL additional funnel and cooled with ice-water bath. To the amine solution was then added 5-(*tert*-butyl)isophthaloyl dichloride dissolved in dichloromethane (100 mL) dropwise *via* an additional funnel. Once the addition was complete, the cooling bath was removed and the reaction was stirred at room temperature overnight. The reaction mixture was washed with water (3 × 100 mL) and brine (100 mL), and dried with sodium sulfate. The volatile components were removed using a rotary evaporator, and the residue was dried under vacuum. The resulting pale yellow solid (15 g, quantitative) was used for the next step without further purification. M.p. 139 °C. ^{1}H NMR (400 MHz, $CDCl_3$, 25 °C) δ 1.31 (s, 9H, CH_3), 4.04 (m, 4 H, NH*C*H_2), 5.14 (dd, 2 H, J = 1.2 and 10 Hz, C=CH*H* cis), 5.22 (dd, 2 H, J 1.2 and 16.8 Hz, C=C*H*H trans), 5.88 (m, 2 H, C*H*=CH_2), 6.54 (s, 2 H, NH), 7.94 (d, 2 H, J = 1.6 Hz, benzene CH), 7.92 (t, 2 H, J = 1.6, benzene CH). ^{13}C NMR (100 MHz, $CDCl_3$, 25 °C) δ 31.16, 35.05, 42.57, 116.92, 122.21, 127.29, 133.87, 134.50, 152.58, 167.00. HRMS (CI^+) *m*/*z* (M + H^+) calcd for $C_{18}H_{25}N_2O_2$: 301.1916, found: 301.1920.

N,N'-Diallyl-5-hexyloxy-isophthaldiamide 109c

Dimethyl-5-hexyloxyisophthalate (**112**; 8.82 g, 30 mmol) was dissolved in allylamine (90 mL), and the mixture was stirred at RT for 4 days. The excess solvent was removed under reduced pressure. Column chromatographic purification (silica gel, 1% CH_3OH in dichloromethane, eluent) of the residue afforded **109c** in the form of a brown oil (9 g, 75%). ^{1}H NMR (400 MHz, $CDCl_3$, 25 °C) δ 0.91 (t, 3 H, J = 7.2 Hz, CH_3), 1.33 (m, 4 H, CH_2), 1.45 (m, 2H, CH_2), 1.78 (m, 2 H, CH_2), 4.01 (t, 2 H, 6.4 Hz, O*CH*$_2$), 4.06 (m, 4 H, NH*CH*$_2$), 5.18 (dd, 2 H, J = 1.2 and 10 Hz, C=CH*H* cis), 5.25 (dd, 2 H, J = 1.2 and 16.8 Hz, C=C*H*H trans), 5.91 (m, 2 H, C*H*=CH_2), 6.46 (s, 2 H, NH), 7.45 (d, 2 H, benzene CH), 7.73 (t, 2 H, benzene CH). ^{13}C NMR (100 MHz, $CDCl_3$, 25 °C) δ 14.00, 22.55, 26.00, 29.03, 31.47, 42.55, 68.57, 116.12, 116.89, 116.99, 133.73, 136.01, 159.57, 166.38. HRMS (CI^+) *m*/*z* ($M + H^+$) calcd for $C_{20}H_{29}N_2O_3$: 345.2178, found: 345.2181.

1,3-Bis(pyrrol-2-yl)benzene 105a

A mixture of **109a** (2.44g, 10 mmol), phosgene (20% solution in toluene, 40 mL), and DMF (4 drops) was stirred for 15 h at room temperature under Ar. The resulting mixture was heated at 40-45 °C for 2 h, followed by evaporation of solvent under *vacuo*. The residue was dissolved in THF (60 mL) and added dropwise with stirring to a solution of potassium *tert*-butoxide (5.89 g, 52 mmol) in THF (60 ml) at 5-10 °C under Ar. After stirring for 1 h at this temperature, the reaction mixture was poured into ice water and extracted with chloroform (3 × 100 mL). The organic phase was dried (Na_2SO_4) and evaporated to dryness. The residue was subjected to column chromatography (silica gel, dichloromethane, eluent) to give crude product, which upon recrystallization from dichloromethane/hexanes afforded **105a** in the form of a white solid (0.6 g, 29%). M.p.

163 °C. ^{1}H NMR (400 MHz, $CDCl_3$, 25 °C) δ 6.32 (q, 2 H, pyrrole CH), 6.56 (m, 2 H, pyrrole CH), 6.89 (m, 2 H, pyrrole CH), 7.30-7.39 (m, 3 H, benzene CH), 7.58 (t, 1 H, benzene CH), 8.47 (br s, 2 H, pyrrole NH). ^{13}C NMR (100 MHz, $CDCl_3$, 25 °C) δ 100.18, 110.16, 118.98, 119.62, 121.77, 129.40, 131.95, 133.36. HRMS (CI^+) *m*/*z* ($M + H^+$) calcd for $C_{14}H_{13}N_2$: 209.1079, found: 209.1079.

5-(tert-Butyl)-1,3-bis(pyrrol-2-yl)benzene 105b

The title compound was prepared from **109b** (3 g, 10 mmol) in the same manner as **105a**. After column chromatography (silica gel, eluent: dichloromethane/hexanes 4:1 v/v), the crude product was recrystalized from benzene/hexanes to afford **105b** in the form of a pale yellow solid (1.13 g, 43%). M.p. 163 °C. ^{1}H NMR (400 MHz, $CDCl_3$, 25 °C) δ 1.37 (s, 9 H, CH_3), 6.32 (m, 2 H, pyrrole CH), 6.54 (m, 2 H, pyrrole CH), 6.88 (m, 2 H, pyrrole CH), 7.4 (d, 2 H, benzene CH), 7.38 (t, 1 H, benzene CH), 8.47 (br s, 2 H, pyrrole NH). ^{13}C NMR (100 MHz, $CDCl_3$, 25 °C) δ 31.33, 34.81, 106.03, 110.06, 117.44, 118.73, 119.40, 132.50, 133.14, 152.30. HRMS (CI^+) *m*/*z* ($M + H^+$) calcd for $C_{18}H_{21}N_2$: 265.1705, found: 265.1700.

5-Hexyloxy-1,3-bis(pyrrol-2-yl)benzene 105c

This compound was prepared from **109c** (5 g, 14.5 mmol) in the same manner as **105a**. Column chromatography (silica gel, dichloromethane/hexanes 1:1, eluent) afforded **105c** in the form of a pale yellow solid (3.30 g, 96%). M.p. 66 °C. ^{1}H NMR (400 MHz, $CDCl_3$, 25 °C) δ 0.91 (t, 3 H, CH_3), 1.36 (m, 4 H, CH_2), 1.49 (m, 2 H, CH_2), 1.81 (m, 2 H, CH_2), 4.02 (t, 2 H, OCH_2), 6.31 (m, 2 H, pyrrole CH), 6.54 (m, 2 H, pyrrole CH), 6.85 (d, 2 H, benzene CH), 6.87 (m, 2 H, pyrrole CH), 7.16 (t, 1 H, benzene CH), 7.38 (t, 1 H, benzene CH), 8.45 (br s, 2 H, pyrrole NH). ^{13}C NMR (100 MHz, $CDCl_3$, 25 °C) δ 14.03,

22.60, 25.73, 29.27, 31.57, 68.11, 106.31, 108.16, 110.07, 112.33, 118.91, 131.96, 134.55, 160.01. HRMS (CI^+) *m*/*z* ($M + H^+$) calcd for $C_{20}H_{25}N_2O$: 309.1967, found: 309.1967.

Calix[*n*]1,3-bis(pyrrol-2-yl)benzenes 106a-108a

Compound **105a** (0.42 g, 2 mmol) was dissolved in acetone (40 mL) and the mixture was degassed by bubbling with Ar for 10 minutes. Trifluoroacetic acid (0.23 g, 2 mmol) was added, and the resulting mixture was stirred at room temperature for 12 h. Triethylamine was added to quench the reaction, and the solvent was evaporated in *vacuo*. Column chromatography (silica gel, gradient of hexanes to hexanes/ethyl acetate 1:9 as eluents) afforded the title compounds **106a-108a**:

106a: White solid (68 mg, 14%). M.p. > 180 °C (decomp.). ^1H NMR (400 MHz, $CDCl_3$, 25 °C) δ 1.74 (s, 12 H, CH_3), 6.17 (t, 4 H, β-pyrrole CH), 6.37 (t, 4 H, β-pyrrole CH), 7.20 (s, 2 H, benzene CH), 7.35 (s, 6 H, benzene CH), 8.09 (s, 4 H, pyrrole NH). ^{13}C NMR (100 MHz, $CDCl_3$, 25 °C) δ 30.13, 35.81, 106.14, 107.32, 120.14, 124.88, 129.56, 131.54, 134.02, 140.27. HRMS (CI^+) *m*/*z* ($M + H^+$) calcd for $C_{34}H_{33}N_4$: 497.2705, found: 497.2700.

107a: White solid (82 mg, 17%). M.p. > 140 °C (decomp.). ^1H NMR (400 MHz, $CDCl_3$, 25 °C) δ 1.72 (s, 18 H, CH_3), 6.20 (t, 6 H, β-pyrrole CH), 6.40 (t, 6 H, β-pyrrole CH), 7.15-7.24 (m, 12 H, benzene CH), 7.96 (s, 6 H, pyrrole NH). ^{13}C NMR (100 MHz, $CDCl_3$, 25 °C) δ 29.29, 35.73, 105.80, 105.89, 118.51, 121.55, 129.21, 131.53, 132.96, 140.08. HRMS (CI^+) *m*/*z* ($M + H^+$) calcd for $C_{51}H_{49}N_6$: 7454019, found: 745.4028.

108a: White solid (64 mg, 13%). M.p. > 140 °C (decomp.). ^{1}H NMR (400 MHz, $CDCl_3$, 25 °C) δ 1.70 (s, 24 H, CH_3), 6.17 (t, 8 H, β-pyrrole CH), 6.41 (t, 8 H, β-pyrrole CH), 7.15-7.23 (m, 12 H, benzene CH), 7.33 (t, 4 H, benzene CH), 8.03 (m, 8 H, pyrrole NH). ^{13}C NMR (100 MHz, $CDCl_3$, 25 °C) δ 29.26, 35.70, 105.83, 105.88, 118.97, 121.45, 129.19, 131.43, 133.05, 140.06. HRMS (CI^+) *m*/*z* ($M + H^+$) calcd for $C_{68}H_{65}N_8$: 993.5332, found: 993.5304.

Calix[*n*]5-(*tert*-butyl)-1,3-bis(pyrrol-2-yl)benzene 106b-108b

This set of title compounds was prepared from **105b** (0.26 g, 1 mmol) in a manner analogous to that used to prepare **106a-108a**. Column chromatography (silica gel, eluent: gradient of hexanes to hexanes-ethyl acetate 1:9 v/v) afforded **106b-108b**:

106b: White solid (50 mg, 16%). M.p. > 200 °C (decomp.). ^{1}H NMR (400 MHz, $CDCl_3$, 25 °C) δ 1.34 (s, 18 H, benzene CH_3), 1.72 (s, 12 H, *meso* CH_3), 6.17 (t, 4 H, β-pyrrole CH), 6.37 (t, 4 H, β-pyrrole CH), 7.03 (t, 2 H, benzene CH), 7.40 (d, 4 H, benzene CH), 8.08 (s, 4 H, pyrrole NH). ^{13}C NMR (100 MHz, $CDCl_3$, 25 °C) δ 30.34, 31.24, 34.77, 35.87, 105.96, 106.86, 118.15, 122.54, 132.02, 133.84, 134.00, 152.56. HRMS (CI^+) *m*/*z* ($M + H^+$) calcd for $C_{42}H_{49}N_4$: 609.3957, found: 609.3966.

107b: White solid (66 mg, 22%). M.p. 194 °C (decomp.). ^{1}H NMR (400 MHz, $CDCl_3$, 25 °C) δ 1.30 (s, 27 H, benzene CH_3), 1.73 (s, 18 H, *meso* CH_3), 6.20 (t, 6 H, β-pyrrole CH), 6.39 (t, 6 H, β-pyrrole CH), 7.07 (t, 3 H, benzene CH), 7.21 (d, 6 H, benzene CH), 8.03 (s, 6 H, pyrrole NH). ^{13}C NMR (100 MHz, $CDCl_3$, 25 °C) δ 29.43, 31.26, 34.71, 35.75, 105.68, 105.80, 116.37, 119.17, 131.99, 132.72, 139.89, 152.11. HRMS (CI^+) *m*/*z* ($M + H^+$) calcd for $C_{63}H_{73}N_6$: 913.5897, found: 913.5912.

108b: White solid (34 mg, 11%). M.p. > 180 °C. ^{1}H NMR (400 MHz, $CDCl_3$, 25 °C) δ 1.29 (s, 36 H, benzene CH_3), 1.70 (s, 24 H, *meso* CH_3), 6.15 (t, 8 H, *β*-pyrrole CH), 6.38 (t, 8 H, *β*-pyrrole CH), 7.11 (t, 4 H, benzene CH), 7.19 (d, 8 H, benzene CH), 8.04 (s, 8 H, pyrrole NH). ^{13}C NMR (100 MHz, $CDCl_3$, 25 °C) δ 29.30, 31.26, 34.70, 35.70, 105.76, 116.78, 119.35, 131.98, 132.91, 139.90, 152.10. HRMS (CI^+) *m*/*z* ($M + H^+$) calcd for $C_{84}H_{97}N_8$: 1217.7836, found: 1217.7833.

Calix[*n*]5-hexyloxy-1,3-bis(pyrrol-2-yl)benzene 106c-108c

This set of title compounds was prepared from **105c** (0.46 g, 1.5 mmol) using the same procedure as used to prepare **106a-108a**. Column chromatography (silica gel, gradient of hexanes to hexanes/ethyl acetate 1:19 as eleuent) afforded **106c-108c**:

106c: White solid (58 mg, 11%). M.p. 172 °C. ^{1}H NMR (400 MHz, $CDCl_3$, 25 °C) *δ* 0.90 (t, 6 H, CH_2CH_3), 1.34 (m, 8 H, CH_2), 1.46 (m, 4 H, CH_2), 1.72 (s, 12 H, *meso* CH_3), 1.79 (m, 4 H, CH_2), 3.99 (t, 4 H, OCH_2), 6.16 (t, 4 H, *β*-pyrrole CH), 6.36 (t, 4 H, *β*-pyrrole CH), 6.80 (t, 2 H, benzene CH), 6.90 (d, 4 H, benzene CH), 8.10 (s, 4 H, pyrrole NH). ^{13}C NMR (100 MHz, $CDCl_3$, 25 °C) *δ* 14.03, 22.60, 25.70, 29.20, 30.17, 31.56, 35.80, 68.10, 106.07, 107.28, 111.01, 112.72, 131.60, 135.28, 140.14, 159.93. HRMS (CI^+) *m*/*z* ($M + H^+$) calcd for $C_{46}H_{57}N_4O_2$: 697.4482, found: 697.4482.

107c: White solid (104 mg, 20%). M.p. > 80 °C (no clear m.p.). ^{1}H NMR (400 MHz, $CDCl_3$, 25 °C) *δ* 0.89 (t, 9 H, CH_2CH_3), 1.31 (m, 12 H, CH_2), 1.44 (m, 6 H, CH_2), 1.71 (s, 18 H, *meso* CH_3), 1.75 (m, 6 H, CH_2), 3.95 (t, 6 H, OCH_2), 6.18 (t, 6 H, *β*-pyrrole CH), 6.38 (t, 6 H, *β*-pyrrole CH), 6.69 (d, 6 H, benzene CH), 6.83 (t, 3 H, benzene CH),

7.93 (s, 6 H, pyrrole NH). ^{13}C NMR (100 MHz, $CDCl_3$, 25 °C) δ 14.03, 22.57, 25.70, 29.26, 29.29, 31.56, 35.71, 68.01, 105.86, 105.96, 107.77, 111.44, 131.54, 134.19, 140.00, 159.80. HRMS (FAB$^+$) *m/z* (M^+) calcd for $C_{69}H_{84}N_6O_3$: 1044.6605, found: 1044.6631.

108c: White solid (34 mg, 11%). M.p. > 120 °C (no clear m.p.). ^{1}H NMR (400 MHz, $CDCl_3$, 25 °C) δ 0.89 (t, 12 H, CH_2CH_3), 1.32 (m, 16 H, CH_2), 1.43 (m, 8 H, CH_2), 1.69 (s, 24 H, *meso* CH_3), 1.75 (m, 8 H, CH_2), 3.94 (t, 8 H, OCH_2), 6.13 (t, 8 H, β-pyrrole CH), 6.38 (t, 4 H, β-pyrrole CH), 6.69 (d, 8 H, benzene CH), 6.90 (s, 4 H, benzene CH), 8.02 (s, 8 H, pyrrole NH). ^{13}C NMR (100 MHz, $CDCl_3$, 25 °C) δ 14.03, 22.57, 25.71, 29.26, 31.57, 35.67, 68.03, 105.83, 106.10, 107.87, 111.80, 131.44, 1354.35, 139.99, 159.82. HRMS (FAB$^+$) *m/z* (M^+) calcd for $C_{92}H_{112}N_8O_4$: 1392.8807, found: 1392.8788.

Appendix A: Non Linear Curve Fitting Equations Used for Derivation of Anion Binding Constants in ^{1}H NMR titration Measurements

Wilcox 1:1 Binding Equation:[1]

$$y = \delta_i+[(\delta_f -\delta_i)/2*H]*[(1/K+H+x)-[(1/K+H+x)^2-4*H*x]^0.5]$$

y: chemical shift measured in the experiment

x: guest concentration (mol/L)

H: host concentration (mol/L)

K: binding constant (L/mol)

δ_i: initial chemical shift (free of guest)

δ_f: final chemical shift (theoretically final chemical shift)

Connor 1:1 Binding Equation:[2]

$$y = [(\delta_f -\delta_i)*K*x]/[1+K*x]$$

y: chemical shift measured in the experiment

x: guest concentration (mol/L)

K: binding constant (L/mol)

δ_i: initial chemical shift (free of guest)

δ_f: final chemical shift (theoretically final chemical shift)

Equation References

1. Wilcox, C. S. in *Frontiers in Supramolecular Organic Chemistry and Photochemistry*; Schneider, H. J., Dürr, H., Eds.; VCH: Weinheim, **1991**.
2. Connors, K. A. in *Binding Constants*, Wiley: New York, **1987**.

Appendix B: X-ray Experimental and Crystallographic Data

All crystals for X-ray crystallographic analyses described in this appendix were grown by the author, and their X-ray diffraction structures were solved by Dr. Vincent Lynch of this department. A general experimental method as provided by Dr. Lynch used in obtaining these structures, along with relevant data tables for each structure now follows.

The data were collected on a Nonius Kappa CCD diffractometer using a graphite monochromator with MoK_α radiation ($\lambda = 0.71073$Å). The data were collected at 153 K using an Oxford Cryostream low temperature device. Data reduction were performed using DENZO-SMN.[1] The structures were solved by direct methods using SIR92[2] or SIR97,[3] and refined by full-matrix least-squares on F^2 with anisotropic displacement parameters for the non-H atoms using SHELXL-97.[4] The hydrogen atoms on carbon were calculated in ideal positions with isotropic displacement parameters set to 1.2 × Ueq of the attached atom (1.5 × Ueq for methyl hydrogen atoms). Neutral atom scattering factors and values used to calculate the linear absorption coefficient are from the International Tables for X-ray Crystallography (1992). [5]

Experimental References

1. Otwinowski, Z.; Minor, W. In *DENZO-SMN., Methods in Enzymology,* 276: Macromolecular Crystallography, part A, 307 – 326, Carter, Jr., C. W.; Sweets, R. M. Eds.; Academic Press 1997.

2. Altomare, A.; Cascarano, G.; Guagliardi, C. *J. Appl. Cryst.* **1993**, *26*, 343-350.

3. Altomare, A; Burla, M. C.; Camalli, M.; Cascarano, G. L.; Giacovazzo, C.; Guagliardi, A.; Moliterni, A. G. G.; Polidori, G.; Spagna, R. *J. Appl. Cryst*. **1999**, *32*, 115-119.

4. Sheldrick, G. M. SHELXL97. *Program for the Refinement of Crystal Structures.* **1994**; University of Gottingen, Germany.

5. International Tables for X-ray Crystallography. Vol. C, Tables 4.2.6.8 and 6.1.1.4, Wilson, A. J. C. Eds.; Boston: Kluwer Academic Press, **1992**.

Table B1. Crystal data and structure refinement for **65**.

Empirical formula	C34 H40 Cl8 N4	
Formula weight	788.30	
Temperature	153(2) K	
Wavelength	0.71073 Å	
Crystal system	Monoclinic	
Space group	P21/c	
Unit cell dimensions	a = 13.5526(1) Å	α= 90°.
	b = 15.0351(2) Å	β= 108.648(1)°.
	c = 19.0304(2) Å	γ = 90°.
Volume	3674.15(7) $Å^3$	
Z	4	
Density (calculated)	1.425 Mg/m^3	
Absorption coefficient	0.644 mm^{-1}	
F(000)	1632	
Crystal size	0.48 x 0.13 x 0.10 mm	
Theta range for data collection	2.94 to 27.50°.	
Index ranges	-17<=h<=17, -19<=k<=14, -24<=l<=24	
Reflections collected	13491	
Independent reflections	8413 [R(int) = 0.0187]	
Completeness to theta = 27.50°	99.6 %	
Absorption correction	None	
Refinement method	Full-matrix least-squares on F^2	
Data / restraints / parameters	8413 / 0 / 432	
Goodness-of-fit on F^2	1.016	
Final R indices [I>2sigma(I)]	R1 = 0.0427, wR2 = 0.0994	
R indices (all data)	R1 = 0.0571, wR2 = 0.1075	
Extinction coefficient	1.1(3) x 10^{-6}	
Largest diff. peak and hole	0.77 and -0.70 $e.Å^{-3}$	

Table B2. Crystal data and structure refinement for [**70**·Cl]$^-$.

Empirical formula	C50 H74 Cl3 N7	
Formula weight	879.51	
Temperature	153(2) K	
Wavelength	0.71073 Å	
Crystal system	Monoclinic	
Space group	P21/c	
Unit cell dimensions	a = 12.6394(3) Å	α= 90°.
	b = 25.0959(6) Å	β= 108.614(1)°.
	c = 16.5497(5) Å	γ = 90°.
Volume	4974.9(2) Å^3	
Z	4	
Density (calculated)	1.174 Mg/m^3	
Absorption coefficient	0.225 mm^{-1}	
F(000)	1896	
Crystal size	0.17 x 0.10 x 0.09 mm	
Theta range for data collection	2.94 to 25.00°.	
Index ranges	-15<=h<=15, -28<=k<=29, -19<=l<=19	
Reflections collected	15672	
Independent reflections	8657 [R(int) = 0.1480]	
Completeness to theta = 25.00°	98.9 %	
Absorption correction	None	
Refinement method	Full-matrix least-squares on F^2	
Data / restraints / parameters	8657 / 0 / 550	
Goodness-of-fit on F^2	1.398	
Final R indices [I>2sigma(I)]	R1 = 0.1420, wR2 = 0.1410	
R indices (all data)	R1 = 0.2969, wR2 = 0.1686	
Largest diff. peak and hole	0.315 and -0.376 e.Å^{-3}	

Table B3. Crystal data and structure refinement for **71**·4THF.

Empirical formula	C30 H40 N4 O2
Formula weight	488.66
Temperature	153(2) K
Wavelength	0.71073 Å
Crystal system	Tetragonal
Space group	I-4
Unit cell dimensions	a = 16.4069(3) Å α= 90°.
	b = 16.4069(3) Å β= 90°.
	c = 10.5522(2) Å γ = 90°.
Volume, Z	2840.51(9) $Å^3$, 4
Density (calculated)	1.143 Mg/m^3
Absorption coefficient	0.072 mm^{-1}
F(000)	1056
Crystal size	0.24 x 0.23 x 0.17 mm
Theta range for data collection	3.38 to 27.49°.
Index ranges	-19<=h<=21, -21<=k<=21, -13<=l<=13
Reflections collected	10600
Independent reflections	3277 [R(int) = 0.0369]
Completeness to theta = 27.49°	99.8 %
Absorption correction	None
Refinement method	Full-matrix least-squares on F^2
Data / restraints / parameters	3277 / 4 / 249
Goodness-of-fit on F^2	1.029
Final R indices [I>2sigma(I)]	R1 = 0.0391, wR2 = 0.0759
R indices (all data)	R1 = 0.0614, wR2 = 0.0833
Absolute structure parameter	-0.6(13)
Extinction coefficient	7.4(6) x 10^{-6}
Largest diff. peak and hole	0.128 and -0.119 $e.Å^{-3}$

Table B4. Crystal data and structure refinement for **71**·2$C_{10}H_8N_2$

Empirical formula	C56 H60 Cl4 N10	
Formula weight	1014.94	
Temperature	153(2) K	
Wavelength	0.71073 Å	
Crystal system	Monoclinic	
Space group	P21/n	
Unit cell dimensions	a = 13.2087(3) Å	α= 90°.
	b = 15.1331(4) Å	β= 91.865(1)°.
	c = 13.2234(4) Å	γ = 90°.
Volume	2641.81(12) $Å^3$	
Z	2	
Density (calculated)	1.276 Mg/m^3	
Absorption coefficient	0.272 mm^{-1}	
F(000)	1068	
Crystal size	0.35 x 0.25 x 0.20 mm	
Theta range for data collection	3.08 to 27.50°.	
Index ranges	-14<=h<=13, -18<=k<=19, -17<=l<=15	
Reflections collected	15770	
Independent reflections	5556 [R(int) = 0.0718]	
Completeness to theta = 27.50°	91.5 %	
Max. and min. transmission	0.9477 and 0.9109	
Refinement method	Full-matrix least-squares on F^2	
Data / restraints / parameters	5556 / 0 / 333	
Goodness-of-fit on F^2	1.035	
Final R indices [I>2sigma(I)]	R1 = 0.0747, wR2 = 0.1179	
R indices (all data)	R1 = 0.1441, wR2 = 0.1372	
Extinction coefficient	3.8(5) x 10^{-6}	
Largest diff. peak and hole	0.290 and -0.583 e.$Å^{-3}$	

Table B5. Crystal data and structure refinement for [**71**·Cl]$^-$.

Empirical formula	C68 H104 Cl N9 O2
Formula weight	1115.05
Temperature	153(2) K
Wavelength	0.71073 Å
Crystal system	Orthorhombic
Space group	P212121
Unit cell dimensions	a = 15.1706(3) Å α= 90°.
	b = 20.1092(4) Å β= 90°.
	c = 21.6320(5) Å γ = 90°.
Volume, Z	6599.2(2) Å^3, 4
Density (calculated)	1.122 Mg/m^3
Absorption coefficient	0.107 mm^{-1}
F(000)	2432
Crystal size	0.3 x 0.3 x 0.15 mm
Theta range for data collection	3.00 to 25.07°.
Index ranges	-18<=h<=18, -23<=k<=23, -25<=l<=25
Reflections collected	11343
Independent reflections	11343
Completeness to theta = 25.07°	98.9 %
Absorption correction	None
Refinement method	Full-matrix least-squares on F^2
Data / restraints / parameters	11343 / 0 / 633
Goodness-of-fit on F^2	1.849
Final R indices [I>2sigma(I)]	R1 = 0.0754, wR2 = 0.1322
R indices (all data)	R1 = 0.1756, wR2 = 0.1387
Absolute structure parameter	0.10(8)
Extinction coefficient	7.1(4) x 10^{-6}
Largest diff. peak and hole	0.241 and -0.186 e.Å^{-3}

Table B6. Crystal data and structure refinement for [**71**·Br]$^-$.

Empirical formula	C52.50 H69 Br Cl N9	
Formula weight	941.53	
Temperature	153(2) K	
Wavelength	0.71073 Å	
Crystal system	Monoclinic	
Space group	P21/c	
Unit cell dimensions	a = 21.4853(3) Å	α= 90°.
	b = 15.7904(2) Å	β= 91.265(1)°.
	c = 29.3770(5) Å	γ = 90°.
Volume	9964.1(3) Å^3	
Z	8	
Density (calculated)	1.255 Mg/m^3	
Absorption coefficient	0.923 mm^{-1}	
F(000)	3992	
Crystal size	0.50 x 0.11 x 0.05 mm	
Theta range for data collection	2.91 to 25.00°.	
Index ranges	-25<=h<=25, -18<=k<=18, -34<=l<=34	
Reflections collected	31386	
Independent reflections	17418 [R(int) = 0.1174]	
Completeness to theta = 25.00°	99.2 %	
Absorption correction	None	
Refinement method	Full-matrix-block least-squares on F^2	
Data / restraints / parameters	17418 / 128 / 1180	
Goodness-of-fit on F^2	1.090	
Final R indices [I>2sigma(I)]	R1 = 0.0647, wR2 = 0.0916	
R indices (all data)	R1 = 0.1693, wR2 = 0.1145	
Largest diff. peak and hole	0.485 and -0.567 e.Å^{-3}	

Table B7. Crystal data and structure refinement for **91**.

Empirical formula	C36 H40 N4 O2
Formula weight	560.72
Temperature	153(2) K
Wavelength	0.71073 Å
Crystal system	Monoclinic
Space group	P21/c
Unit cell dimensions	a = 10.60460(10) Å α= 90°.
	b = 18.4424(4) Å β= 107.2090(10)°.
	c = 7.9205(2) Å γ = 90°.
Volume	1479.70(5) $Å^3$
Z	2
Density (calculated)	1.258 Mg/m^3
Absorption coefficient	0.079 mm^{-1}
F(000)	600
Crystal size	0.20 x 0.17 x 0.17 mm
Theta range for data collection	2.91 to 27.50°.
Index ranges	-13<=h<=13, -22<=k<=23, -10<=l<=10
Reflections collected	6179
Independent reflections	3392 [R(int) = 0.0540]
Completeness to theta = 27.50°	99.7 %
Absorption correction	None
Refinement method	Full-matrix least-squares on F^2
Data / restraints / parameters	3392 / 0 / 271
Goodness-of-fit on F^2	1.198
Final R indices [I>2sigma(I)]	R1 = 0.0946, wR2 = 0.1249
R indices (all data)	R1 = 0.1372, wR2 = 0.1356
Extinction coefficient	8(2) x 10^{-6}
Largest diff. peak and hole	0.249 and -0.229 $e.Å^{-3}$

Table B8. Crystal data and structure refinement for **92**·2C_4H_8O.

Empirical formula	C44 H56 N4 O2 S2	
Formula weight	737.05	
Temperature	153(2) K	
Wavelength	0.71073 Å	
Crystal system	Monoclinic	
Space group	P21/n	
Unit cell dimensions	a = 10.0674(3) Å	α= 90°.
	b = 20.8027(5) Å	β= 97.053(1)°.
	c = 19.2138(6) Å	γ = 90°.
Volume	3993.5(2) $Å^3$	
Z	4	
Density (calculated)	1.226 Mg/m^3	
Absorption coefficient	0.175 mm^{-1}	
F(000)	1584	
Crystal size	0.26 x 0.21 x 0.21 mm	
Theta range for data collection	2.93 to 25.00°.	
Index ranges	-11<=h<=11, -23<=k<=24, -22<=l<=22	
Reflections collected	12651	
Independent reflections	6996 [R(int) = 0.0373]	
Completeness to theta = 25.00°	99.6 %	
Absorption correction	None	
Refinement method	Full-matrix least-squares on F^2	
Data / restraints / parameters	6996 / 138 / 522	
Goodness-of-fit on F^2	3.072	
Final R indices [I>2sigma(I)]	R1 = 0.1223, wR2 = 0.1846	
R indices (all data)	R1 = 0.1571, wR2 = 0.1885	
Largest diff. peak and hole	0.724 and -0.418 $e.Å^{-3}$	

Table B9. Crystal data and structure refinement for **93**·$2CH_2Cl_2$.

Empirical formula	C38 H44 Cl4 N4 O S	
Formula weight	746.63	
Temperature	153(2) K	
Wavelength	0.71073 Å	
Crystal system	Monoclinic	
Space group	P21/n	
Unit cell dimensions	a = 10.4748(2) Å	α= 90°.
	b = 13.6047(2) Å	β= 92.435(1)°.
	c = 13.2513(2) Å	γ = 90°.
Volume	1886.69(5) $Å^3$	
Z	2	
Density (calculated)	1.314 Mg/m^3	
Absorption coefficient	0.405 mm^{-1}	
F(000)	784	
Crystal size	0.24 x 0.22 x 0.20 mm	
Theta range for data collection	2.94 to 27.48°.	
Index ranges	-13<=h<=13, -16<=k<=17, -17<=l<=17	
Reflections collected	7911	
Independent reflections	4314 [R(int) = 0.0414]	
Completeness to theta = 27.48°	99.5 %	
Absorption correction	None	
Refinement method	Full-matrix least-squares on F^2	
Data / restraints / parameters	4314 / 0 / 243	
Goodness-of-fit on F^2	1.044	
Final R indices [I>2sigma(I)]	R1 = 0.0467, wR2 = 0.1002	
R indices (all data)	R1 = 0.1085, wR2 = 0.1170	
Extinction coefficient	9.0(11) x 10^{-6}	
Largest diff. peak and hole	0.287 and -0.274 e.$Å^{-3}$	

Table B10. Crystal data and structure refinement for [**92**·$PhCO_2$]$^-$.

Empirical formula	C60 H83 Cl2 N5 O2 S2	
Formula weight	1041.33	
Temperature	153(2) K	
Wavelength	0.71073 Å	
Crystal system	Monoclinic	
Space group	P21	
Unit cell dimensions	a = 11.5806(2) Å	α= 90°.
	b = 22.8486(4) Å	β= 113.6230(10)°.
	c = 12.1009(2) Å	γ = 90°.
Volume	2933.59(9) Å^3	
Z	2	
Density (calculated)	1.179 Mg/m^3	
Absorption coefficient	0.227 mm^{-1}	
F(000)	1120	
Crystal size	0.55 x 0.18 x 0.10 mm	
Theta range for data collection	3.14 to 27.49°.	
Index ranges	-15<=h<=15, -20<=k<=29, -15<=l<=15	
Reflections collected	10518	
Independent reflections	10518	
Completeness to theta = 27.49°	99.3 %	
Absorption correction	None	
Refinement method	Full-matrix least-squares on F^2	
Data / restraints / parameters	10518 / 3 / 668	
Goodness-of-fit on F^2	0.986	
Final R indices [I>2sigma(I)]	R1 = 0.0507, wR2 = 0.0909	
R indices (all data)	R1 = 0.0988, wR2 = 0.1074	
Absolute structure parameter	0.00(6)	
Largest diff. peak and hole	0.276 and -0.297 e.Å^{-3}	

Table B11. Crystal data and structure refinement for [**92**·CH_3CO_2]$^-$.

Empirical formula	C55 H81 Cl2 N5 O2 S2	
Formula weight	979.27	
Temperature	153(2) K	
Wavelength	0.71073 Å	
Crystal system	Triclinic	
Space group	P-1	
Unit cell dimensions	a = 12.0220(2) Å	α= 70.8010(9)°.
	b = 14.4610(2) Å	β= 88.9990(8)°.
	c = 17.7050(3) Å	γ = 72.4930(8)°.
Volume	2760.82(8) Å^3	
Z	2	
Density (calculated)	1.178 Mg/m^3	
Absorption coefficient	0.237 mm^{-1}	
F(000)	1056	
Crystal size	0.27 x 0.26 x 0.10 mm	
Theta range for data collection	2.96 to 27.44°.	
Index ranges	-15<=h<=15, -18<=k<=18, -22<=l<=20	
Reflections collected	19709	
Independent reflections	12485 [R(int) = 0.0431]	
Completeness to theta = 27.44°	99.0 %	
Absorption correction	None	
Refinement method	Full-matrix least-squares on F^2	
Data / restraints / parameters	12485 / 64 / 666	
Goodness-of-fit on F^2	1.607	
Final R indices [I>2sigma(I)]	R1 = 0.0754, wR2 = 0.1271	
R indices (all data)	R1 = 0.1929, wR2 = 0.1416	
Extinction coefficient	2.0(5) x 10^{-6}	
Largest diff. peak and hole	0.610 and -0.581 e.Å^{-3}	

Table B12. Crystal data and structure refinement for [**92**·Cl]$^-$.

Empirical formula	C54 H82 Cl5 N5 O S2	
Formula weight	1058.62	
Temperature	153(2) K	
Wavelength	0.71073 Å	
Crystal system	Monoclinic	
Space group	P21/n	
Unit cell dimensions	a = 15.1902(5) Å	α= 90°.
	b = 18.6941(6) Å	β= 98.979(2)°.
	c = 20.9059(8) Å	γ = 90°.
Volume	5863.8(4) Å^3	
Z	4	
Density (calculated)	1.199 Mg/m^3	
Absorption coefficient	0.359 mm^{-1}	
F(000)	2264	
Crystal size	0.36 x 0.28 x 0.15 mm	
Theta range for data collection	2.93 to 25.00°.	
Index ranges	-18<=h<=18, -22<=k<=20, -24<=l<=24	
Reflections collected	17723	
Independent reflections	10250 [R(int) = 0.0718]	
Completeness to theta = 25.00°	99.3 %	
Absorption correction	None	
Refinement method	Full-matrix least-squares on F^2	
Data / restraints / parameters	10250 / 379 / 603	
Goodness-of-fit on F^2	1.727	
Final R indices [I>2sigma(I)]	R1 = 0.0956, wR2 = 0.1495	
R indices (all data)	R1 = 0.1892, wR2 = 0.1583	
Extinction coefficient	1.2(2) x 10^{-6}	
Largest diff. peak and hole	0.384 and -0.256 e.Å^{-3}	

Table B13. Crystal data and structure refinement for **105a**.

Empirical formula	C14 H12 N2	
Formula weight	208.26	
Temperature	153(2) K	
Wavelength	0.71073 Å	
Crystal system	Orthorhombic	
Space group	Pnma	
Unit cell dimensions	a = 6.4010(2) Å	α= 90°.
	b = 23.0270(6) Å	β= 90°.
	c = 7.2189(2) Å	γ = 90°.
Volume	1064.04(5) $Å^3$	
Z	4	
Density (calculated)	1.300 Mg/m^3	
Absorption coefficient	0.078 mm^{-1}	
F(000)	440	
Crystal size	0.27 x 0.17 x 0.09 mm	
Theta range for data collection	2.96 to 27.49°.	
Index ranges	-8<=h<=8, -29<=k<=29, -9<=l<=9	
Reflections collected	2206	
Independent reflections	1250 [R(int) = 0.0410]	
Completeness to theta = 27.49°	99.3 %	
Absorption correction	None	
Refinement method	Full-matrix least-squares on F^2	
Data / restraints / parameters	1250 / 0 / 103	
Goodness-of-fit on F^2	1.142	
Final R indices [I>2sigma(I)]	R1 = 0.0550, wR2 = 0.1160	
R indices (all data)	R1 = 0.1016, wR2 = 0.1287	
Extinction coefficient	2.0(5) x 10^{-5}	
Largest diff. peak and hole	0.224 and -0.275 $e.Å^{-3}$	

Table B14. Crystal data and structure refinement for **106a**·$2C_3H_6O$.

Empirical formula	C40 H44 N4 O2
Formula weight	612.79
Temperature	153(2) K
Wavelength	0.71073 Å
Crystal system	Orthorhombic
Space group	P212121
Unit cell dimensions	a = 7.25800(10) Å α= 90°.
	b = 21.3115(4) Å β= 90°.
	c = 21.5388(4) Å γ = 90°.
Volume	3331.60(10) $Å^3$
Z	4
Density (calculated)	1.222 Mg/m^3
Absorption coefficient	0.076 mm^{-1}
F(000)	1312
Crystal size	0.20 x 0.20 x 0.08 mm
Theta range for data collection	2.96 to 27.48°.
Index ranges	-9<=h<=9, -27<=k<=27, -27<=l<=27
Reflections collected	7584
Independent reflections	4315 [R(int) = 0.0672]
Completeness to theta = 27.48°	99.7 %
Absorption correction	None
Refinement method	Full-matrix least-squares on F^2
Data / restraints / parameters	4315 / 0 / 432
Goodness-of-fit on F^2	1.005
Final R indices [I>2sigma(I)]	R1 = 0.0455, wR2 = 0.0766
R indices (all data)	R1 = 0.1039, wR2 = 0.0924
Extinction coefficient	1.8(4) x 10^{-6}
Largest diff. peak and hole	0.196 and -0.204 $e.Å^{-3}$

Table B15. Crystal data and structure refinement for [**107a**·PF_6]$^-$.

Empirical formula	C70 H90 Cl6 F6 N7 P	
Formula weight	1387.16	
Temperature	153(2) K	
Wavelength	0.71073 Å	
Crystal system	Monoclinic	
Space group	P21/c	
Unit cell dimensions	a = 19.570(2) Å	α= 90°.
	b = 17.228(2) Å	β= 104.622(4)°.
	c = 21.934(3) Å	γ = 90°.
Volume	7155.6(15) Å^3	
Z	4	
Density (calculated)	1.288 Mg/m^3	
Absorption coefficient	0.323 mm^{-1}	
F(000)	2920	
Crystal size	0.56 x 0.24 x 0.07 mm	
Theta range for data collection	3.05 to 22.50°.	
Index ranges	-21<=h<=21, -18<=k<=17, -23<=l<=23	
Reflections collected	12703	
Independent reflections	7963 [R(int) = 0.1369]	
Completeness to theta = 22.50°	85.2 %	
Absorption correction	None	
Refinement method	Full-matrix least-squares on F^2	
Data / restraints / parameters	7963 / 540 / 811	
Goodness-of-fit on F^2	1.614	
Final R indices [I>2sigma(I)]	R1 = 0.1542, wR2 = 0.1716	
R indices (all data)	R1 = 0.3317, wR2 = 0.1989	
Largest diff. peak and hole	0.622 and -0.386 e.Å^{-3}	

Table B16. Crystal data and structure refinement for **108a**·$4C_4H_8O_2$.

Empirical formula	C42 H48 N4 O4	
Formula weight	672.84	
Temperature	173(2) K	
Wavelength	0.71073 Å	
Crystal system	Monoclinic	
Space group	P21/n	
Unit cell dimensions	a = 20.1548(6) Å	α= 90°.
	b = 6.5134(2) Å	β= 91.508(2)°.
	c = 28.2362(10) Å	γ = 90°.
Volume	3705.5(2) $Å^3$	
Z	4	
Density (calculated)	1.206 Mg/m^3	
Absorption coefficient	0.078 mm^{-1}	
F(000)	1440	
Crystal size	0.48 x 0.22 x 0.11 mm	
Theta range for data collection	3.10 to 25.00°.	
Index ranges	-23<=h<=23, -7<=k<=7, -33<=l<=33	
Reflections collected	11762	
Independent reflections	11762	
Completeness to theta = 25.00°	99.6 %	
Absorption correction	None	
Refinement method	Full-matrix least-squares on F^2	
Data / restraints / parameters	11762 / 36 / 415	
Goodness-of-fit on F^2	1.809	
Final R indices [I>2sigma(I)]	R1 = 0.1060, wR2 = 0.1716	
R indices (all data)	R1 = 0.2203, wR2 = 0.1890	
Extinction coefficient	6.5(7) x	10^{-6}
Largest diff. peak and hole	0.687 and -0.450 $e.Å^{-3}$	

Table B17. Crystal data and structure refinement for [**106a**·Cl]$^-$.

Empirical formula	C50 H68 Cl N5	
Formula weight	774.54	
Temperature	153(2) K	
Wavelength	0.71073 Å	
Crystal system	Orthorhombic	
Space group	Pbcn	
Unit cell dimensions	a = 41.0311(5) Å	α= 90°.
	b = 12.6474(1) Å	β= 90°.
	c = 17.3594(2) Å	γ = 90°.
Volume	9008.43(17) Å^3	
Z	8	
Density (calculated)	1.142 Mg/m^3	
Absorption coefficient	0.124 mm^{-1}	
F(000)	3360	
Crystal size	0.43 x 0.21 x 0.12 mm	
Theta range for data collection	2.96 to 27.50°.	
Index ranges	-53<=h<=53, -16<=k<=16, -22<=l<=22	
Reflections collected	18826	
Independent reflections	10137 [R(int) = 0.1062]	
Completeness to theta = 27.50°	97.9 %	
Absorption correction	None	
Refinement method	Full-matrix least-squares on F^2	
Data / restraints / parameters	10137 / 0 / 522	
Goodness-of-fit on F^2	1.065	
Final R indices [I>2sigma(I)]	R1 = 0.0607, wR2 = 0.1243	
R indices (all data)	R1 = 0.1930, wR2 = 0.1537	
Extinction coefficient	1.8(2) x 10^{-6}	
Largest diff. peak and hole	0.498 and -0.223 e.Å^{-3}	

Table B18. Crystal data and structure refinement for [**106a**·NO_3]$^-$.

Empirical formula	C50 H68 N6 O3
Formula weight	801.10
Temperature	153(2) K
Wavelength	0.71073 Å
Crystal system	Orthorhombic
Space group	Pbcn
Unit cell dimensions	a = 40.79880(10) Å α= 90°.
	b = 12.5954(2) Å β= 90°.
	c = 17.7740(6) Å γ = 90°.
Volume	9133.7(3) Å^3
Z	8
Density (calculated)	1.165 Mg/m^3
Absorption coefficient	0.073 mm^{-1}
F(000)	3472
Crystal size	0.51 x 0.16 x 0.08 mm
Theta range for data collection	2.97 to 27.49°.
Index ranges	-52<=h<=52, -16<=k<=16, -23<=l<=23
Reflections collected	18428
Independent reflections	10412 [R(int) = 0.1244]
Completeness to theta = 27.49°	99.3 %
Absorption correction	None
Refinement method	Full-matrix least-squares on F^2
Data / restraints / parameters	10412 / 0 / 549
Goodness-of-fit on F^2	1.213
Final R indices [I>2sigma(I)]	R1 = 0.0676, wR2 = 0.1262
R indices (all data)	R1 = 0.2298, wR2 = 0.1531
Extinction coefficient	2.8(2) x 10^{-6}
Largest diff. peak and hole	0.796 and -0.298 e.Å^{-3}

Table B19. Crystal data and structure refinement for [**107a**·NO_3]$^-$.

Empirical formula	C70 H90 Cl6 N8 O3	
Formula weight	1304.20	
Temperature	153(2) K	
Wavelength	0.71073 Å	
Crystal system	Monoclinic	
Space group	P21/c	
Unit cell dimensions	a = 18.6292(3) Å	α= 90°.
	b = 16.9861(3) Å	β= 102.662(1)°.
	c = 22.4638(4) Å	γ = 90°.
Volume	6935.5(2) Å^3	
Z	4	
Density (calculated)	1.249 Mg/m^3	
Absorption coefficient	0.299 mm^{-1}	
F(000)	2768	
Crystal size	0.30 x 0.24 x 0.17 mm	
Theta range for data collection	3.02 to 27.48°.	
Index ranges	-24<=h<=24, -21<=k<=22, -29<=l<=29	
Reflections collected	27570	
Independent reflections	15772 [R(int) = 0.0710]	
Completeness to theta = 27.48°	99.2 %	
Absorption correction	None	
Refinement method	Full-matrix-block least-squares on F^2	
Data / restraints / parameters	15772 / 54 / 808	
Goodness-of-fit on F^2	2.350	
Final R indices [I>2sigma(I)]	R1 = 0.1160, wR2 = 0.1898	
R indices (all data)	R1 = 0.2549, wR2 = 0.2012	
Largest diff. peak and hole	1.725 (near solvent) and -0.771 e.Å^{-3}	

References

1. Park, C. H.; Simmons, H. E. *J. Am. Chem. Soc.* **1968**, *90*, 2431-2432.

2. Schmidtchen, F. P.; Berger, M. *Chem. Rev.* **1997**, *97*, 1609-1646.

3. Martijn, M. G.; Reinhoudt, D. N. *Chem. Commun.* **1998**, 443-448.

4. Gale, P. A. *Coord. Chem. Rev.* **2000**, *199*, 181-223. Gale, P. A. *Coord. Chem. Rev.* 2001, 213, 79-128. Gale, P. A. *Coord. Chem. Rev.* **2003**, *240*, 191-221.

5. Beer, P. D.; Gale, P. A. *Angew. Chem. Int. Ed.* **2001**, *40*, 486-516.

6. *Supramolecular Chemistry of Anions* (Eds: Bianchi, A.; Bowman-James, K.; Garcia-España, E.), WILEY-VCH, New York, 1997.

7. Baeyer, A. *Ber. Dtsch. Chem. Ges*. **1886**, *19*, 2184-2185.

8. Chelintzev, V. V.; Tronov, B. V. *J. Russ. Phys. Chem. Soc.* **1916**, *48*, 105.

9. Rothemund, P.; Gage, C. L. *J. Am. Chem. Soc.* **1955**, *77*, 3340-3342.

10. Chelintzev, V. V.; Tronov, B. V. *J. Russ. Phys. Chem. Soc.* **1916**, *48*, 1197.

11. Brown, W. H.; Hutchinson, B. J.; MacKinnon, M. H. *Can. J. Chem.* **1971**, *49*, 4017-4022.

12. Lalloz, J. C.; Lehn, J. M. Unpublished results reported in Macrocyclic Chemistry; Dietrich, B.; Viout, P.; Lehn, J. M., Eds.; VCH: Weinheim, **1993**. Lalloz, J. C.; Lehn, J. M.; Willard, A. K. Unpublished results reported in Macrocyclic Chemistry; Dietrich, B.; Viout, P.; Lehn, J. M., Eds.; VCH: Weinheim, **1993**. Cesario, M.; Pascard, C. Unpublished results reported in Macrocyclic Chemistry; Dietrich, B.; Viout, P.; Lehn, J. M., Eds.; VCH: Weinheim, **1993**.

13. Floriani, C.; Floriani-Moro, R. *Porphyrin Handbook*, **2000**, *3*, 385-403.

14. Gale, P. A.; Sessler, J. L.; Král, V.; Lynch, V. *J. Am. Chem. Soc.* **1996**, *118*, 5140-5141.

15. Gale, P. A.; Sessler, J. L.; Král, V. *Chem. Commun.* **1998**, 1-8.

16. Gale, P. A.; Anzenbacher Jr., P.; Sessler, J. L. *Coord. Chem. Rev.* **2001**, *222*, 57-102.

17. Sessler, J. L.; Gale, P. A. *The Porphyrin Handbook*, **2000**, *6*, 257-277.

18. Sessler, J. L.; Cyr, M. J.; Lynch, V.; McGhee, E.; Ibers, J. A. *J. Am. Chem. Soc.* **1990**, *112*, 2810-2813.

19. Shionoya, M.; Furuta, H.; Lynch, V.; Harriman, A.; Sessler, J. L. *J. Am. Chem. Soc.* **1992**, *114*, 5714-5722.

20. Kral, V.; Furuta, H.; Shreder, K.; Lynch, V.; Sessler, J. L. *J. Am. Chem. Soc.* **1996**, *118*, 1595-1607.

21. van Hoorn, W. P.; Jorgensen, W. L. *J. Org. Chem.* **1999**, *64*, 7439-7444.

22. Blas, J. R.; Márquez, M.; Sessler, J. L.; Luque, F. J.; Orozco, M. *J. Am. Chem. Soc.* **2002**, *124*, 12796-12805.

23. Wu, Y-D.; Wang, D-F.; Sessler, J. L. *J. Org. Chem.* **2001**, *66*, 3739-3746.

24. Anzenbacher Jr., P; Jursíková, K.; Lynch, V. M.; Gale, P. A.; Sessler, J. L. *J. Am. Chem. Soc.* **1999**, *121*, 11020-11021.

25. Sessler, J. L.; Andrievsky, A.; Gale, P. A.; Lynch, V. *Angew. Chem. Int. Ed.* **1996**, *35*, 2782-2785.

26. Turner, B.; Botoshansky, M.; Eichen, Y. *Angew. Chem. Int. Ed.* **1998**, *37*, 2475-2478.

27. Nielsen, K. A.; Jeppesen, J. O.; Levillain, E.; Becher, J. *Angew. Chem. Int. Ed.* **2003**, *42*, 187-191.

28. Bucher, C.; Zimmerman, R. S.; Lynch, V.; Sessler, J. L. *J. Am. Chem. Soc.* **2001**, *123*, 9716-9717.

29. Gale, P. A.; Sessler, J. L.; Allen, W. E.; Tvermoes, N. A.; Lynch, V. *Chem. Commun.* **1997**, 665-666.

30. Anzenbacher Jr., P; Jursíková, K.; Shriver, J. A.; Miyaji, H.; Lynch, V. M.; Sessler, J. L.; Gale, P. A. *J. Org. Chem.* **2000**, *65*, 7641-7645.

31. Miyaji, H.; Sato, W.; Sessler, J. L.; Lynch, V. M. *Tetrahedron Lett.* **2000**, *41*, 1369.

32. Dukh, M.; Drašar, P.; Černý, I.; Pouzar, V.; Shriver, J. A.; Král, V.; Sessler, J. L. *Supramol. Chem.* **2002**, *14*, 237-244.

33. Warriner, C.; Gale, P. A.; Light, M. E.; Hursthouse, M. B. *Chem. Commun.* **2003**, 1810-1811.

34. Sato, W.; Miyaji, H.; Sessler, J. L. *Tetrahedron Lett.* **2000**, *41*, 6731-6736.

35. Yoon, D. W.; Hwang, H.; Lee, C. H. *Angew. Chem. Int. Ed.* **2002**, *41*, 1757-1759.

36. Lee, C. H.; Na, H. K.; Yoon, D. W.; Won, D. H.; Cho, W. S.; Lynch, V. M.; Shevchuk, S. V.; Sessler, J. L. *J. Am. Chem. Soc.* **2003**, *125*, 7301-7306.

37. Panda, P. K.; Lee, C. H. *Org. Lett.* **2004**, *6*, 671-674.

38. Miyaji, H.; Anzenbacher Jr., P.; Sessler, J. L.; Bleasdale, E. R.; Gale, P. A. *Chem. Commun.* **1999**, 1723-1724.

39. Miyaji, H.; Sato, W.; Sessler, J. L. *Angew. Chem. Int. Ed.* **2000**, *39*, 1777-1780.

40. Anzenbacher Jr., P; Jursíková, K.; Sessler, J. L. *J. Am. Chem. Soc.* **2000**, *122*, 9350-9351.

41. Sessler, J. L.; Gebauer, A.; Gale, P. A. *Gazz. Chim. Ital.* **1997**, *127*, 723-726.

42. Gale, P. A.; Hursthouse, M. B.; Light, M. E.; Sessler, J. L.; Warriner, C. N.; Zimmerman, R. S. *Tetrahedron Lett.* **2001**, *42*, 6759-6762.

43. Kral, V.; Sessler, J. L.; Shishkanova, T. V.; Gale, P. A.; Volf, R. *J. Am. Chem. Soc.* **1999**, *121*, 8771-8775.

44. Sessler, J. L.; Gale, P. A.; Genge, J. W. *Chem. Eur. J.* **1998**, *4*, 1095-1099.

45. Sessler, J. L.; Král, V.; Shishkanova, T. V.; Gale, P. A. *Proc. Natl. Acad. Sci. U. S. A.* **2002**, *99*, 4848-4853.

46. Gale, P. A.; Genge, J. W.; Král, V.; McKervey, M. A.; Sessler, J. L.; Walker, A. *Tetrahedron Lett.* **1997**, *38*, 8443-8444.

47. Gale, P. A.; Sessler, J. L.; Lynch, V.; Sansom, P. I. *Tetrahedron Lett.* **1996**, *37*, 7881-7884.

48. Turner, B.; Shterenberg, A.; Kapon, M.; Suwinska, K.; Eichen, Y. *Chem. Commun.* **2001**, 13-14. Turner, B.; Shterenberg, A.; Kapon, M.; Suwinska, K.; Eichen, Y. *Chem. Commun.* **2002**, 404-405. Turner, B.; Shterenberg, A.; Kapon, M.; Suwinska, K.; Eichen, Y. *Chem. Commun.* **2002**, 726-727.

49. Cafeo, G.; Kohnke, F. H.; Parisi, M. F.; Nascone, R. P.; La Torre, G. L.; Williams, D. J. *Org. Lett.* **2002**, *4*, 2695-2697.

50. Cafeo, G.; Kohnke, F. H.; La Torre, G. L.; White, A. J. P.; Williams, D. J. *Angew. Chem. Int. Ed.* **2000**, *39*, 1496-1498. Cafeo, G.; Kohnke, F. H.; La Torre, G. L.; White, A. J. P.; Williams, D. J. *Chem. Commun.* **2000**, 1207-1208. Cafeo, G.; Kohnke, F. H.; La Torre, G. L.; Parisi, M. F.; Nascone, R. P.; White, A. J. P.; Williams, D. J. *Chem. Eur. J.* **2002**, *8*, 3148-3156.

51. Sessler, J. L.; Anzenbacher Jr., P; Shriver, J. A.; Jursíková, K.; Lynch, V. M.; Marquez, M. *J. Am. Chem. Soc.* **2000**, *122*, 12061-12062.

52. Shriver, J. A. *Dissertation*, The University of Texas at Austin (USA), **2002**.

53. Unpublished results from Won-Seob Cho, a graduate student in the Sessler lab.

54. Anzenbacher Jr., P.; Try, A. C.; Miyaji, H.; Jursíková, K.; Lynch, V. M.; Marquez, M.; Sessler, J. L. *J. Am. Chem. Soc.* **2000**, *122*, 10268-10272.

55. d'A, A. M.; Gonsalves, R.; Johnstone, R. A. W.; Pereira, M. M.; Shaw, J.; do N. Sobral, A. J. F. *Tetrahedron Lett.* **1991**, *32*, 1355-1358.

56. Motekaitis, R. J.; Heinert, D. H.; Martell, Arthur E. *J. Org. Chem.* **1970**, *35*, 2504-2511.

57. Miyaji, H.; An, D.; Sessler, J. L. *Supramol. Chem.* **2001**, *13*, 661-669.

58. Sessler, J. L.; Weghorn, S. J.; Morishima, T.; Rosingana, M.; Lynch, V.; Lee, V. *J. Am. Chem. Soc.* **1992**, *114*, 8306-8307.

59. Setsune, J.; Katakami, Y.; Iizuna, N. *J. Am. Chem. Soc.* **1999**, *121*, 8957-8958. Setsune, J.; Maeda, S. *J. Am. Chem. Soc.* **2000**, *122*, 12405-12406.

60. Sessler, J. L.; An, D.; Cho, W. S.; Lynch, V. *Angew. Chem. Int. Ed.* **2003**, *42*, 2278-2281.

61. Groenendaal, L.; Peerlings, H. W. I.; van Dongen, J. L. J.; Havinga, E. E.; Vekemans, J. A. J. M.; Meijer, E. W. *Macromolecules* **1995**, *28*, 116-123. Burger, U.; Dreier, F. *Helv. Chim. Acta* **1980**, *63*, 1190-1197.

62. 3,3',4,4'-Tetrafluoro-2,2'-bipyrrole was obtained from Dr. Piotr Piatek, a postdoctoral fellow in this group.

63. Camiolo, S.; Gale, P. A. *Chem. Commun.* **2000**, 1129-1130.

64. Bauer, V. J.; Clive, D. L.; Dolphin, D.; Paine III, J. B.; Harris, F. L.; King, M. M.; Loder, J.; Wang, S.-W. C.; Woodward, R. B. *J. Am. Chem. Soc.* **1983**, *105*, 6429.

65. Sessler, J. L.; Morishima, T.; Lynch, V. *Angew. Chem. Int. Ed.* **1991**, *30*, 977-980.

66. Srinivasan, A.; Mahajan, S.; Pushpan, S. K.; Ravikumar, M.; Chandrashekar, T. K. *Tetrahedron Lett.* **1998**, 39, 1961-1964. Srinivasan, A.; Reddy, V. M.; Narayanan, S. J.; Sridevi, B.; Pushpan, S. K.; Ravikumar, M.; Chandrashekar, T. K. *Angew. Chem. Int. Ed.* **1997**, *36*, 2598-2601.

67. Jang Y. S.; Kim, H. J.; Lee, P. H.; Lee, C. H. *Tetrahedron Lett.* **2000**, *41*, 2919-2923. Arumugam, N.; Jang, Y. S.; Lee, C. H. *Org. Lett.* **2000**, *2*, 3115-3117. Nagarajan, A.; Ka, J. W.; Lee, C.-H. *Tetrahedron* **2001**, *57*, 7323-7330. Lee, E. C.; Park, Y. K.; Kim, J. H.; Hwang, H.; Kim, Y.-R.; Lee, C. H. *Tetrahedron Lett.* **2002**, *43*, 9493-9495.

68. Chadwick, D. J.; Will be, C. *J. Chem. Soc., Perkin Trans. 1* **1977**, 887-893.

69. Sessler, J. L.; An, D.; Cho, W. S.; Lynch, V. *J. Am. Chem. Soc.* **2003**, *125*, 13646-13647.

70. Sessler, J. L.; Andrievsky, A.; Gale, P. A.; Lynch, V. *Angew. Chem. Int. Ed.* **1996**, *35*, 2782-2785.

71. Sessler, J. L.; Cho, W. S.; Lynch, V.; Král, V. *Chem. Eur. J.* **2002**, *8*, 1134-1143.

72. Chérioux, F.; Therrien, B.; Süss-Fink, G. *Chem. Commun.* **2004**, 204-205.

73. Merrill, B. A.; LeGoff, E. *J. Org. Chem.* **1990**, *55*, 2904-2908.

74. Sessler, J. L.; Weghorn, S. J.; Hiseada, Y.; Lynch, V. *Chem. Eur. J.* **1995**, *1*, 56-67.

75. Corriu, R. J. P.; Bolin, G; Moreau, J. J. E.; Vernhet, C. *J. Chem. Soc., Chem. Commun.* **1991**, 211-213.

76. Carré, F. H.; Corriu, R. J. P.; Bolin, G.; Moreau, J. J. E.; Vernhet, C. *Organometallics* **1993**, *12*, 2478-2486.

77. Sotzing, G. A. ; Reynolds, J. R. ; Katritzky, A. R. ; Soloducho, J. ; Belyakov, S. ; Musgrave, R. *Macromolecules* **1996**, *29*, 1679-1684.

78. Littler, B. J.; Miller, M. A.; Hung, C.-H.; Wagner, R. W.; O'Shea, D. F.; Boyle, P. D.; Lindsey, J. S. *J. Org. Chem.* **1999**, *64*, 1391-1396.

79. Seidel, D.; Lynch, V.; Sessler, J. L. *Angew. Chem. Int. Ed.* **2002**, *41*, 1422-1425.

80. Köhler, T.; Seidel, D.; Lynch, V.; Arp, F. O.; Ou, Z.; Kadish, K. M.; Sessler, J. L. *J. Am. Chem. Soc.* **2003**, *125*, 6872-6873.

Vita

Deqiang An was born in Siping, Jilin Province, P. R. China on December 17, 1971, the son of Yuliang An and Chunxiang Ma. After completing secondary education at Siping No.1 high school, Siping, Jilin Province, P. R. China in 1989, he entered Jilin University in Changchun, Jilin Province, P. R. China. He received a Bachelor of Science in Chemistry from Jilin University in July 1993. He then continued his education at Jilin University and was awarded with a Master of Science in Chemistry in July 1996. After working in industry for two years, he entered the Graduate School of the University of Missouri-Rolla in 1998. In 1999 he transferred to the Graduate School of the University of Texas at Austin.

Permanent address: No. 82 Nan Youdian Street
Siping, Jilin Province
P.R. China 136000

This dissertation was typed by the author.